

Time-series machine-learning error models for approximate solutions to parameterized dynamical systems

Eric J. Parish^a, Kevin T. Carlberg^a

^a*Sandia National Laboratories, 7011 East Ave, Livermore, CA 94550*

Abstract

This work proposes a machine-learning framework for modeling the error incurred by approximate solutions to parameterized dynamical systems. In particular, we extend the machine-learning error models (MLEM) framework proposed in Ref. [15] to dynamical systems. The proposed Time-Series Machine-Learning Error Modeling (T-MLEM) method constructs a regression model that maps features—which comprise error indicators that are derived from standard *a posteriori* error-quantification techniques—to a random variable for the approximate-solution error at each time instance. The proposed framework considers a wide range of candidate features, regression methods, and additive noise models. We consider primarily recursive regression techniques developed for time-series modeling, including both classical time-series models (e.g., autoregressive models) and recurrent neural networks (RNNs), but also analyze standard non-recursive regression techniques (e.g., feed-forward neural networks) for comparative purposes. Numerical experiments conducted on multiple benchmark problems illustrate that the long short-term memory (LSTM) neural network, which is a type of RNN, outperforms other methods and yields substantial improvements in error predictions over traditional approaches.

1. Introduction

Myriad applications in engineering and science require many simulations of a (parameterized) dynamical-system model. Examples of such “many-query” problems include uncertainty propagation, design optimization, and statistical inference. When the cost of a single dynamical-system simulation is computationally expensive—as is the case for partial-differential-equation (PDE) models characterized by a fine spatiotemporal discretization—such many-query problems are intractable. In these cases, analysts often replace the original (high-fidelity) dynamical-system model with a surrogate model that can generate low-cost *approximate solutions*, which can in turn make the many-query problem computationally tractable. Examples of surrogate models include *inexact solutions* arising from early termination of an iterative method, *lower-fidelity models* characterized by simplifying physical assumptions (e.g., linearized dynamics, inviscid flow, elastic deformation) or a coarse discretization, and projection-based *reduced-order models (ROMs)* (e.g., Galerkin projection with a proper orthogonal decomposition basis).

The use of an approximate solution introduces error; as such, it is critical to quantify this error and properly account for it in the analysis underpinning the many-query problem. For this purpose, researchers have developed a wide range of methods for *a posteriori* error quantification. These efforts, which date back to the pioneering work of Babuška and Rheinboldt for finite element analysis [24, 3, 2], have resulted in a techniques that can be categorized as (1) *a posteriori* error bounds, (2) error indicators, and (3) error models.

A posteriori error bounds place bounds on the (normed) state or quantity-of-interest (QoI) error arising from the use of an approximate solution. These methods were originally developed in the finite-element [36, 35, 29] and model-reduction communities. In the reduced-basis community, Refs. [8, 38] derived *a posteriori*

Email addresses: ejparis@sandia.gov (Eric J. Parish), ktcarlb@sandia.gov (Kevin T. Carlberg)

QoI error bounds for the reduced-basis method applied to linear elliptic and parabolic PDEs. Refs. [18, 41] extended these results to time-dependent linear parabolic PDEs. In the context of model reduction for nonlinear dynamical systems, Ref. [21] derived error bounds for the linearized Galerkin ROM, while Ref. [9] derived error bounds for Galerkin and least-squares Petrov-Galerkin (LSPG) ROMs. These error bounds are *residual-based*, meaning that they depend on the (dual) norm of the high-fidelity-model residual evaluated at the approximate solution. Such bounds are appealing because they can provide guaranteed, rigorous bounds on the errors of interest, thus providing a critical tool for certified predictions. However, these bounds often suffer from lack of sharpness, i.e., they are often orders-of-magnitude larger than the approximate-solution error itself. This is exacerbated in dynamical systems, where error bounds for many types of approximate solutions grow exponentially in time (see, e.g., Ref. [9]). In addition, these bounds typically require (difficult-to-compute) estimates or bounds of operator quantities such as Lipschitz and inf-sup constants. These drawbacks often limit the utility of *a posteriori* error bounds in practical applications.

Alternatively, *error indicators* are computable quantities that are *indicative* of the approximate-solution error. Error indicators typically do not provide unbiased estimates of the error, nor do they rigorously bound the error; instead, they are often correlated with the error, correspond to a low-order approximation of the error, and/or appear as terms in error bounds. The two most common error indicators are the (dual) norm of the high-fidelity-model residual evaluated at the approximate solution (i.e., the residual norm) and the dual-weighted residual. The residual norm is informative of the error, as it typically appears in *a posteriori* error bounds and is usually strongly correlated with the error; it is often used within greedy methods for snapshot collection [7, 6, 19, 48, 49] and when using ROMs for PDE-constrained optimization within a trust-region framework [52, 50, 51]. In contrast, dual-weighted residuals are derived from a Taylor-series approximation of the error, and are typically used for goal-oriented error estimation and mesh adaptation [28, 1, 46, 47]. Due to their practical utility, error indicators have been largely successful in quantifying and controlling errors through mesh adaptation for static problems (i.e., problems without time evolution). However, their success has been more limited for dynamical systems due to the fact that errors for such systems exhibit dependence on *non-local* quantities, i.e., the approximate-solution error at a given time instance depends on the past time history of the system. Thus, the residual norm at the current time instance is no longer directly indicative of the approximate-solution error; the error additionally depends on non-local quantities. This can be clearly seen from *a posteriori* error bounds, as the bound for the error at a given time instance depends on the residual norm at previous time instances. Similarly, dual-weighted-residual error estimation requires computing solutions to either the forward-in-time linearized sensitivity equations or the backward-in-time linearized adjoint equations. Not only does this incur significant computational and storage costs, it can also be linearly unstable and produce exploding gradients when applied to chaotic systems (although this can be mitigated by approaches such as least-squares shadowing [5, 44]). Further, it is often practically challenging to implement adjoint-based methods, e.g., due to the requirement of residual-Jacobian transposes, which are not always easily exposed.

Error models seek to model the state and QoI errors directly via regression techniques. The most popular such approach is the so-called “model-discrepancy” method of Kennedy and O’Hagan [25] (and related approaches [22, 13, 30, 16]). The model-discrepancy approach computes a Gaussian process (GP) that provides a mapping from any finite number of points in parameter space to a Gaussian random vector representing the approximate-solution error at those points. As such, this technique can be considered a regression approach, where the *regression model* is provided by a GP, the *features* are the system parameters, and the *response* is the approximate-solution error. Recently, researchers have pursued improvements over this technique by (1) considering a wider class of modern machine-learning regression methods than simply Gaussian processes (which do not scale well to high-dimensional feature spaces), and (2) considering more informative features than the system parameters alone. First, the reduced-order model error surrogates (ROMES) method [12] was proposed in the context of static problems. ROMES employs the same regression model (GP) as the model-discrepancy approach, but it employs different features; namely, it employs the aforementioned *error indicators* (i.e., residual norm, approximated dual-weighted residual) as features. Because these quantities are indicative of the error, they provide more informative features for predicting the error than the system parameters. Numerical experiments illustrated the ability of the ROMES method to pro-

duce significantly more accurate error predictions than the model-discrepancy approach. More recently, the ROMES method was applied to construct error models for the in-plane and out-of-plane state error incurred by reduced-order models for static problems [33]. Subsequent work [15] again considered static problems, but constructed machine-learning error models that considered a wide range of candidate regression models (e.g., neural networks, support vector machines, random forests) and error-indicator-based features (e.g., residual samples) in order to predict the approximate-solution error response. This work showed the ability of machine-learning methods to predict the error with near perfect accuracy across a range of static problems and approximate-solution types.

The construction of error models for dynamical systems is significantly more challenging than doing so for static systems, as the errors exhibit dependence on non-local quantities. Relevant work on constructing error models for dynamical systems accounts for the time-dependent nature of the approximate-solution error either (1) by using both time itself and time-lagged error indicators as features [45] or (2) by constructing a different regression method for each time instance or window [34]. In the first case, Ref. [45] proposes the error modeling via machine learning (EMML) method. EMML is a regression approach, where the regression model is provided by random forests or LASSO, the features correspond to application-specific quantities that include time itself and time-lagged quantities, and the response is the (relative) QoI or state error at a given time instance. While this work generated promising results on an oil–water subsurface flow problem, it suffers from a noticeable limitation: it treats error modeling as a classical (non-recursive) regression problem as opposed to a time-series-prediction problem. As such, it does not capture the intrinsic recursive structure of the error. In the second case, Ref. [34] proposes a regression model that is tantamount to applying the model-discrepancy method [25] to model the approximate-solution error at each time instance or window, as the regression model corresponds to a GP, the features are system parameters, and the response is the QoI error at a given time instance/window. Unfortunately, this approach also fails to capture non-local dependencies of the error, and—as with the original model-discrepancy method—does not use particularly informative features to predict the error.

The objective of this work is to construct accurate error models for dynamical systems by (1) applying the same machine-learning error modeling framework of Ref. [15], but (2) considering recursive regression techniques developed for time-series modeling, as this naturally enables the method to capture the non-local dependencies of the error. The proposed Time-Series Machine-Learning Error Modeling (T-MLEM) method, which views the error modeling problem from the time-series-prediction perspective, is characterized by a *regression model* provided by a recursive time-series-prediction model (e.g., autoregressive model, recurrent neural network [43]), *features* corresponding to time-local error indicators (e.g., residual samples), and a *response* corresponding to the normed state or QoI error at a given time instance. For comparative purposes, we also consider classical non-recursive regression methods (e.g., feed-forward neural networks) within the T-MLEM framework, which is analogous to the approach proposed in Ref. [45]. To produce a statistical model of the approximate-solution error, we also consider several noise models (e.g., Gaussian, Laplacian). The net result is a random variable for the error whose statistics can be used to assess the uncertainty in the error prediction.

The paper proceeds as follows. Section 2 sets the mathematical context by introducing parameterized dynamical systems, approximate solutions, and classical methods for error quantification. Section 3 outlines the proposed T-MLEM method, including the structure of the regression model, feature engineering, data generation, and training of the regression and noise models. Section 4 provides numerical experiments that apply the proposed framework to 1) the parameterized advection–diffusion equation, where the approximate solution is provided by a proper orthogonal decomposition (POD) ROM with Galerkin projection, 2) the parameterized shallow-water equations, where the approximate solution is again provided by a POD–Galerkin ROM, and 3) the parameterized Burgers’ equation, where the approximate solution is provided by a coarse-mesh model. Finally, Section 5 provides conclusions.

2. Parametrized nonlinear dynamical systems

This work considers the high-fidelity model to be a parameterized dynamical system characterized by a parameterized system of nonlinear ordinary differential equations (ODEs) of the form

$$\frac{d\mathbf{x}}{dt} = \mathbf{f}(\mathbf{x}, t; \boldsymbol{\mu}), \quad \mathbf{x}(0) = \mathbf{x}_0(\boldsymbol{\mu}), \quad t \in [0, T], \quad (1)$$

where $T \in \mathbb{R}^+$ denotes the final time; $\mathbf{x} \equiv \mathbf{x}(t, \boldsymbol{\mu})$ with $\mathbf{x} : [0, T] \times \mathcal{D} \rightarrow \mathbb{R}^N$ denotes the state implicitly defined as the solution to the initial-value problem (1); $\mathbf{x}_0 : \mathcal{D} \rightarrow \mathbb{R}^N$ denotes the parameterized initial condition; $\boldsymbol{\mu} \in \mathcal{D} \subseteq \mathbb{R}^{N_\mu}$ denote parametric inputs to the system; and $\mathbf{f} : \mathbb{R}^N \times [0, T] \times \mathcal{D} \rightarrow \mathbb{R}^N$ denotes the parameterized velocity, which may be linear or nonlinear in its first argument. We refer to Eq. (1) as the full-order-model system of ordinary differential equations (FOM ODE), which may arise, for example, from the spatial discretization of a system of PDEs.

Numerically computing a solution to Eq. (1) requires applying a time-discretization method. In this work, we assume the use of a linear multistep method for this purpose. For notational simplicity, we assume a uniform time discretization characterized by N_t time instances $t^n = n\Delta t$, $n = 0, \dots, N_t$ with time step $\Delta t = T/N_t$; however, the proposed methodology does not rely on this restriction. Applying a linear multistep method to discretize the FOM ODE (1) yields the following system of algebraic equations arising at the n th time instance, which we refer to as the FOM OΔE:

$$\mathbf{r}^n(\mathbf{x}^n; \mathbf{x}^{n-1}, \dots, \mathbf{x}^{n-k^n}, \boldsymbol{\mu}) = \mathbf{0}, \quad n = 1, \dots, N_t. \quad (2)$$

The discrete state \mathbf{x}^n comprises the numerical approximation to $\mathbf{x}(t^n)$ and is implicitly defined as the solution to Eq. (2) given the discrete state at the previous k^n time instances and the parameters $\boldsymbol{\mu}$. Here, the discrete residual $\mathbf{r}^n : \mathbb{R}^N \otimes \mathbb{R}^{k^n+1} \times \mathcal{D} \rightarrow \mathbb{R}^N$ is defined as

$$\mathbf{r}^n : (\mathbf{w}; \mathbf{x}^{n-1}, \dots, \mathbf{x}^{n-k^n}, \boldsymbol{\mu}) \mapsto \alpha_0 \mathbf{w} - \Delta t \beta_0 \mathbf{f}(\mathbf{w}, t^n; \boldsymbol{\mu}) + \sum_{i=1}^{k^n} \alpha_i \mathbf{x}^{n-i} - \Delta t \sum_{i=1}^{k^n} \beta_i \mathbf{f}(\mathbf{x}^{n-i}, t^{n-i}; \boldsymbol{\mu}). \quad (3)$$

Given the initial state $\mathbf{x}^0(\boldsymbol{\mu}) = \mathbf{x}_0(\boldsymbol{\mu})$, solving the FOM OΔE (2) for $n = 1, \dots, N_t$ yields the sequence of (discrete) FOM solutions $\mathbf{x}^n(\boldsymbol{\mu})$, $n = 0, \dots, N_t$.

In many cases, the analyst is primarily interested in computing a scalar-valued quantity of interest (QoI) at each time instance, which we define as

$$s^n : \boldsymbol{\mu} \mapsto g(\mathbf{x}^n(\boldsymbol{\mu}); t^n, \boldsymbol{\mu}), \quad n = 0, \dots, N_t, \quad (4)$$

where $s^n : \mathcal{D} \rightarrow \mathbb{R}$ and $g : \mathbb{R}^N \times [0, T] \times \mathcal{D} \rightarrow \mathbb{R}$ denotes the QoI functional.

If the FOM state-space dimension N or the number of time instances N_t is large, then computing the sequence of FOM solutions $\mathbf{x}^n(\boldsymbol{\mu})$, $n = 0, \dots, N_t$ and associated QoIs $s^n(\boldsymbol{\mu})$, $n = 0, \dots, N_t$ can be computationally expensive. If additionally these solutions are sought at many parameter instances, then the resulting *many-query* problem is computationally intractable. In such scenarios, analysts typically aim to overcome this computational barrier by replacing the FOM with a surrogate model that can generate low-cost *approximate solutions*.

2.1. Approximate solutions

When a surrogate model is employed to mitigate the aforementioned computational bottleneck, it generates a sequence of *approximate solutions* $\tilde{\mathbf{x}}^n : \mathcal{D} \rightarrow \mathbb{R}^N$, $n = 0, \dots, N_t$ with $\tilde{\mathbf{x}}^0(\boldsymbol{\mu}) = \tilde{\mathbf{x}}_0(\boldsymbol{\mu})$ given and attendant approximate QoIs

$$\tilde{s}^n : \boldsymbol{\mu} \mapsto g(\tilde{\mathbf{x}}^n(\boldsymbol{\mu}); t^n, \boldsymbol{\mu}), \quad n = 0, \dots, N_t, \quad (5)$$

where $\tilde{s}^n : \mathcal{D} \rightarrow \mathbb{R}$. As in Ref. [15], we now discuss three types of surrogate models that are often employed to generate the approximate solutions $\tilde{\mathbf{x}}^n(\boldsymbol{\mu})$, $n = 0, \dots, N_t$.

2.1.1. Inexact solutions

If one applies an iterative method (e.g., Newton's method) to solve the FOM OΔE system (2) arising at each time instance, then inexact tolerances $\varepsilon^n > 0$, $n = 1, \dots, N_t$ can be employed such that the approximate solutions satisfy

$$\|\mathbf{r}^n(\tilde{\mathbf{x}}^n; \tilde{\mathbf{x}}^{n-1}, \dots, \tilde{\mathbf{x}}^{n-k^n}, \boldsymbol{\mu})\|_2 \leq \varepsilon^n, \quad n = 1, \dots, N_t. \quad (6)$$

In such cases, the surrogate model merely corresponds to early termination of the associated iterative method.

2.1.2. Lower-fidelity models

Approximate solutions can also be obtained by employing a computational model of lower fidelity, which can be achieved, for example, by introducing simplifying physical assumptions or coarsening the spatial discretization. In such cases, the corresponding low-fidelity-model (LFM) ODE takes the form

$$\frac{d\mathbf{x}_{\text{LF}}}{dt} = \mathbf{f}_{\text{LF}}(\mathbf{x}_{\text{LF}}, t; \boldsymbol{\mu}), \quad \mathbf{x}_{\text{LF}}(0) = \mathbf{x}_{\text{LF},0}(\boldsymbol{\mu}), \quad t \in [0, T], \quad (7)$$

where $\mathbf{x}_{\text{LF}} \equiv \mathbf{x}_{\text{LF}}(t, \boldsymbol{\mu})$ with $\mathbf{x}_{\text{LF}} : [0, T] \times \mathcal{D} \rightarrow \mathbb{R}^{N_{\text{LF}}}$ denotes the LFM state of dimension $N_{\text{LF}} (\ll N)$; $\mathbf{x}_{\text{LF},0} : \mathcal{D} \rightarrow \mathbb{R}^{N_{\text{LF}}}$ denotes the parameterized initial conditions; and $\mathbf{f}_{\text{LF}} : \mathbb{R}^{N_{\text{LF}}} \times [0, T] \times \mathcal{D} \rightarrow \mathbb{R}^{N_{\text{LF}}}$ denotes the parameterized LFM velocity.

Applying a linear multistep method (with the same uniform time step Δt as the FOM) to the discretized LFM ODE (7) yields the LFM OΔE arising at the n th time instance

$$\mathbf{r}_{\text{LF}}^n(\mathbf{x}_{\text{LF}}^n; \mathbf{x}_{\text{LF}}^{n-1}, \dots, \mathbf{x}_{\text{LF}}^{n-k^n}, \boldsymbol{\mu}) = \mathbf{0}, \quad n = 1, \dots, N_t, \quad (8)$$

where the discrete state \mathbf{x}_{LF}^n is the numerical approximation to $\mathbf{x}_{\text{LF}}(t^n)$ and is implicitly defined as the solution to Eq. (8) given the LFM state at the previous k^n time instances and the parameters $\boldsymbol{\mu}$. Analogously to definition (3), the LFM OΔE residual $\mathbf{r}^n : \mathbb{R}^{N_{\text{LF}}} \otimes \mathbb{R}^{k^n+1} \times \mathcal{D} \rightarrow \mathbb{R}^N$ is defined as

$$\mathbf{r}_{\text{LF}}^n : (\mathbf{w}_{\text{LF}}; \mathbf{x}_{\text{LF}}^{n-1}, \dots, \mathbf{x}_{\text{LF}}^{n-k^n}, \boldsymbol{\mu}) \mapsto \alpha_{\text{LF},0} \mathbf{w}_{\text{LF}} - \Delta t \beta_{\text{LF},0} \mathbf{f}_{\text{LF}}(\mathbf{w}_{\text{LF}}, t^n; \boldsymbol{\mu}) + \sum_{i=1}^{k^n} \alpha_{\text{LF},i} \mathbf{x}_{\text{LF}}^{n-i} - \Delta t \sum_{i=1}^{k^n} \beta_{\text{LF},i} \mathbf{f}_{\text{LF}}(\mathbf{x}_{\text{LF}}^{n-i}, t^{n-i}; \boldsymbol{\mu}). \quad (9)$$

We emphasize that the time integrators for the FOM and LFM can be different, as denoted by the LF subscripts on the coefficients in definition (9). As with the FOM, given the initial LFM state $\mathbf{x}_{\text{LF}}^0(\boldsymbol{\mu}) = \mathbf{x}_{\text{LF},0}(\boldsymbol{\mu})$, solving the LFM OΔE (8) yields the sequence of (discrete) LFM solutions \mathbf{x}_{LF}^n , $n = 0, \dots, N_t$.

Critically, to recover the approximate solution in the FOM state space \mathbb{R}^N , we assume the existence of a prolongation operator $\mathbf{p} : \mathbb{R}^{N_{\text{LF}}} \times \mathcal{D} \rightarrow \mathbb{R}^N$ such that

$$\tilde{\mathbf{x}}^n(\boldsymbol{\mu}) = \mathbf{p}(\mathbf{x}_{\text{LF}}^n(\boldsymbol{\mu}); \boldsymbol{\mu}), \quad n = 0, \dots, N_t. \quad (10)$$

2.1.3. Projection-based reduced-order models

Projection-based reduced-order models (ROMs) comprise a popular technique for generating approximate solutions. Such approaches can be derived by applying projection to either the FOM ODE (1) or OΔE (2). In the former case, ROMs correspond to a particular type of low-fidelity model as described in Section 2.1.2. In particular, introducing a trial-basis matrix $\boldsymbol{\Phi} \in \mathbb{R}_{\star}^{N \times K}$ (e.g., computed via proper orthogonal decomposition [4]) and a test-basis matrix $\boldsymbol{\Psi} \in \mathbb{R}_{\star}^{N \times K}$ (e.g., $\boldsymbol{\Psi} = \boldsymbol{\Phi}$ in the case of Galerkin projection), where $K \ll N$ and $\mathbb{R}_{\star}^{m \times n}$ denotes the set of $m \times n$ full-column-rank matrices (i.e., the non-compact Stiefel manifold), ROMs seek an approximate solution in a K -dimensional affine trial subspace, i.e.,

$$\mathbf{x}(t; \boldsymbol{\mu}) \approx \tilde{\mathbf{x}}(t; \boldsymbol{\mu}) = \mathbf{x}_{\text{ref}}(\boldsymbol{\mu}) + \boldsymbol{\Phi} \hat{\mathbf{x}}(t; \boldsymbol{\mu}), \quad (11)$$

where $\hat{\mathbf{x}} : [0, T] \times \mathcal{D} \rightarrow \mathbb{R}^K$ are the generalized coordinates and $\mathbf{x}_{\text{ref}} : \mathcal{D} \rightarrow \mathbb{R}^K$ denotes the reference state (typically chosen to be either $\mathbf{x}_{\text{ref}}(\boldsymbol{\mu}) = \mathbf{x}_0(\boldsymbol{\mu})$ or $\mathbf{x}_{\text{ref}}(\boldsymbol{\mu}) = \mathbf{0}$). The generalized coordinates are computed by performing a projection process performed on the FOM ODE (1). Namely, the approximation (11) is

substituted in the FOM ODE (1), and the resulting residual is enforced to be orthogonal to range of the test-basis matrix. This projection process yields

$$\frac{d\hat{\mathbf{x}}}{dt} = [\Psi^T \Phi]^{-1} \Psi^T \mathbf{f}(\mathbf{x}_{\text{ref}}(\boldsymbol{\mu}) + \Phi \hat{\mathbf{x}}, t; \boldsymbol{\mu}), \quad \hat{\mathbf{x}}(0; \boldsymbol{\mu}) = \Phi^+(\mathbf{x}_0(\boldsymbol{\mu}) - \mathbf{x}_{\text{ref}}(\boldsymbol{\mu})), \quad (12)$$

where the superscript $+$ denotes the Moore–Penrose pseudo-inverse. This approach to model reduction is equivalent to a low-fidelity model of the form (7) with $\mathbf{x}_{\text{LF}} = \hat{\mathbf{x}}$, $\mathbf{f}_{\text{LF}} : (\hat{\mathbf{x}}, t; \boldsymbol{\mu}) \mapsto [\Psi^T \Phi]^{-1} \Psi^T \mathbf{f}(\mathbf{x}_{\text{ref}}(\boldsymbol{\mu}) + \Phi \hat{\mathbf{x}}, t; \boldsymbol{\mu})$, and $\mathbf{p} : (\hat{\mathbf{x}}, \boldsymbol{\mu}) \mapsto \mathbf{x}_{\text{ref}}(\boldsymbol{\mu}) + \Phi \hat{\mathbf{x}}$.

The most common method that associates with applying projection to the FOM ODE (2) is the least-squares Petrov–Galerkin (LSPG) method [9], which substitutes the approximation (11) into the FOM ODE (2) and minimizes the resulting residual in the ℓ^2 -norm. In this case, the approximate solutions satisfy

$$\tilde{\mathbf{x}}^n \in \arg \min_{\tilde{\mathbf{x}} \in \mathbf{x}_{\text{ref}}(\boldsymbol{\mu}) + \text{Ran}(\Phi)} \|\mathbf{r}^n(\tilde{\mathbf{x}}; \tilde{\mathbf{x}}^{n-1}, \dots, \tilde{\mathbf{x}}^{n-k^n}, \boldsymbol{\mu})\|_2. \quad (13)$$

It can be shown [9] that this LSPG approach can be expressed as a time-continuous projection (12) with $\Psi = \Psi(\hat{\mathbf{x}}, t; \boldsymbol{\mu}) = (\alpha_0 \mathbf{I} - \Delta t \beta_0 \partial \mathbf{f} / \partial \mathbf{x}(\mathbf{x}_{\text{ref}}(\boldsymbol{\mu}) + \Phi \hat{\mathbf{x}}, t; \boldsymbol{\mu})) \Phi$ if $\beta_j = 0$ for $j \geq 1$ (i.e., a single-step method is used), the velocity \mathbf{f} is linear in its first argument, or if $\beta_0 = 0$ (i.e., an explicit scheme is used).

2.2. Approximate-solution errors

Employing an approximate solution in lieu of the FOM solution incurs an error that must be accounted for in the ultimate analysis. This work focuses on quantifying two types of such errors, namely

1. the quantity-of-interest error $\delta_s^n(\boldsymbol{\mu}) := s^n(\boldsymbol{\mu}) - \tilde{s}^n(\boldsymbol{\mu})$, $n = 1, \dots, N_t$ and
2. the normed state error $\delta_x^n(\boldsymbol{\mu}) := \|\mathbf{x}^n(\boldsymbol{\mu}) - \tilde{\mathbf{x}}^n(\boldsymbol{\mu})\|_2$, $n = 1, \dots, N_t$.

Because $\tilde{\mathbf{x}}^0(\boldsymbol{\mu})$ and $\mathbf{x}^0(\boldsymbol{\mu})$ are given, we can compute $\delta_s^0(\boldsymbol{\mu})$ and $\delta_x^0(\boldsymbol{\mu})$ explicitly.

2.3. Classical approaches for error quantification

Classical approaches for quantifying approximate-solution errors for parameterized dynamical systems correspond to a *posteriori* error bounds and error indicators. We proceed by briefly reviewing these methods, as they serve as a starting point for our work and will be used to engineer features for the proposed regression framework. We focus in particular on the dual-weighted-residual error indicator.

2.3.1. A posteriori error bounds

We now state a *posteriori* error bounds for both the errors $|\delta_s^n(\boldsymbol{\mu})|$ and $\delta_x^n(\boldsymbol{\mu})$, $n = 1, \dots, N_t$, which arise from any arbitrary sequence of approximate solutions $\tilde{\mathbf{x}}^n(\boldsymbol{\mu})$, $n = 0, \dots, N_t$. The first result was presented in Ref. [27, Theorem 4.3].

Proposition 2.1 (*A posteriori* error bounds [27]). For a given parameter instance $\boldsymbol{\mu} \in \mathcal{D}$, if the velocity \mathbf{f} is Lipschitz continuous, i.e., there exists a constant $\kappa > 0$ such that $\|\mathbf{f}(\mathbf{x}, t; \boldsymbol{\mu}) - \mathbf{f}(\mathbf{y}, t; \boldsymbol{\mu})\|_2 \leq \kappa \|\mathbf{x} - \mathbf{y}\|_2$ for all $\mathbf{x}, \mathbf{y} \in \mathbb{R}^N$ and $t \in \{t^n\}_{i=1}^{N_t}$, and the time step is sufficiently small such that $\Delta t < |\alpha_0|/|\beta_0| \kappa$, then

$$\delta_x^n(\boldsymbol{\mu}) \leq \frac{1}{h} \left\| \mathbf{r}^n \left(\tilde{\mathbf{x}}^n(\boldsymbol{\mu}); \tilde{\mathbf{x}}^{n-1}(\boldsymbol{\mu}), \dots, \tilde{\mathbf{x}}^{n-k^n}(\boldsymbol{\mu}), \boldsymbol{\mu} \right) \right\|_2 + \sum_{j=1}^{k^n} \gamma_j \delta_x^{n-j}(\boldsymbol{\mu}) \quad (14)$$

for all $n = 1, \dots, N_t$. Here, $h := |\alpha_0| - |\beta_0| \kappa \Delta t$ and $\gamma_j := (|\alpha_j| + |\beta_j| \kappa \Delta t) / h$. If additionally the QoI functional g is Lipschitz continuous, i.e., there exists a constant $\kappa_g > 0$ such that $|g(\mathbf{x}; t, \boldsymbol{\mu}) - g(\mathbf{y}; t, \boldsymbol{\mu})| \leq \kappa_g \|\mathbf{x} - \mathbf{y}\|_2$ for all $\mathbf{x}, \mathbf{y} \in \mathbb{R}^N$ and $t \in \{t^n\}_{i=1}^{N_t}$, then

$$|\delta_s^n(\boldsymbol{\mu})| \leq \frac{\kappa_g}{h} \left\| \mathbf{r}^n \left(\tilde{\mathbf{x}}^n(\boldsymbol{\mu}); \tilde{\mathbf{x}}^{n-1}(\boldsymbol{\mu}), \dots, \tilde{\mathbf{x}}^{n-k^n}(\boldsymbol{\mu}), \boldsymbol{\mu} \right) \right\|_2 + \kappa_g \sum_{j=1}^{k^n} \gamma_j \delta_x^{n-j}(\boldsymbol{\mu}) \quad (15)$$

for all $n = 1, \dots, N_t$.

Proof. Bound (14) was derived in Ref. [27, Theorem 4.3]. Bound (15) follows directly from Lipschitz continuity of the QoI functional and the bound 14. \square

We make three critical observations from inequalities (14) and (15):

1. The error bounds are *residual based*, i.e., the magnitudes of the error bounds are driven by the FOM residual operator \mathbf{r}^n evaluated at the sequence of approximate solutions $\tilde{\mathbf{x}}^n(\boldsymbol{\mu})$, $n = 0, \dots, N_t$. Note that the approximate solution incurs no error if the approximate solutions exactly satisfy the FOM ODE (2) such that the residual is zero at all time instances. This also illustrates why the residual norm is often viewed as a useful *error indicator* for guiding greedy methods for snapshot collection [7, 6, 19, 48, 49] or trust-region optimization algorithms [52, 50, 51].
2. The error bounds exhibit dependence on *non-local* quantities, i.e., the error at the n th time instance depends on the error at the previous k^n time instances through recursion via the rightmost term in inequalities (14) and (15). This comprises a fundamental difference from error bounds for static problems.
3. The error bounds often *lack sharpness*, i.e., they are often significant larger than the magnitudes of the actual errors. This overestimation is exacerbated for ill-conditioned problems (in which case the Lipschitz constants κ and κ_g are large) and long time horizons (as the error bounds grow exponentially in time). As such, their practical utility for error estimation itself is often limited.
4. The error bounds are *difficult to compute*, i.e., they require computing Lipschitz constants κ and κ_g , which is challenging for general nonlinear dynamical systems. While bounding these constants is possible in some contexts [23], this often incurs substantial additional computational costs.

2.3.2. Error indicator: dual-weighted residuals

Besides the residual norm, the dual-weighted residual is perhaps the most popular error indicator. The dual-weighted residual is derived from a low-order approximation of the QoI error and, as such, is often strongly correlated with the error [12]. Because deriving dual-weighted residuals for dynamical systems requires considering the problem from the monolithic “space–time” perspective, we now introduce the required space–time formulation of the problem.

We begin by defining a “vectorization” function that assembles the full space–time solution from a tuple of time-local solutions as

$$\begin{aligned} \text{vec} : (\mathbf{y}^1, \dots, \mathbf{y}^{N_t}) &\mapsto \begin{bmatrix} [\mathbf{y}^1]^T & \dots & [\mathbf{y}^{N_t}]^T \end{bmatrix}^T \\ &: \mathbb{R}^p \otimes \mathbb{R}^{N_t} \rightarrow \mathbb{R}^{pN_t}, \end{aligned}$$

for arbitrary p . Then, we define the space–time FOM state and space–time approximate solution as $\bar{\mathbf{x}}(\boldsymbol{\mu}) := \text{vec}(\mathbf{x}^1(\boldsymbol{\mu}), \dots, \mathbf{x}^{N_t}(\boldsymbol{\mu}))$ and $\tilde{\bar{\mathbf{x}}}(\boldsymbol{\mu}) := \text{vec}(\tilde{\mathbf{x}}^1(\boldsymbol{\mu}), \dots, \tilde{\mathbf{x}}^{N_t}(\boldsymbol{\mu}))$, respectively, where $\bar{\mathbf{x}}, \tilde{\bar{\mathbf{x}}} : \mathcal{D} \rightarrow \mathbb{R}^{Np}$. We also define the space–time residual as

$$\begin{aligned} \bar{\mathbf{r}} : (\bar{\mathbf{w}}; \boldsymbol{\mu}) &\mapsto \text{vec}(\mathbf{r}^1(\mathbf{w}^1; \boldsymbol{\mu}), \dots, \mathbf{r}^{N_t}(\mathbf{w}^{N_t}; \mathbf{w}^{N_t-1}, \dots, \mathbf{w}^{N_t-k^{N_t}}, \boldsymbol{\mu})), \\ &: \mathbb{R}^{Np} \times \mathcal{D} \rightarrow \mathbb{R}^{Np}, \end{aligned}$$

where $\bar{\mathbf{w}} \equiv \text{vec}(\mathbf{w}^1, \dots, \mathbf{w}^{N_t})$. Lastly, we define the space–time QoI functional as

$$\begin{aligned} \bar{g} : (\bar{\mathbf{w}}; \boldsymbol{\mu}) &\mapsto \text{vec}(g(\mathbf{w}^1; t^1, \boldsymbol{\mu}), \dots, g(\mathbf{w}^{N_t}; t^{N_t}, \boldsymbol{\mu})), \\ &: \mathbb{R}^{Np} \times \mathcal{D} \rightarrow \mathbb{R}^{Np}, \end{aligned}$$

such that the space–time QoIs computed from the FOM and approximate solutions are given by

$$\bar{s} : \boldsymbol{\mu} \mapsto \bar{g}(\bar{\mathbf{x}}(\boldsymbol{\mu}); \boldsymbol{\mu}), \quad \tilde{\bar{s}} : \boldsymbol{\mu} \mapsto \bar{g}(\tilde{\bar{\mathbf{x}}}(\boldsymbol{\mu}); \boldsymbol{\mu}),$$

respectively, where $\bar{s}, \tilde{s} : \mathcal{D} \rightarrow \mathbb{R}^{N_t}$.

Assuming the residual is twice continuously differentiable in its first argument and noting that $\bar{\mathbf{r}}(\bar{\mathbf{x}}(\boldsymbol{\mu}); \boldsymbol{\mu}) = \mathbf{0}$, we can write

$$-\bar{\mathbf{r}}(\tilde{\mathbf{x}}(\boldsymbol{\mu}); \boldsymbol{\mu}) = \left[\frac{\partial \bar{\mathbf{r}}}{\partial \bar{\mathbf{w}}}(\tilde{\mathbf{x}}(\boldsymbol{\mu}); \boldsymbol{\mu}) \right] \left(\bar{\mathbf{x}}(\boldsymbol{\mu}) - \tilde{\mathbf{x}}(\boldsymbol{\mu}) \right) + \mathcal{O} \left(\|\bar{\mathbf{x}}(\boldsymbol{\mu}) - \tilde{\mathbf{x}}(\boldsymbol{\mu})\|_2^2 \right). \quad (16)$$

Assuming the space-time residual Jacobian $\left[\frac{\partial \bar{\mathbf{r}}}{\partial \bar{\mathbf{w}}}(\tilde{\mathbf{x}}(\boldsymbol{\mu}); \boldsymbol{\mu}) \right]$ is invertible, Eq. (16) can be solved for a first-order approximation of the solution error

$$\bar{\mathbf{x}}(\boldsymbol{\mu}) - \tilde{\mathbf{x}}(\boldsymbol{\mu}) = - \left[\frac{\partial \bar{\mathbf{r}}}{\partial \bar{\mathbf{w}}}(\tilde{\mathbf{x}}(\boldsymbol{\mu}); \boldsymbol{\mu}) \right]^{-1} \bar{\mathbf{r}}(\tilde{\mathbf{x}}(\boldsymbol{\mu}); \boldsymbol{\mu}) + \mathcal{O} \left(\|\bar{\mathbf{x}}(\boldsymbol{\mu}) - \tilde{\mathbf{x}}(\boldsymbol{\mu})\|_2^2 \right). \quad (17)$$

If we additionally assume the space-time QoI functional \bar{g} is twice continuously differentiable in its first argument, the error in the space-time QoI can be represented to first order as,

$$\bar{s}(\boldsymbol{\mu}) - \tilde{s}(\boldsymbol{\mu}) = \left[\frac{\partial \bar{g}}{\partial \bar{\mathbf{w}}}(\tilde{\mathbf{x}}(\boldsymbol{\mu}); \boldsymbol{\mu}) \right] \left(\bar{\mathbf{x}}(\boldsymbol{\mu}) - \tilde{\mathbf{x}}(\boldsymbol{\mu}) \right) + \mathcal{O} \left(\|\bar{\mathbf{x}}(\boldsymbol{\mu}) - \tilde{\mathbf{x}}(\boldsymbol{\mu})\|_2^2 \right). \quad (18)$$

Substituting Eq. (17) into Eq. (18) yields,

$$\bar{s}(\boldsymbol{\mu}) - \tilde{s}(\boldsymbol{\mu}) = d(\boldsymbol{\mu}) + \mathcal{O} \left(\|\bar{\mathbf{x}}(\boldsymbol{\mu}) - \tilde{\mathbf{x}}(\boldsymbol{\mu})\|_2^2 \right), \quad (19)$$

where the dual-weighted residual comprises a first-order approximation of the QoI error and is defined as

$$d(\boldsymbol{\mu}) := - \underbrace{\left[\frac{\partial \bar{g}}{\partial \bar{\mathbf{w}}}(\tilde{\mathbf{x}}(\boldsymbol{\mu}); \boldsymbol{\mu}) \right]}_{N_t \times NN_t} \underbrace{\left[\frac{\partial \bar{\mathbf{r}}}{\partial \bar{\mathbf{w}}}(\tilde{\mathbf{x}}(\boldsymbol{\mu}); \boldsymbol{\mu}) \right]^{-1}}_{NN_t \times NN_t} \underbrace{\bar{\mathbf{r}}(\tilde{\mathbf{x}}(\boldsymbol{\mu}); \boldsymbol{\mu})}_{NN_t \times 1}, \quad (20)$$

$$= \begin{bmatrix} \text{---} & \text{---} & \dots & \text{---} \end{bmatrix} \begin{bmatrix} \square & & & \\ \square & \square & & \\ \vdots & \vdots & \ddots & \\ \square & \dots & \dots & \square \end{bmatrix} \begin{bmatrix} \vdots \\ \vdots \\ \vdots \\ \vdots \end{bmatrix}. \quad (21)$$

Computing the dual-weighted residual (20) involves applying the inverse of the $NN_t \times NN_t$ space-time residual Jacobian and can be computed in one of two ways: (1) the direct (forward) method, or (2) the adjoint (backward) method. The direct method solves the (linear) *sensitivity equations*

$$\frac{\partial \bar{\mathbf{r}}}{\partial \bar{\mathbf{w}}}(\tilde{\mathbf{x}}(\boldsymbol{\mu}); \boldsymbol{\mu}) \bar{\mathbf{q}} = \bar{\mathbf{r}}(\tilde{\mathbf{x}}(\boldsymbol{\mu}); \boldsymbol{\mu}), \quad (22)$$

where $\bar{\mathbf{q}} \equiv \bar{\mathbf{q}}(\boldsymbol{\mu}) \equiv \text{vec}(\mathbf{q}^1(\boldsymbol{\mu}), \dots, \mathbf{q}^{N_t}(\boldsymbol{\mu}))$ with $\mathbf{q}^n : \mathcal{D} \rightarrow \mathbb{R}^N$, $n = 1, \dots, N_t$ is implicitly defined as the solution to Eq. (22) and denotes the space-time *sensitivity vector*. The direct method subsequently computes the dual-weighted residual as

$$d(\boldsymbol{\mu}) = - \left[\frac{\partial \bar{g}}{\partial \bar{\mathbf{w}}}(\tilde{\mathbf{x}}(\boldsymbol{\mu}); \boldsymbol{\mu}) \right] \bar{\mathbf{q}}(\boldsymbol{\mu}). \quad (23)$$

Due to the sparsity pattern of the space-time residual Jacobian $\frac{\partial \bar{\mathbf{r}}}{\partial \bar{\mathbf{w}}}(\tilde{\mathbf{x}}(\boldsymbol{\mu}); \boldsymbol{\mu})$, this approach is equivalent to performing a linear forward-in-time solve, which can be executed simultaneously with the forward-in-time

solve used to generate the approximate solutions, i.e., the sensitivities $\mathbf{q}^n(\boldsymbol{\mu})$ can be computed contemporaneously with $\tilde{\mathbf{x}}^n(\boldsymbol{\mu})$. In contrast, the adjoint method solves the multiple-right-hand-side (linear) *adjoint equations*

$$\left[\frac{\partial \bar{\mathbf{r}}}{\partial \bar{\mathbf{w}}}(\tilde{\mathbf{x}}(\boldsymbol{\mu}); \boldsymbol{\mu}) \right]^T \bar{\mathbf{y}} = \left[\frac{\partial \bar{g}}{\partial \bar{\mathbf{w}}}(\tilde{\mathbf{x}}(\boldsymbol{\mu}); \boldsymbol{\mu}) \right]^T, \quad (24)$$

where

$$\bar{\mathbf{y}} \equiv \bar{\mathbf{y}}(\boldsymbol{\mu}) \equiv [\text{vec}(\mathbf{y}_1^1(\boldsymbol{\mu}), \dots, \mathbf{y}_1^{N_t}(\boldsymbol{\mu})) \quad \dots \quad \text{vec}(\mathbf{y}_{N_t}^1(\boldsymbol{\mu}), \dots, \mathbf{y}_{N_t}^{N_t}(\boldsymbol{\mu}))] \in \mathbb{R}^{NN_t \times N_t},$$

with $\mathbf{y}_i^n : \mathcal{D} \rightarrow \mathbb{R}^N$, $i, n = 1, \dots, N_t$ is implicitly defined as the solution to Eq. (24) and denotes N_t space–time *dual vectors*. The adjoint method subsequently computes the dual-weighted residual as

$$d(\boldsymbol{\mu}) = -\bar{\mathbf{y}}(\boldsymbol{\mu})^T \bar{\mathbf{r}}(\tilde{\mathbf{x}}(\boldsymbol{\mu}); \boldsymbol{\mu}). \quad (25)$$

Due to the sparsity pattern of the space–time residual Jacobian transpose, this approach is tantamount to performing a linear backward-in-time solve, and must be computed *after* the approximate-solution sequence has been fully computed, as this sequence defines the argument at which the space–time residual Jacobian is evaluated.

Analogously to the observations made about error bounds in the Section 2.3.1, we now make several observations about the dual-weighted residual:

1. The dual-weighted residual is *residual-based*, i.e., it corresponds to a linear combination of elements of the space–time residual, where the weights in the linear combination are provided by the dual according to Eq. (25).
2. The dual-weighted residual exhibits dependence on *non-local* quantities, i.e., computing the dual-weighted residual using either the direct method (23) or the adjoint method (25) requires solving a linear system either forward-in-time or backward-in-time over the entire time domain. Further, the sparsity pattern of the operators in Eq. (20) illustrates that the QoI error at the n th time instance depends on quantities computed at all previous time instances.
3. The dual-weighted residual may be an *inaccurate* approximation of the error, i.e., it is a first-order approximation valid in the limit $\|\bar{\mathbf{x}}(\boldsymbol{\mu}) - \tilde{\mathbf{x}}(\boldsymbol{\mu})\|_2 = \sqrt{\sum_{n=1}^{N_t} (\delta_{\mathbf{x}}^n(\boldsymbol{\mu}))^2} \rightarrow 0$, and thus can be inaccurate for cases where the normed state error is not negligible. This is precisely the case we are interested in, as we aim to model this error.
4. Dual-weighted residuals can be *difficult to compute*, i.e., they require solving either the forward sensitivity (22) or adjoint equations (24), each of which is characterized by a block triangular system matrix of dimension $NN_t \times NN_t$, with NN_t the space–time dimension of the original full-order-model problem. The use of approximate solutions aims to avoid any computations that scale with the dimension N , and thus computing the dual-weighted residual in this manner is often impractical. To mitigate this computational burden, analysts often adopt the adjoint method, solve the adjoint equations (24) using a coarse model (e.g., a coarse mesh), and prolongate the computed (coarse) dual vector to a representation compatible with the (fine) full-order model in order to compute the dual-weighted residual [46]. In addition to these computational-cost issues, adopting the adjoint method introduces other challenges, as it requires access to the residual-Jacobian transpose to solve Eq. (24), which may not be available.

2.3.3. Discussion

This work aims to overcome the most prominent shortcomings of *a posteriori* error bounds and dual-weighted residuals: (1) their lack of sharpness or inaccuracy, and (2) the difficulty in their computation. We aim to achieve this by applying modern machine-learning methods within a regression setting, wherein the *regression model* is provided by a recursive time-series-prediction model that can capture dependencies on non-local quantities, the *features* correspond to residual-based time-local error indicators that appear in the definitions of the *a posteriori* error bounds and dual-weighted residuals, and the *response* corresponds

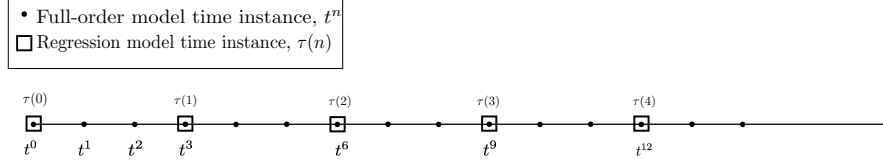


Figure 1: Example of time discretizations for the full-order model and machine learning model. In this case, the regression model is solved on a temporal grid that is three times as coarse as the approximate and full-order models such that $\mathbb{T} = \{3, 6, 9, 12, \dots\}$.

to the time-local normed state or QoI error. Thus, we employ the classical methods for error quantification to guide the design of the both the regression model and features. We also aim to construct a statistical model of the response error by considering several noise models. The next section describes the proposed methodology, which adopts this strategy.

3. Time-Series Machine-Learning Error Modeling

We now present the proposed Time-Series Machine-Learning Error Modeling (T-MLEM) method, which constructs a mapping from residual-based features to a random variable for the error using regression techniques that can capture dependencies on non-local quantities. The method comprises an extension of the machine-learning error modeling (MLEM) framework presented in Ref. [15]—which was applicable to parameterized static systems—to parameterized dynamical systems. Because the method is applicable to modeling both the QoI error $\delta_s^n(\boldsymbol{\mu})$ and normed-state error $\delta_x^n(\boldsymbol{\mu})$, we denote the error of interest generically as $\delta^n(\boldsymbol{\mu})$ in this section.

3.1. Machine-learning framework

The proposed method aims to predict errors on a *subset* of the time grid $t^n = n\Delta t$, $n = 0, \dots, N_t$ used to define the FOM OΔE (2). We make this choice because the time step Δt is typically chosen to control time-discretization errors, while we may be interested in modeling the error at only a (relatively small) subset of these grid points; furthermore, constructing a time-series model of these errors on a coarser time grid reduces the computational cost of training the regression model. We define this coarse time grid as $t^n = n\Delta t$, $n \in \mathbb{T}$, where $\mathbb{T} \subseteq \{1, \dots, N_t\}$ denotes the coarse time-index set comprising $\bar{N}_t := |\mathbb{T}| (\leq N_t)$ time instances and equipped with a mapping $\tau : \{0, \dots, \bar{N}_t\} \rightarrow \{0, \dots, N_t\}$ from a coarse time index to the corresponding fine time index, which satisfies $\tau(0) = 0$.

We assume that we can compute *features* $\boldsymbol{\rho}^n(\boldsymbol{\mu}) \in \mathbb{R}^{N_\rho}$ that are informative of the *response* $\delta^n(\boldsymbol{\mu}) \in \mathbb{R}$ —which is the time-local error of interest—at time instances $n \in \mathbb{T}$. Section 3.1.1 provides candidate features, which are inspired by the classical error-quantification methods described in Section 2.3. Given the ability to compute these features, we propose to construct error models $\hat{\delta}^n(\boldsymbol{\mu}) (\approx \delta^n(\boldsymbol{\mu}))$ of the form

$$\hat{\delta}^n(\boldsymbol{\mu}) = \hat{\delta}_f^n(\boldsymbol{\mu}) + \hat{\delta}_\epsilon^n(\boldsymbol{\mu}), \quad n \in \mathbb{T}, \quad (26)$$

where $\hat{\delta}_f^n : \mathcal{D} \rightarrow \mathbb{R}$, $n \in \{0\} \cup \mathbb{T}$ denotes the sequence of *deterministic regression-function models* and $\hat{\delta}_\epsilon^n : \mathcal{D} \rightarrow \mathbb{V}$, $n \in \{0\} \cup \mathbb{T}$ denotes a sequence of mean-zero random variables that serve as the *stochastic noise models* such that $\hat{\delta}^n : \mathcal{D} \rightarrow \mathbb{V}$, $n \in \mathbb{T}$ with $\mathbb{E}[\hat{\delta}^n(\boldsymbol{\mu})] = \hat{\delta}_f^n(\boldsymbol{\mu})$; we denote the set of real-valued random variables by \mathbb{V} .

As previously described, we propose to construct the regression model using a recursive time-series-prediction model that can capture dependencies on non-local quantities. In particular, we impose the following structure on the regression-function model:

$$\hat{\delta}_f^n(\boldsymbol{\mu}) = \hat{f}(\boldsymbol{\rho}^n(\boldsymbol{\mu}), \mathbf{h}^n(\boldsymbol{\mu})), \quad n \in \mathbb{T}. \quad (27)$$

Here, $\hat{f} : \mathbb{R}^{N_\rho} \times \mathbb{R}^{N_h} \rightarrow \mathbb{R}$, while $\mathbf{h}^n : \mathcal{D} \rightarrow \mathbb{R}^{N_h}$, $n \in \{0\} \cup \mathbb{T}$ denotes the sequence of *latent variables*. Critically, the inclusion of these latent variables enables the proposed method to capture dependencies on non-local quantities, as we enforce the latent variables to be governed by the recursion

$$\mathbf{h}^{\tau(n)}(\boldsymbol{\mu}) = \mathbf{g}(\boldsymbol{\rho}^{\tau(n)}(\boldsymbol{\mu}), \mathbf{h}^{\tau(n-1)}(\boldsymbol{\mu}), \hat{\delta}_f^{\tau(n-1)}(\boldsymbol{\mu})), \quad n = 1, \dots, \bar{N}_t, \quad (28)$$

where $\mathbf{g} : \mathbb{R}^{N_\rho} \times \mathbb{R}^{N_h} \times \mathbb{R} \rightarrow \mathbb{R}^{N_h}$; $\hat{\delta}_f^0(\boldsymbol{\mu}) = \delta^0(\boldsymbol{\mu})$ is given; and $\mathbf{h}^0(\boldsymbol{\mu}) = \mathbf{0}$. Similarly, we impose the following structure on the noise model:

$$\hat{\delta}_\epsilon^{\tau(n)}(\boldsymbol{\mu}) = \hat{\epsilon}(\hat{\delta}_\epsilon^{\tau(n-1)}(\boldsymbol{\mu}), \epsilon^{\tau(n)}), \quad n = 1, \dots, \bar{N}_t. \quad (29)$$

Here, $\hat{\epsilon} : \mathbb{V} \times \mathbb{V} \rightarrow \mathbb{V}$, $\hat{\delta}_\epsilon^0(\boldsymbol{\mu}) = 0$, and $\epsilon^n \in \mathbb{V}$, $n \in \mathbb{T}$ denotes a sequence of independent and identically distributed mean-zero random variables.

Remark 3.1 (Classical non-recursive regression). We note that classical non-recursive regression methods can be described by omitting latent variables from the regression function approximation such that $\hat{f}(\boldsymbol{\rho}^n(\boldsymbol{\mu}), \mathbf{h}^n(\boldsymbol{\mu})) \equiv \hat{f}(\boldsymbol{\rho}^n(\boldsymbol{\mu}))$, omitting latent-variable dynamics (28), and employing a simple non-recursive noise model such that $\hat{\delta}_\epsilon^n(\boldsymbol{\mu}) = \epsilon^n$, $n \in \mathbb{T}$.

Remark 3.2 (Noise models). We note that more sophisticated functional forms of $\hat{\epsilon}$ could be considered, e.g., by allowing parameters that define the probability distribution of ϵ^n for $n \in \mathbb{T}$ to depend on features, or by including latent variables as inputs to the function $\hat{\epsilon}$.

The primary distinction between the proposed T-MLEM method and the methods proposed in Refs. [15, 45] is the consideration of recursive regression models that employ latent variables. The MLEM method [15] considered only static problems and thus did not require the use of such variables. The EMLL framework [45] accounted for dependencies on non-local quantities by explicitly considering features corresponding to quantities computed at previous time instances. This introduces difficulties, as it requires knowledge about the memory of the system (i.e., how many previous time instances to consider in constructing the features) and can lead to a prohibitively large set of features. In contrast, the use of latent variables and the specific functional forms (27)–(29) allow the proposed T-MLEM method to capture non-local effects naturally.

As in Ref. [15], we aim to construct regression models that exhibit the following properties:

Objective 1 Low cost. The error model $\hat{\delta}^n(\boldsymbol{\mu})$ should be computationally inexpensive to deploy, i.e., its evaluation should not dominate the computational cost of computing the approximate solutions $\tilde{\mathbf{x}}^n(\boldsymbol{\mu})$, $n = 0, \dots, N_t$. This requirement implies that the features $\boldsymbol{\rho}^n(\boldsymbol{\mu})$ should be cheap to compute, the latent-variable dimension N_h should be relatively small, and it should be inexpensive to evaluate the functions \hat{f} , \mathbf{g} , and $\hat{\epsilon}$.

Objective 2 Low noise variance. Because the variance of the noise model $\hat{\delta}_\epsilon^n(\boldsymbol{\mu})$ reflects the magnitude of epistemic uncertainty introduced by the use of an approximate solution, reducing this variance in turn reduces the uncertainty introduced into the analysis. A model with low noise variance has not been underfit to training data.

Objective 3 Generalizability. For the regression model to be trustworthy, the distributions of the true error $\delta^n(\boldsymbol{\mu})$ and the error model $\hat{\delta}^n(\boldsymbol{\mu})$ should closely match on an independent test set, which was not used to train the error model. A model exhibiting generalizability has not been overfit to training data.

We adopt the machine-learning framework proposed in Ref. [15] to satisfy these objectives. This framework comprises the following steps:

- Step 1 Feature engineering.** Select features that are inexpensive to compute (Objective 1), informative of the error such that a low-noise-variance model can be constructed (Objective 2), and low dimensional (i.e., N_ρ small) such that less training data are required for the resulting model to generalize (Objective 3). To satisfy these requirements, we engineer residual-based features informed by classical error-quantification methods as described in Section 2.3. We ensure these features are low dimensional and inexpensive to compute through the use of sampling-based approximations (e.g., gappy principal component analysis). Section 3.1.1 describes this step.
- Step 2 Data generation.** After selecting candidate features, generate both training and test data in the form of a set of response–feature pairs on the coarse time-index set \mathbb{T} for parameter instances sampled according to the imposed probability distribution on the parameter domain \mathcal{D} . Constructing these data requires computing *both* the FOM solutions and approximate solutions for the selected parameter instances. Sections 3.1.2–3.1.3 describe this step.
- Step 3 Train the deterministic regression-function model $\hat{\delta}_f^n(\boldsymbol{\mu})$.** Define candidate functional forms for the functions \hat{f} and \mathbf{g} , compute model parameters by (approximately) minimizing a loss function defined on the training data, and perform hyperparameter selection using (cross-)validation. Sections 3.1.4–3.1.5 describes this step.
- Step 4 Train the stochastic noise model $\hat{\delta}_\epsilon^n(\boldsymbol{\mu})$.** Finally, define candidate functional forms for the function $\hat{\epsilon}$, and compute model parameters via maximum likelihood estimation on a training set independent from that used to train the deterministic regression function. In this work, we employ a subset of the test set used to evaluate the deterministic regression function for this purpose. Sections 3.1.6–3.1.7 describe this step.

3.1.1. Feature engineering

We now describe Step 1 of the proposed framework: feature engineering. Namely, we describe the candidate features $\boldsymbol{\rho}^n$ that we consider, which are inspired by those proposed in Ref. [15]. Several considerations drive feature engineering, which balance Objective 1–Objective 3:

Consideration 1 Feature cost. To satisfy Objective 1, we aim to develop features that are inexpensive to compute. Satisfying this objective can compromise quality, as high-quality features are often costly to compute.

Consideration 2 Feature quality. To satisfy Objective 2, we aim to develop features that are as informative of the error as possible, because employing high-quality explanatory features can lead to a low-noise-variance regression model.

Consideration 3 Number of features. Employing a large number of features often leads to a high-capacity model that can yield low noise variance with sufficient training data (i.e., Objective 2 is bolstered). However, computing a large number of features can be computationally expensive (i.e., Objective 1 suffers), and often requires a large amount of training data to generalize well and avoid overfitting (i.e., Objective 3 suffers). Regularization strategies can be employed when training a regression model with a large number of features to mitigate overfitting.

The remainder of this section details a variety of candidate features that differ in terms of the above considerations.

Feature 1 Parameters: The system’s parametric inputs $\boldsymbol{\mu}$ correspond to free-to-compute but low-quality features, where the number of features is equal to the number of parameters $N_{\boldsymbol{\mu}}$. Simply setting $\boldsymbol{\rho}^n(\boldsymbol{\mu}) = \boldsymbol{\mu}$ comprises the same feature choice as that employed by the classical model-discrepancy approach [25], which uses Gaussian-process regression to construct the regression model. These features are time independent.

Feature 2 Time: The time variable t^n is a single, free-to-compute feature, which is likely to be low quality in most scenarios. This low quality arises from the fact that—in most applications—the error is not driven by the time variable itself. Instead, the classical error-quantification methods discussed in Section 2.3 suggest that the error is instead determined by the residual, Lipschitz constants, and dual vectors. Intuitively, employing time as a feature can cause the resulting regression model to be “tied” to the particular time coordinates associated with the behavior observed during training. This implies that the resulting regression method will lack invariance with respect to the time grid, i.e., the model will not generalize well for problems characterized by phase shifts or for prediction beyond the training time interval. The EML framework considered time as a feature [45, Table I].

Feature 3 Residual norm: As discussed in Section 2.3, classical error-quantification methods are residual based. In particular, the first term on the right-hand side of a *a posteriori* error bound (14) demonstrates that the residual norm $\|\tilde{\mathbf{r}}^n(\boldsymbol{\mu})\|_2$, where $\tilde{\mathbf{r}}^n : \boldsymbol{\mu} \mapsto \mathbf{r}^n(\tilde{\mathbf{x}}^n(\boldsymbol{\mu}); \tilde{\mathbf{x}}^{n-1}(\boldsymbol{\mu}), \dots, \tilde{\mathbf{x}}^{n-k^n}(\boldsymbol{\mu}), \boldsymbol{\mu})$, is informative of the state error $\delta_{\mathbf{x}}^n(\boldsymbol{\mu})$; bound (15) shows that the residual norm $\|\tilde{\mathbf{r}}^n(\boldsymbol{\mu})\|_2$ is also informative of the magnitude of the QoI error $|\delta_s^n(\boldsymbol{\mu})|$. This feature is computationally expensive to compute, as it requires computing all N elements of the vector $\tilde{\mathbf{r}}^n(\boldsymbol{\mu})$ before computing its norm. However, this (single) feature is likely of higher quality than the both Feature 1 and Feature 2, as it appears explicitly in classical *a posteriori* error bounds (14)–(15). Yet, this feature will likely be of lower quality for predicting the (signed) QoI error $\delta_s^n(\boldsymbol{\mu})$ because it is not informative of the error’s sign. We note that—in contrast to static systems—the residual norm $\|\tilde{\mathbf{r}}^n(\boldsymbol{\mu})\|_2$ (along with stability constants) is not sufficient to bound the errors $\delta_{\mathbf{x}}^n(\boldsymbol{\mu})$ and $|\delta_s^n(\boldsymbol{\mu})|$. Instead, inequalities (14)–(15) illustrate that these bounds depend additionally on non-local quantities, namely $\delta_{\mathbf{x}}^{n-j}(\boldsymbol{\mu})$, $j = 1, \dots, k^n$. Thus, we expect this feature choice—as well as all subsequent residual-based features—to perform best when used with recursive regression methods that can capture dependencies on non-local quantities. We note that the ROMES method [12] employed features $\boldsymbol{\rho} = \|\tilde{\mathbf{r}}^n(\boldsymbol{\mu})\|_2$ with Gaussian-process regression to construct a regression model for the normed state error.

Feature 4 Residual: To increase the number of features relative to Feature 3 yet maintain high feature quality, one may employ all N elements of the residual vector $\tilde{\mathbf{r}}^n(\boldsymbol{\mu})$ as features. This has the effect of changing the number of features from one extreme to another, as we assume the full-order-model dimension N is large. Employing N features can enable very high-capacity regression models, which can lead to low noise variance given sufficient training data; however, the amount of training data needed to ensure generalizability may be excessive. Further, these features are costly to compute. These features are of high quality, as the residual not only appears in the *a posteriori* error bounds (14)–(15), but it also appears in the dual-weighted residual discussed in Section 2.3.2. Namely, inserting Eq. (25) into Eq. (19) shows that the QoI error can be approximated to first order by a linear combination of space–time residual elements.

Feature 5 Residual principal components $\hat{\mathbf{r}}^n(\boldsymbol{\mu})$. As proposed in Ref. [15], to retain the high quality of Feature 4, but reduce the number of features such that less training data is needed for generalization, we can employ *principal components* of the residual as features. In particular, one can use

$$\hat{\mathbf{r}}^n(\boldsymbol{\mu}) := \boldsymbol{\Phi}_{\mathbf{r}}^T(\tilde{\mathbf{r}}^n(\boldsymbol{\mu}) - \bar{\tilde{\mathbf{r}}})$$

as features, where the columns of $\boldsymbol{\Phi}_{\mathbf{r}} \in \mathbb{R}_*^{N \times n_r}$ comprise the first $n_r (\ll N)$ principal components of the training set $\mathcal{T}_{\mathbf{r}, \text{train}} \subset \mathbb{R}^N$ (which will be described in Section 3.1.3), and $\bar{\tilde{\mathbf{r}}} := \frac{1}{|\mathcal{T}_{\mathbf{r}, \text{train}}|} \sum_{\tilde{\mathbf{r}} \in \mathcal{T}_{\mathbf{r}, \text{train}}} \tilde{\mathbf{r}}$ denotes the training-set mean. These features are costly to compute, as they require computing all N elements of the residual $\tilde{\mathbf{r}}^n(\boldsymbol{\mu})$ before applying projection with the principal-component matrix $\boldsymbol{\Phi}_{\mathbf{r}}$. However, these features retain the high quality of the residual vector if the truncation level n_r is set such that the principal components explain most of the variance of the data in the training set $\mathcal{T}_{\mathbf{r}, \text{train}}$. Critically, this approach associates with using n_r features and thus constitutes a compromise between Feature 3 and Feature 4: it will lead to a higher-capacity model than can be obtained using Feature 3, but will likely generalize with significantly less training data than would be the case with Feature 4.

Feature 6 Residual gappy principal components: This approach aims to address the primary shortcoming of Feature 5: the high computational cost incurred by the need to compute all N elements of the residual $\tilde{\mathbf{r}}^n(\boldsymbol{\mu})$. In particular, this feature choice aims to approximate the residual principal components using the gappy POD method [14], which replaces orthogonal projection with a sampling-based linear least-squares approximation to realize computational-cost savings. Specifically, introducing a sampling matrix $\mathbf{P} \in \{0, 1\}^{n_s \times N}$ comprising n_s selected rows of the identity matrix (with $n_r \leq n_s \ll N$), the residual gappy principal components are

$$\hat{\mathbf{r}}_g^n(\boldsymbol{\mu}) := [\mathbf{P}\Phi_r]^+ \mathbf{P}(\tilde{\mathbf{r}}^n(\boldsymbol{\mu}) - \bar{\tilde{\mathbf{r}}}).$$

In this work, we construct the sampling matrix \mathbf{P} according to the q-sampling method [11]; Appendix B presents the associated algorithm. We note that the number of features for this method is the same as that for Feature 5, and the feature quality is similar to that of Feature 5 if least-squares reconstruction yields similar results to orthogonal projection. However, computing these features requires computing only $n_s (\ll N)$ elements of the residual vector $\tilde{\mathbf{r}}^n(\boldsymbol{\mu})$; thus, this feature choice is substantially less costly to compute than Feature 5.

Feature 7 Sampled residual: Feature 6 constitutes an affine transformation applied to the sampled residual $\mathbf{P}\tilde{\mathbf{r}}^n(\boldsymbol{\mu})$. Thus, it is sensible to consider employing only the underlying sampled residual $\mathbf{P}\tilde{\mathbf{r}}^n(\boldsymbol{\mu})$ as features, given that many regression techniques are likely to discover this affine transformation if it yields superior prediction performance. Further, employing the sampled residual does not require computing the residual principal components Φ_r (although q-sampling employs this matrix to construct the sampling matrix \mathbf{P}). We note that the number of features in this case is $n_s (\geq n_r)$.

In the numerical experiments, we consider feature-engineering methods that employ different combinations of the above features. However, all considered methods use at most one of the residual-based features, i.e., at most one of Feature 3–Feature 7. Table 1 summarizes the feature-engineering methods considered in the numerical experiments.

3.1.2. Data generation

We now describe Step 2 of the proposed framework: data generation. After selecting the features, the method generates response–feature pairs that comprise the training, validation, and test sets used to select the deterministic regression-function model and stochastic noise model, respectively. Specifically, we first define

$$\mathcal{T}(\overline{\mathcal{D}}, \overline{\mathbb{T}}) := \{(\delta^n(\boldsymbol{\mu}), \boldsymbol{\rho}^n(\boldsymbol{\mu})) \mid \boldsymbol{\mu} \in \overline{\mathcal{D}}, n \in \overline{\mathbb{T}}\}$$

as the set of response–feature pairs generated by computing the full-order and approximate states for $\boldsymbol{\mu} \in \overline{\mathcal{D}}$ and computing the features and errors at time instances t^n with $n \in \overline{\mathbb{T}} \subseteq \{1, \dots, N_t\}$. We then define the training, validation, and test data as

$$\mathcal{T}_{\text{train}} := \mathcal{T}(\mathcal{D}_{\text{train}}, \mathbb{T}_{\text{train}}), \quad \mathcal{T}_{\text{val}} := \mathcal{T}(\mathcal{D}_{\text{val}}, \mathbb{T}_{\text{val}}), \quad \mathcal{T}_{\text{test}} := \mathcal{T}(\mathcal{D}_{\text{test}}, \mathbb{T}_{\text{test}}), \quad (30)$$

respectively, where $\mathcal{D}_{\text{train}}, \mathcal{D}_{\text{val}}, \mathcal{D}_{\text{test}} \subset \mathcal{D}$; and $\mathbb{T}_{\text{train}} := \{\tau(1), \dots, \tau(|\mathbb{T}_{\text{train}}|)\} \subseteq \mathbb{T}$, $\mathbb{T}_{\text{val}} := \{\tau(1), \dots, \tau(|\mathbb{T}_{\text{val}}|)\} \subseteq \mathbb{T}$, and $\mathbb{T}_{\text{test}} := \{\tau(1), \dots, \tau(|\mathbb{T}_{\text{test}}|)\} \subseteq \mathbb{T}$. For example, $\mathcal{D}_{\text{train}}, \mathcal{D}_{\text{val}}$, and $\mathcal{D}_{\text{test}}$ can be generated by drawing samples from a probability distribution defined on the parameter domain \mathcal{D} , and the time indices can be set to $\mathbb{T}_{\text{train}} = \mathbb{T}_{\text{val}} = \mathbb{T}_{\text{test}} = \mathbb{T}$ (which we do in the numerical experiments).

3.1.3. Training data for principal component analysis and q-sampling

Feature 5 and Feature 6 require computing principal components of the residual; Feature 6 and Feature 7 require constructing the sampling matrix \mathbf{P} , which we do via q-sampling [11] (which in turn requires residual principal components). In these cases, computing residual principal components requires the additional training set

$$\mathcal{T}_{r,\text{train}} := \{\tilde{\mathbf{r}}^n(\boldsymbol{\mu}) \mid \boldsymbol{\mu} \in \mathcal{D}_{\text{train}}, n \in \mathbb{T}_{\text{train}}\}. \quad (31)$$

Because principal component analysis is an unsupervised machine learning method, it does not require validation or test sets.

Description	Features $\boldsymbol{\rho}^n$	Number of features N_ρ	Number of residual elements required
Parameters	$\boldsymbol{\mu}$	N_μ	0
Parameters and time	$[\boldsymbol{\mu}; t^n]$	$N_\mu + 1$	0
Residual norm	$\ \tilde{\mathbf{r}}^n(\boldsymbol{\mu})\ _2$	1	N
Parameters and residual norm	$[\boldsymbol{\mu}; \ \tilde{\mathbf{r}}^n(\boldsymbol{\mu})\ _2]$	$N_\mu + 1$	N
Parameters, residual norm, and time	$[\boldsymbol{\mu}; \ \tilde{\mathbf{r}}^n(\boldsymbol{\mu})\ _2; t^n]$	$N_\mu + 2$	N
Parameters and residual	$[\boldsymbol{\mu}; \tilde{\mathbf{r}}^n(\boldsymbol{\mu})]$	$N_\mu + N$	N
Parameters, residual, and time	$[\boldsymbol{\mu}; \tilde{\mathbf{r}}^n(\boldsymbol{\mu}); t^n]$	$N_\mu + N + 1$	N
Parameters and residual principal components	$[\boldsymbol{\mu}; \hat{\mathbf{r}}^n(\boldsymbol{\mu})]$	$N_\mu + n_r$	N
Parameters, residual principal components, and time	$[\boldsymbol{\mu}; \hat{\mathbf{r}}^n(\boldsymbol{\mu}); t^n]$	$N_\mu + n_r + 1$	N
Parameters and gappy residual principal components	$[\boldsymbol{\mu}; \hat{\mathbf{r}}_g^n(\boldsymbol{\mu})]$	$N_\mu + n_r$	n_s
Parameters, gappy residual principal components, and time	$[\boldsymbol{\mu}; \hat{\mathbf{r}}_g^n(\boldsymbol{\mu}); t^n]$	$N_\mu + n_r + 1$	n_s
Parameters and sampled residual	$[\boldsymbol{\mu}; \mathbf{P}\tilde{\mathbf{r}}^n(\boldsymbol{\mu})]$	$N_\mu + n_s$	n_s
Parameters, sampled residual, and time	$[\boldsymbol{\mu}; \mathbf{P}\tilde{\mathbf{r}}^n(\boldsymbol{\mu}); t^n]$	$N_\mu + n_s + 1$	n_s

Table 1: Summary of considered feature-engineering methods.

Description	Description	Classification	Latent dynamics	Latent dimension N_h
k -nearest neighbors	kNN	Category 1	None	N/A
Artificial neural network	ANN	Category 1	None	N/A
Autoregressive w/ exogenous inputs	ARX	Category 2	Linear	1
Integrated artificial neural network	ANN-I	Category 2	Linear	1
Latent autoregressive w/ exogenous inputs	LARX	Category 3	Linear	Arbitrary
Recurrent neural network	RNN	Category 3	Nonlinear	Arbitrary
Long short-term memory network	LSTM	Category 3	Nonlinear	Arbitrary

Table 2: Summary of considered regression methods.

3.1.4. Regression function

We now describe Step 3 of the proposed framework: training the deterministic regression-function model $\hat{\delta}_f^n(\boldsymbol{\mu})$ of the form (27)–(28). In particular, this step constructs the mappings \hat{f} and \mathbf{g} . To achieve this, we consider a variety of both recursive and non-recursive regression methods from classical time-series analysis and supervised machine learning. In particular, we consider three categories of regression methods:

Category 1 Non-recursive. Non-recursive regression methods do not include latent variables or latent-variable dynamics. In this case, the latent variables can be omitted from the regression function arguments, i.e., $\hat{f}(\boldsymbol{\rho}, \mathbf{h}) \equiv \hat{f}(\boldsymbol{\rho})$, and the mapping \mathbf{g} is not employed.

Category 2 Recursive with latent state equal to previous prediction. This category of methods employs latent variables, but sets them equal to the predicted response at the previous time instance, i.e., $\mathbf{h}^{\tau(n)} = \hat{\delta}_f^{\tau(n-1)}$, $n = 1, \dots, \bar{N}_t$. This is equivalent to prescribing the recursion function as simply

$$\mathbf{g} : (\boldsymbol{\rho}, \mathbf{h}, \hat{\delta}_f) \mapsto \hat{\delta}_f. \quad (32)$$

These methods place no particular restriction on the mapping \hat{f} .

Category 3 Recursive. This category of methods follows the general framework outlined in Section 3.1 with no particular restrictions on the forms of the mappings \hat{f} or \mathbf{g} .

Table 2 summarizes the considered methods and their associated categories.

- **k -nearest neighbors (kNN)** (Category 1): kNN is a simple regression method wherein the prediction comprises a weighted average of the nearest neighbors in feature space such that

$$\hat{f} : \boldsymbol{\rho} \mapsto \frac{1}{k} \sum_{(\bar{\delta}, \bar{\rho}) \in \mathcal{T}_{\text{kNN}}(\boldsymbol{\rho})} w(\boldsymbol{\rho}, \bar{\rho}) \bar{\delta} \quad (33)$$

where $\mathcal{T}_{\text{kNN}}(\boldsymbol{\rho}) \subseteq \mathcal{T}_{\text{train}}$ with $|\mathcal{T}_{\text{kNN}}(\boldsymbol{\rho})| = k$ denotes the k response–feature pairs of the training set $\mathcal{T}_{\text{train}}$ whose features are closest to the vector $\boldsymbol{\rho}$ in feature space. Common choices for the weights are uniform weights, $w : (\boldsymbol{\rho}, \bar{\rho}) \mapsto 1/k$ and weights based on Euclidean distance, i.e.,

$$w : (\boldsymbol{\rho}, \bar{\rho}) \mapsto \frac{(\sum_{(\bar{\delta}, \bar{\rho}) \in \mathcal{T}_{\text{kNN}}(\boldsymbol{\rho})} \|\boldsymbol{\rho} - \bar{\rho}\|_2^{-1})^{-1}}{\|\boldsymbol{\rho} - \bar{\rho}\|_2}. \quad (34)$$

The hyperparameters associated with this method correspond to the number of neighbors k , and the definition of the weights w . We note that all parameters characterizing this model are hyperparameters; there are no parameters that are subject to training via optimization.

- **Artificial neural network (ANN)** (Category 1): Feed-forward ANNs (i.e., multilayer perceptrons) employ function composition to create nonlinear input–output maps. In the context of error modeling, Ref. [15] observed ANNs to yield the best performance for static systems. In the present context, feed-forward ANNs can be used to construct the (parameterized) non-recursive regression function that satisfies $\hat{f}(\boldsymbol{\rho}, \mathbf{h}) \equiv \hat{f}(\boldsymbol{\rho})$ and is given by

$$\hat{f} : (\boldsymbol{\rho}; \boldsymbol{\theta}_f) \mapsto \mathbf{z}_d(\cdot, \boldsymbol{\theta}_d) \circ \cdots \circ \mathbf{z}_1(\boldsymbol{\rho}; \boldsymbol{\theta}_1),$$

where $\boldsymbol{\theta}_f \equiv (\boldsymbol{\theta}_1, \dots, \boldsymbol{\theta}_d)$ with $\boldsymbol{\theta}_i \equiv (\mathbf{W}_i, \mathbf{b}_i) \in \mathbb{R}^{p_i \times p_{i-1}} \times \mathbb{R}^{p_i}$, $i = 1, \dots, d$ denotes neural-network weights and biases; $\mathbf{z}_i(\cdot; \boldsymbol{\theta}_i) : \mathbb{R}^{p_{i-1}} \rightarrow \mathbb{R}^{p_i}$, $i = 1, \dots, d$ denotes the activation function employed at the i th layer; d denotes the depth of the network; and p_i , $i = 0, \dots, d$ (with $p_0 = N_\rho$ and $p_d = 1$) denotes the number of neurons at layer i . The activation function takes the form

$$\mathbf{z}_i : (\mathbf{w}; \boldsymbol{\theta}_i) \mapsto \boldsymbol{\zeta}_i(\mathbf{W}_i \mathbf{w} + \mathbf{b}_i), \quad i = 1, \dots, d,$$

where $\boldsymbol{\zeta}_i : \mathbb{R}^{p_i} \rightarrow \mathbb{R}^{p_i}$, $i = 1, \dots, d$ denote activations (e.g., rectified linear unit (ReLU), hyperbolic tangent) applied elementwise.

In this work, we consider only fully connected feed-forward ANNs with ReLU activation functions. As such, we consider the number of layers d and the number of neurons at each layer p_i , $i = 1, \dots, d - 1$ to be hyperparameters.

- **Autoregressive with exogenous inputs (ARX)** (Category 2): Autoregressive methods are linear models that have been widely adopted for time-series analysis. The ARX model is an extension of the autoregressive (AR) model that allows for exogenous inputs, which we treat as the features. ARX(p, r) methods regress the response at given time index as a linear combination of the value of the response at the previous p time instances and the exogenous inputs at both the current time instance and the previous $r - 1$ time instances. This work considers the ARX(1, 1) model, in which case the (parameterized) regression function is given by

$$\hat{f} : (\boldsymbol{\rho}, \mathbf{h}; \boldsymbol{\theta}_f) \mapsto \boldsymbol{\theta}_1^T \boldsymbol{\rho} + \theta_2 \mathbf{h} + b, \quad (35)$$

where $\boldsymbol{\theta}_f \equiv (\boldsymbol{\theta}_1, \theta_2, b) \in \mathbb{R}^{N_\rho} \times \mathbb{R} \times \mathbb{R}$ denote the regression-function weights and bias, and the latent variable (of dimension $N_{\mathbf{h}} = 1$) corresponds to the predicted response at the previous time instance such that $\mathbf{h}^{\tau(n)} = \hat{\delta}_f^{\tau(n-1)}$, $n = 1, \dots, \bar{N}_t$ and the latent-variables dynamics are prescribed via (32).

We remark that classical autoregressive models typically include the noise term directly within the recursion, i.e., the latent variables $\mathbf{h}^{\tau(n)}$ correspond to the regression-function prediction perturbed by stochastic noise. As a result, generating statistical predictions requires simulating an ensemble of model realizations. To avoid this complication, this work constructs the stochastic noise model *separately* from the deterministic regression-function model; for the stochastic noise models considered in this work, the statistical distribution of the response is given analytically. Sections 3.1.6–3.1.7 describe this step. We also note that it is possible to construct higher-order autoregressive models (i.e., AR(p, q) with $p > 1$ and/or $q > 1$) that include additional lagged states. While we do not consider such approaches in this work, the ARX formulation presented above could be modified to address this case by changing the definition of the latent variables and recursion function.

- **Integrated artificial neural network (ANN-I)** (Category 2): To facilitate time-series modeling, it is common to apply transformations to the training data in order to make the associated processes weakly stationary. The most commonly adopted transformation is time differencing. This process leads to *integrated* methods. Here, we investigate the use of an “integrated” artificial neural network

(ANN-I) model, wherein a neural network is used to predict the time-differenced error. This leads to a modification of the ANN model wherein the (parameterized) recursive regression function takes the form

$$\hat{f} : (\boldsymbol{\rho}, \mathbf{h}; \boldsymbol{\theta}_f) \mapsto \mathbf{h} + \mathbf{z}_d(\cdot, \boldsymbol{\theta}_d) \circ \cdots \circ \mathbf{z}_1(\boldsymbol{\rho}, \boldsymbol{\theta}_1),$$

where the parameters $\boldsymbol{\theta}_f \equiv (\boldsymbol{\theta}_1, \dots, \boldsymbol{\theta}_d)$ and activations \mathbf{z}_i , $i = 1, \dots, d$ are defined as in the ANN model and the latent variable (of dimension $N_{\mathbf{h}} = 1$) corresponds to the predicted response at the previous time instance such that $\mathbf{h}^{\tau(n)} = \hat{\delta}_f^{\tau(n-1)}$, $n = 1, \dots, \bar{N}_t$ and (32) holds. As with ANN, we consider only fully connected feed-forward networks with ReLU activation functions such that the hyperparameters correspond to the number of layers d and the number of neurons at each layer p_i , $i = 1, \dots, d - 1$.

- **Latent autoregressive with exogenous inputs (LARX)** (Category 3): Because ARX falls into Category 2, it employs the predicted response at the previous time instance as the latent variables according to Eq. (32). The LARX method relaxes this assumption and considers higher-dimensional latent variables governed by general linear dynamics. This equips the model with a higher capacity than ARX and thus enables it to capture more complex non-local dependencies. In particular, LARX defines the (parameterized) regression function as a linear mapping from the latent variables to the prediction that satisfies $\hat{f}(\boldsymbol{\rho}, \mathbf{h}) \equiv \hat{f}(\mathbf{h})$ and is given by

$$\hat{f} : (\mathbf{h}; \boldsymbol{\theta}_f) \mapsto \boldsymbol{\theta}_1^T \mathbf{h} + b$$

where $\boldsymbol{\theta}_f \equiv (\boldsymbol{\theta}_1, b) \in \mathbb{R}^{N_{\mathbf{h}}} \times \mathbb{R}$. The latent-variable recursion operator is linear in its first two arguments such that $\mathbf{g}(\boldsymbol{\rho}, \mathbf{h}, \hat{\delta}_f) \equiv \mathbf{g}(\boldsymbol{\rho}, \mathbf{h})$ with

$$\mathbf{g} : (\boldsymbol{\rho}, \mathbf{h}; \boldsymbol{\theta}_g) \mapsto \boldsymbol{\Theta}_{\boldsymbol{\rho}} \boldsymbol{\rho} + \boldsymbol{\Theta}_{\mathbf{h}} \mathbf{h} + b_{\mathbf{h}},$$

where $\boldsymbol{\theta}_g \equiv (\boldsymbol{\Theta}_{\boldsymbol{\rho}}, \boldsymbol{\Theta}_{\mathbf{h}}, b_{\mathbf{h}}) \in \mathbb{R}^{N_{\mathbf{h}} \times N_{\boldsymbol{\rho}}} \times \mathbb{R}^{N_{\mathbf{h}} \times N_{\mathbf{h}}} \times \mathbb{R}^{N_{\mathbf{h}}}$.

LARX is characterized by one hyperparameter: the number of latent variables $N_{\mathbf{h}}$.

- **Recurrent neural network (RNN)** (Category 3): RNNs [42] comprise a particular neural-network architecture that have been widely adopted for modeling time sequences. The main idea of an RNN is to employ the same feed-forward neural network for prediction at each point in a sequence, but to treat the hidden layer of the neural network as inputs to the neural network at the next point in the sequence; these hidden layers associate with the latent variables. RNNs comprise a generalization of LARX models: LARX methods develop a linear recursion for the latent-variable dynamics, while RNNs enable nonlinear latent-variable dynamics. Figure 2 illustrates the computational graph for an “unrolled” RNN. An RNN of depth d employs latent variables $\mathbf{h} \equiv (\mathbf{h}_1, \dots, \mathbf{h}_d)$, with $\mathbf{h}_i \in \mathbb{R}^{p_i}$, $i = 1, \dots, d$ and $N_{\mathbf{h}} = \sum_{i=1}^d p_i$. For RNNs, the deterministic regression-function model is given by an output activation function acting on the latent variables at the final layer; it satisfies $\hat{f}(\boldsymbol{\rho}, \mathbf{h}) \equiv \hat{f}(\mathbf{h})$ and is given by

$$\hat{f} : (\mathbf{h}; \boldsymbol{\theta}_f) \mapsto \zeta(\mathbf{w}_f^T \mathbf{h}_d + b_f) \quad (36)$$

where $\boldsymbol{\theta}_f \equiv (\mathbf{w}_f, b_f) \in \mathbb{R}^{p_d} \times \mathbb{R}$ and $\zeta(\cdot)$ is typically the identity operator.

The latent variables satisfy the recursive relationships

$$\mathbf{h}_i^{\tau(n)} = \mathbf{r}_i(\mathbf{h}_{i-1}^{\tau(n)}, \mathbf{h}_i^{\tau(n-1)}; \boldsymbol{\theta}_i), \quad i = 1, \dots, d, \quad n = 1, \dots, \bar{N}_t, \quad (37)$$

where $\mathbf{r}_i(\cdot, \cdot, \boldsymbol{\theta}_i) : \mathbb{R}^{p_{i-1}} \times \mathbb{R}^{p_i} \rightarrow \mathbb{R}^{p_i}$, $i = 1, \dots, d$ denote activation functions and the latent state at layer zero is defined from the input features such that $\mathbf{h}_0^{\tau(n)} = \mathbf{h}_0(\boldsymbol{\rho}^{\tau(n)})$ with $\mathbf{h}_0 : \mathbb{R}^{N_{\boldsymbol{\rho}}} \rightarrow \mathbb{R}^{p_0}$. These recursive relationships can be expressed by a latent-variable recursion operator, which satisfies

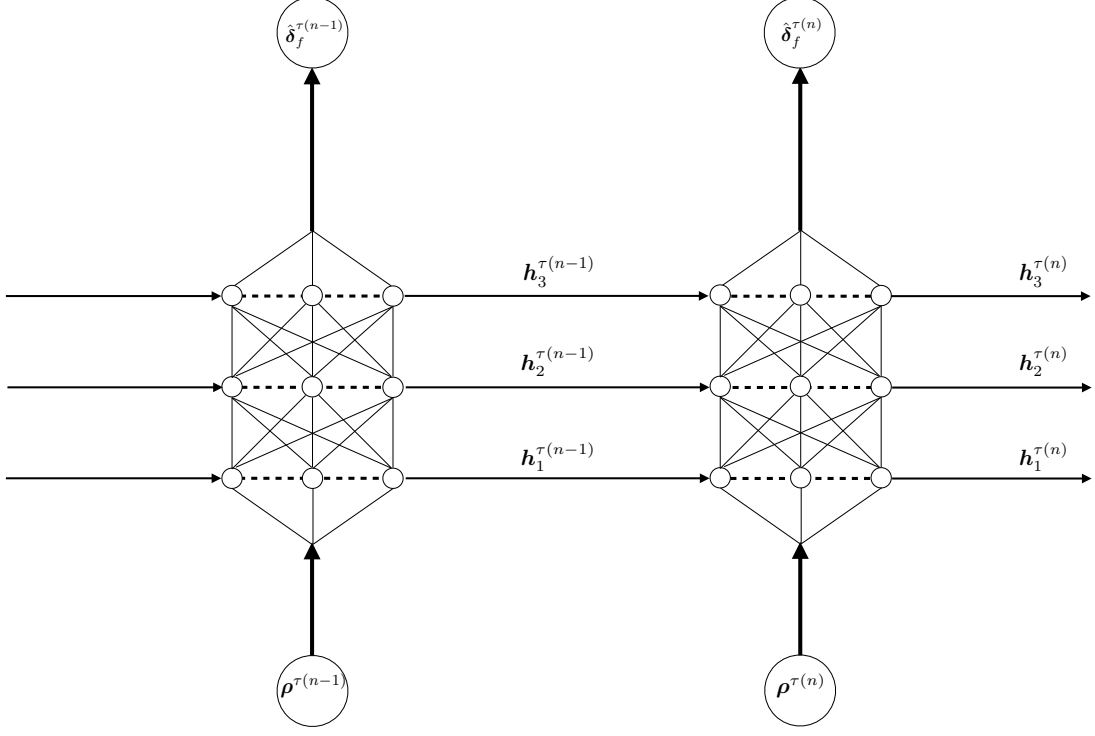


Figure 2: Diagram of an “unrolled” recurrent neural network with depth $d = 3$.

$\mathbf{g}(\boldsymbol{\rho}, \mathbf{h}, \hat{\delta}_f) \equiv \mathbf{g}(\boldsymbol{\rho}, \mathbf{h})$ and is given by

$$\mathbf{g} : (\boldsymbol{\rho}, \mathbf{h}; \boldsymbol{\theta}_{\mathbf{g}}) \mapsto \begin{bmatrix} r_1(\mathbf{h}_0(\boldsymbol{\rho}), \mathbf{h}_1; \boldsymbol{\theta}_1) \\ r_2(\cdot, \mathbf{h}_2; \boldsymbol{\theta}_2) \circ r_1(\mathbf{h}_0(\boldsymbol{\rho}), \mathbf{h}_1; \boldsymbol{\theta}_1) \\ \vdots \\ r_d(\cdot, \mathbf{h}_d; \boldsymbol{\theta}_d) \circ \cdots \circ r_1(\mathbf{h}_0(\boldsymbol{\rho}), \mathbf{h}_1; \boldsymbol{\theta}_1) \end{bmatrix}, \quad (38)$$

where $\boldsymbol{\theta}_{\mathbf{g}} \equiv (\boldsymbol{\theta}_1, \dots, \boldsymbol{\theta}_d)$.

For standard RNNs, the function applied at the i th layer takes the form

$$\mathbf{r}_i : (\mathbf{h}_{i-1}, \mathbf{h}_i; \boldsymbol{\theta}_i) \mapsto \zeta_i(\mathbf{W}_{i,1}\mathbf{h}_{i-1} + \mathbf{W}_{i,2}\mathbf{h}_i + \mathbf{b}_i), \quad (39)$$

where $\boldsymbol{\theta}_i \equiv (\mathbf{W}_{i,1}, \mathbf{W}_{i,2}, \mathbf{b}_i) \in \mathbb{R}^{p_i \times p_{i-1}} \times \mathbb{R}^{p_i \times p_i} \times \mathbb{R}^{p_i}$, $i = 1, \dots, d$ denote the recursive weights and biases, $\zeta_i : \mathbb{R}^{p_i} \rightarrow \mathbb{R}^{p_i}$, $i = 1, \dots, d$ again denote activations (e.g., ReLU) applied elementwise, and \mathbf{h}_0 is the identity operator such that $\mathbf{h}_0^{\tau(n)} = \boldsymbol{\rho}^{\tau(n)}$, $n = 1, \dots, \bar{N}_t$ and $p_0 = N_p$.

Different RNN architectures can be obtained, for example, by modifying the activation functions, the number of latent variables, or the network depth. The LARX method can be recovered from RNN by setting the depth $d = 1$ and setting $\zeta(\cdot)$ and $\zeta_1(\cdot)$ to be the identity mappings. We consider hyperparameters corresponding to the number of neurons at each layer and the depth of the network.

- **Long short-term memory network (LSTM)** (Category 3): The LSTM network [20] is a particular type of RNN designed to capture dependencies on long-term non-local quantities. Figure 3 provides a diagram of an “unrolled” LSTM. LSTMs are able to capture long-term non-local dependencies through

the use of two latent variables: the *hidden state* and the *cell state*. The cell state, which is depicted as the topmost horizontal line running through the cells in Figure 3, undergoes only minor interactions [32]: elementwise multiplication and elementwise addition. Due to the minor changes experienced by the cell state, it can (in principle) more easily capture long-term dependencies. The LSTM architecture is arguably the most widely adopted RNN architecture as of this writing.

Formally, an LSTM decomposes latent variables at the i th layer as $\mathbf{h}_i \equiv (\tilde{\mathbf{h}}_i, \mathbf{c}_i)$, where $\tilde{\mathbf{h}}_i \in \mathbb{R}^{p_i/2}$ and $\mathbf{c}_i \in \mathbb{R}^{p_i/2}$ denote the hidden state and cell state, respectively. The deterministic regression function for LSTMs is defined as in (36), but with elements $p_i/2 + 1$ to p_i of the weighting vector \mathbf{w}_f set to zero so that the output depends only on $\tilde{\mathbf{h}}_d$.

The latent-variable recursion is also defined as in (37)–(38); however, the activations take a special form based on the LSTM “cell”. In particular, the LSTM cell corresponds to defining the i th layer’s function as

$$\mathbf{r}_i : (\mathbf{h}_{i-1}, \mathbf{h}_i; \boldsymbol{\theta}_i) \mapsto \begin{bmatrix} \mathbf{r}_{\sigma,i}(\tilde{\mathbf{h}}_{i-1}, \tilde{\mathbf{h}}_i; \boldsymbol{\theta}_{i,1}) \odot \tanh(\mathbf{r}_{\text{cell},i}(\tilde{\mathbf{h}}_{i-1}, \mathbf{h}_i; \boldsymbol{\theta}_i)) \\ \mathbf{r}_{\text{cell},i}(\tilde{\mathbf{h}}_{i-1}, \mathbf{h}_i; \boldsymbol{\theta}_i) \end{bmatrix}, \quad (40)$$

where $\mathbf{h}_i \equiv (\tilde{\mathbf{h}}_i, \mathbf{c}_i)$, $\boldsymbol{\theta}_i \equiv (\boldsymbol{\theta}_{i,1}, \dots, \boldsymbol{\theta}_{i,4})$, and \odot denotes the elementwise (Hadamard) product, and

$$\mathbf{r}_{\text{cell},i} : (\tilde{\mathbf{h}}_{i-1}, \mathbf{h}_i; \boldsymbol{\theta}_i) \mapsto \mathbf{r}_{\sigma,i}(\tilde{\mathbf{h}}_{i-1}, \tilde{\mathbf{h}}_i; \boldsymbol{\theta}_{i,2}) \odot \mathbf{c}_i + \mathbf{r}_{\sigma,i}(\tilde{\mathbf{h}}_{i-1}, \tilde{\mathbf{h}}_i; \boldsymbol{\theta}_{i,3}) \odot \mathbf{r}_{\tanh,i}(\tilde{\mathbf{h}}_{i-1}, \tilde{\mathbf{h}}_i; \boldsymbol{\theta}_{i,4})$$

denotes the cell activation. Here,

$$\begin{aligned} \mathbf{r}_{\sigma,i} : (\tilde{\mathbf{h}}_{i-1}, \tilde{\mathbf{h}}_i; \boldsymbol{\theta}_{i,j}) &\mapsto \sigma(\mathbf{W}_{i,j,1}\tilde{\mathbf{h}}_{i-1} + \mathbf{W}_{i,j,2}\tilde{\mathbf{h}}_i + \mathbf{b}_{i,j}), \quad j = 1, \dots, 3 \\ \mathbf{r}_{\tanh,i} : (\tilde{\mathbf{h}}_{i-1}, \tilde{\mathbf{h}}_i; \boldsymbol{\theta}_{i,4}) &\mapsto \tanh(\mathbf{W}_{i,4,1}\tilde{\mathbf{h}}_{i-1} + \mathbf{W}_{i,4,2}\tilde{\mathbf{h}}_i + \mathbf{b}_{i,4}), \end{aligned}$$

where $\boldsymbol{\theta}_{i,j} \equiv (\mathbf{W}_{i,j,1}, \mathbf{W}_{i,j,2}, \mathbf{b}_{i,j}) \in \mathbb{R}^{p_i/2 \times p_{i-1}/2} \times \mathbb{R}^{p_i/2 \times p_i/2} \times \mathbb{R}^{p_i/2}$, $i = 1, \dots, d$, $j = 1, \dots, 4$ denote the sigmoid and hyperbolic tangent operators, respectively. For LSTM, the latent state at layer zero is defined via $\mathbf{h}_0 : \boldsymbol{\rho} \mapsto [\boldsymbol{\rho}^T \mathbf{0}^T]^T$ such that $\tilde{\mathbf{h}}_0^{\tau(n)} = \boldsymbol{\rho}^{\tau(n)}$, $n = 1, \dots, \bar{N}_t$ and $p_0 = 2N_\rho$.

Different types of LSTM networks can be constructed, e.g., by modifying the definition of the LSTM cell. For instance, the “peephole” LSTM network can be obtained by replacing the hyperbolic tangent function in Eq. (40) with the identity function. We consider hyperparameters corresponding to the number of neurons p_i , $i = 1, \dots, d$ and the network depth d .

To summarize, this section outlined a variety of non-recursive and recursive regression-function models. This exposition started with a description of the kNN and ANN regression-function models. These regression-function models are non-recurrent and employ no latent variables; non-local effects cannot be captured with kNN and ANN. To capture non-local effects, we introduced the ARX and ANN-I regression-function models. Both of these models employ a single latent variable corresponding to the prediction at the previous time instance; both methods are thus characterized by linear latent dynamics with a latent dimension of $N_{\mathbf{h}} = 1$. To increase the capacity of the latent-dynamics recursion, we introduced the LARX regression-function model. Unlike ARX and ANN-I, LARX employs an arbitrary number of latent variables governed by general linear dynamics. Finally, to further increase the capacity of the latent dynamics recursion, we introduced the RNN and LSTM regression-function models. These methods comprise an extension of LARX as, in addition to supporting an arbitrary number of latent variables, they allow for nonlinear latent-variable dynamics. The regression-function models described in this section are thus characterized by the following hierarchy of models with increasing capacity: no latent variables (kNN, ANN), one latent variable with linear latent-variable dynamics (ARX, ANN-I), an arbitrary number of latent variables with linear latent-variable dynamics (LARX), and an arbitrary number of latent variables with nonlinear latent-variable dynamics (RNN, LSTM).

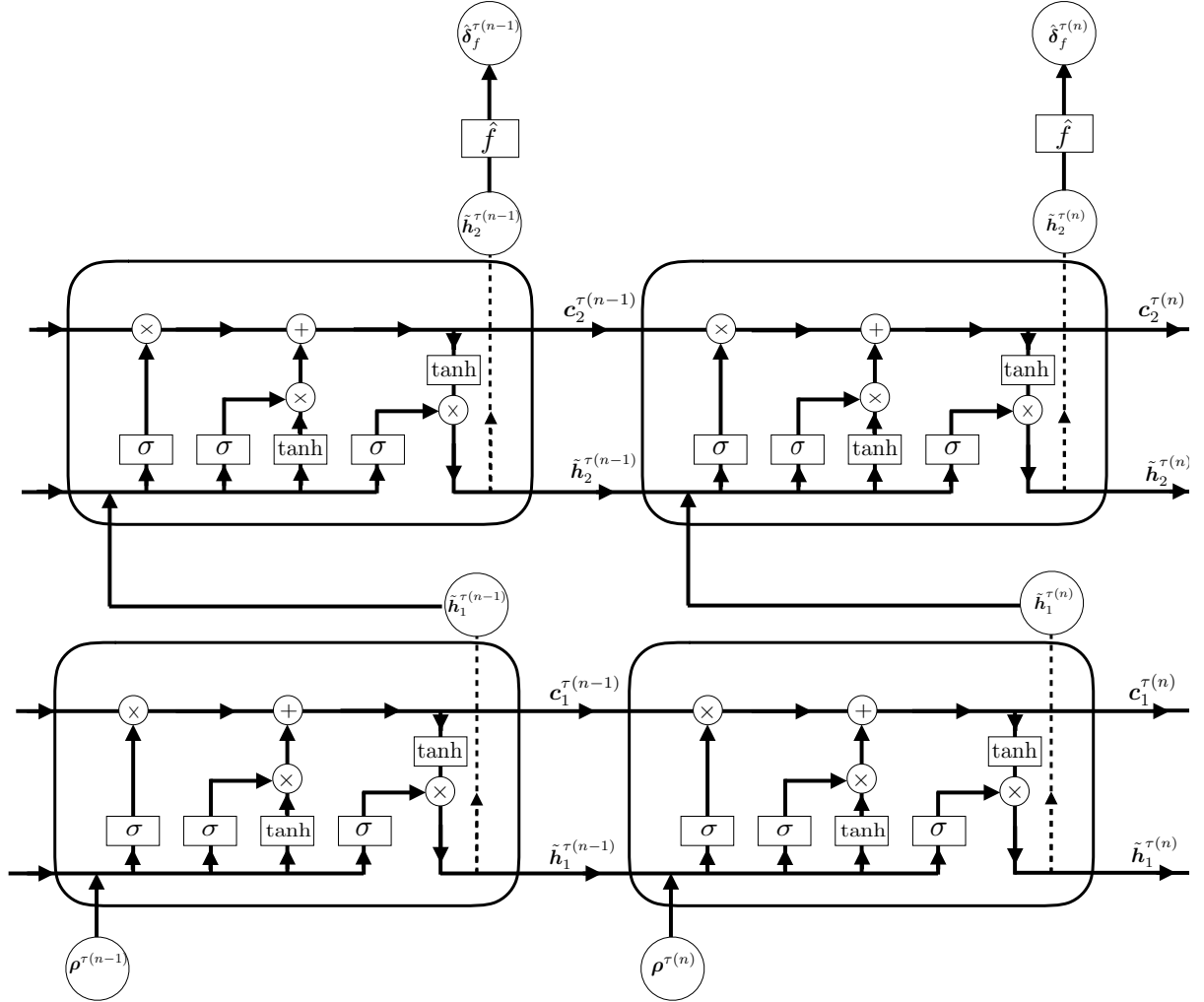


Figure 3: Diagram for a deterministic regression-function model utilizing the LSTM architecture with a depth of $d = 2$. Figure concept adopted from Ref. [32].

3.1.5. Regression-function training

To train a regression model, we employ a validation procedure consisting of two loops: the outer loop modifies hyperparameters characterizing the model, while the inner loop computes optimal model parameters θ_f^* and θ_g^* via optimization executing on the training set $\mathcal{T}_{\text{train}}$ given fixed hyperparameter values. The final model is chosen based on hyperparameter values that yield the smallest MSE on the validation set \mathcal{T}_{val} . In the case of limited data, this process can be replaced by executing cross-validation within the training set $\mathcal{T}_{\text{train}}$; this obviates the need for an independent validation set \mathcal{T}_{val} .

The inner-loop optimization problem depends on the category within which the regression model falls.¹

1. For regression models in Category 1, we compute optimal model parameters θ_f^* as the solution to the minimization problem

$$\underset{\theta_f}{\text{minimize}} \sum_{\mu \in \mathcal{D}_{\text{train}}} \sum_{n \in \mathbb{T}_{\text{train}}} \left\| \delta^n(\mu) - \hat{f}(\rho^n(\mu); \theta_f) \right\|_2^2 + \kappa_f(\theta_f), \quad (41)$$

where $\kappa_f(\cdot) \in \mathbb{R}_+$ is a regularization operator, e.g., LASSO, ridge, elastic-net. We note that optimization problem (41) is nonrecursive, as the prediction at one time instance does not affect the objective-function contribution associated with the prediction at the next time instance.

2. For regression models in Category 2, we can train the models in one of two ways. The first approach is non-recursive in nature and computes the optimal model parameters θ_f^* as the solution to the minimization problem

$$\underset{\theta_f}{\text{minimize}} \sum_{\mu \in \mathcal{D}_{\text{train}}} \sum_{n=1}^{|\mathbb{T}_{\text{train}}|} \left\| \delta^{\tau(n)}(\mu) - \hat{f}(\rho^{\tau(n)}(\mu), \delta^{\tau(n-1)}(\mu); \theta_f) \right\|_2^2 + \kappa_f(\theta_f). \quad (42)$$

Because the actual error $\delta^{\tau(n-1)}(\mu)$ from the training data is employed as the second argument in \hat{f} rather than the predicted value $\hat{\delta}_f^{\tau(n-1)}$ (which is the actual value of the hidden state), the optimization problem (42) is non-recursive. We refer to this approach as non-recursive training (NRT).

3. Finally, regression models in either Category 2 and Category 3 can be trained via a dynamics-constrained recursive training strategy. In this approach, the optimal weights θ_f^* and θ_g^* are the solution to the problem

$$\underset{\theta_f, \theta_g}{\text{minimize}} \sum_{\mu \in \mathcal{D}_{\text{train}}} \sum_{n \in \mathbb{T}_{\text{train}}} \left\| \delta^n(\mu) - \hat{f}(\rho^n(\mu), \mathbf{h}^n(\mu); \theta_f) \right\|_2^2 + \kappa_f(\theta_f) + \kappa_g(\theta_g) \quad (43)$$

subject to $\mathbf{h}^{\tau(n)}(\mu) = \mathbf{g}(\rho^{\tau(n)}(\mu), \mathbf{h}^{\tau(n-1)}(\mu), \hat{\delta}_f^{\tau(n-1)}(\mu); \theta_g), \quad \mu \in \mathcal{D}_{\text{train}}, \quad n = 1, \dots, |\mathbb{T}_{\text{train}}|,$

where $\kappa_g(\cdot) \in \mathbb{R}_+$ is a regularization operator and the latent-variable dynamics appear explicitly as constraints. In this approach, the prediction $\hat{\delta}_f^{\tau(n-1)}(\mu)$ *does* affect the contribution to the objective function at time instance $\tau(n)$ and parameters μ through the constraints. Thus, this formulation reflects the recursive nature of the regression model and can enable more accurate long-time predictions at the expense of more computationally expensive training. We refer to this approach as recursive training (RT). We note that the “backpropagation through time” (BPTT) method [31, 40, 17] is a popular approach for solving the minimization problem 43. We additionally note that for models in Category 2, problem (43) can be derived by substituting $\delta^{\tau(n-1)}(\mu) \leftarrow \hat{\delta}_f^{\tau(n-1)}(\mu)$ in problem (42).

¹We note that kNN is characterized by only hyperparameters and thus the inner loop does not require solving an optimization problem.

Description	Noise Distribution	Time-dependent
Stationary Gaussian	Gaussian	No
Stationary Laplacian	Laplacian	No
Autoregressive 1 (AR1)	Gaussian	Yes

Table 3: Summary of considered noise models.

In the outer loop, for each candidate value of the hyperparameters, optimization problem (41), (42), or (43) is solved for parameters θ_f^* and θ_g^* , and the resulting model is evaluated on the validation set \mathcal{T}_{val} . For regression models in Category 1, we evaluate the validation criterion

$$\sum_{\mu \in \mathcal{D}_{\text{val}}} \sum_{n \in \mathbb{T}_{\text{val}}} \left\| \delta^n(\mu) - \hat{f}(\rho^n(\mu); \theta_f^*) \right\|_2^2, \quad (44)$$

while for methods in Category 2 or Category 3, we evaluate the validation criterion

$$\sum_{\mu \in \mathcal{D}_{\text{val}}} \sum_{n \in \mathbb{T}_{\text{val}}} \left\| \delta^n(\mu) - \hat{f}(\rho^n(\mu), h^n(\mu); \theta_f^*) \right\|_2^2, \quad (45)$$

where the dynamics of the latent variables are defined as $h^{\tau(n)}(\mu) = g(\rho^{\tau(n)}(\mu), h^{\tau(n-1)}(\mu), \hat{\delta}_f^{\tau(n-1)}(\mu); \theta_g^*)$, $\mu \in \mathcal{D}_{\text{val}}$, $n = 1, \dots, |\mathbb{T}_{\text{val}}|$. For each regression model, the hyperparameter values yielding the smallest validation-criterion value are selected.

3.1.6. Noise model

We now describe Step 4 of the proposed framework: training the stochastic noise model $\hat{\delta}_\epsilon^n(\mu)$ of the form (29). While complex noise models could be considered in principle, for the sake of simplicity, we consider here only three types of noise models: a homoscedastic Gaussian model, a homoscedastic Laplacian model, and an autoregressive model.

- **Stationary Gaussian homoscedastic noise model:** Arguably, the simplest way to quantify the discrepancy between the error model and the true error is to assume the errors to be uncorrelated, Gaussian, stationary, and homoscedastic. The resulting error model is independent of the prediction at the previous time instance such that $\hat{\epsilon}(\hat{\delta}_\epsilon, \epsilon) \equiv \hat{\epsilon}(\epsilon)$ with

$$\hat{\epsilon} : \epsilon \mapsto \epsilon, \quad (46)$$

and defining $\epsilon^n \in \mathbb{V}$, $n \in \mathbb{T}$ as a sequence of independent and identically distributed mean-zero Gaussian random variables, i.e.,

$$\epsilon^n \sim \mathcal{N}(0, \sigma^2), \quad n \in \mathbb{T}. \quad (47)$$

This model does not have any latent variables and requires estimating only the variance parameter σ^2 .

- **Stationary Laplacian homoscedastic noise model:** This approach is similar to the Gaussian model, but instead models the random variables as Laplacian, i.e., (46) holds with

$$\epsilon^n \sim \mathcal{L}(0, b), \quad n \in \mathbb{T},$$

where $b > 0$ denotes the diversity, which must be estimated. Again, this error model does not require any input features or latent variables.

- **Autoregressive Gaussian homoscedastic discrepancy model:** Finally, we consider an autoregressive noise model, as we expect errors to display time correlations. We refer to this model as AR1. The model is given by

$$\hat{\epsilon} : (\hat{\delta}_\epsilon, \epsilon) \mapsto c\hat{\delta}_\epsilon + \epsilon,$$

where $c \in \mathbb{R}$ is a model constant, and defining $\epsilon^n \in \mathbb{V}$, $n \in \mathbb{T}$ as a sequence of independent and identically distributed mean-zero Gaussian random variables such that (47) holds. This method requires estimating the parameters c and σ^2 . The auto-regressive model produces a series of (correlated) mean-zero Gaussian distributions where the variance at time-instance $\tau(n)$ is defined recursively as

$$\sigma_\epsilon^{\tau(n)} := \sqrt{\sigma^2 + \sum_{i=1}^{n-1} (c\sigma^{\tau(i)})^2}, \quad n = 1, \dots, \bar{N}_t. \quad (48)$$

3.1.7. Noise-model training

The stationary Gaussian, stationary Laplacian, and AR1 noise models require specification of the parameters σ^2 , b , and (c, σ^2) , respectively. We compute these parameters via maximum likelihood estimation (MLE) on a training set $\mathcal{T}_{\text{train},\epsilon} \subseteq \mathcal{T}_{\text{test}}$, and evaluate the performance of the noise model on a test set $\mathcal{T}_{\text{test},\epsilon} \subseteq \mathcal{T}_{\text{test}}$, where $\mathcal{T}_{\text{train},\epsilon} \cap \mathcal{T}_{\text{test},\epsilon} = \emptyset$ and

$$\mathcal{T}_{\text{train},\epsilon} := \mathcal{T}(\mathcal{D}_{\text{train},\epsilon}, \mathbb{T}_{\text{train},\epsilon}), \quad \mathcal{T}_{\text{test},\epsilon} := \mathcal{T}(\mathcal{D}_{\text{test},\epsilon}, \mathbb{T}_{\text{test},\epsilon}). \quad (49)$$

In this work, we employ $\mathcal{D}_{\text{train},\epsilon}, \mathcal{D}_{\text{test},\epsilon} \subseteq \mathcal{D}_{\text{test}}$ with $\mathcal{D}_{\text{train},\epsilon} \cap \mathcal{D}_{\text{test},\epsilon} = \emptyset$ and $\mathcal{D}_{\text{train},\epsilon} \cup \mathcal{D}_{\text{test},\epsilon} = \mathcal{D}_{\text{test}}$ with $\mathbb{T}_{\text{train},\epsilon} = \mathbb{T}_{\text{test},\epsilon} = \mathbb{T}$. For the stationary Gaussian model, the MLE estimate for σ^2 is given by

$$\sigma_{\text{MLE}}^2 = \frac{1}{|\mathcal{T}_{\text{train},\epsilon}|} \sum_{\mu \in \mathcal{D}_{\text{train},\epsilon}} \sum_{n \in \mathbb{T}_{\text{train},\epsilon}} (\delta^n(\mu) - \hat{\delta}_f^n(\mu))^2. \quad (50)$$

For the stationary Laplacian model, the MLE estimate for b is given by

$$b_{\text{MLE}} = \frac{1}{|\mathcal{T}_{\text{train},\epsilon}|} \sum_{\mu \in \mathcal{D}_{\text{train},\epsilon}} \sum_{n \in \mathbb{T}_{\text{train},\epsilon}} |\delta^n(\mu) - \hat{\delta}_f^n(\mu)|. \quad (51)$$

Lastly, for the AR1 model, the MLE estimates for the parameters are given by

$$\begin{aligned} c_{\text{MLE}} &= \frac{\sum_{\mu \in \mathcal{D}_{\text{train},\epsilon}} \sum_{n=1}^{|\mathbb{T}_{\text{train},\epsilon}|} (\delta^{\tau(n-1)}(\mu) - \hat{\delta}_f^{\tau(n-1)}(\mu))(\delta^{\tau(n)}(\mu) - \hat{\delta}_f^{\tau(n)}(\mu))}{\sum_{\mu \in \mathcal{D}_{\text{train},\epsilon}} \sum_{n=1}^{|\mathbb{T}_{\text{train},\epsilon}|} (\delta^{\tau(n-1)}(\mu) - \hat{\delta}_f^{\tau(n-1)}(\mu))^2}, \\ \sigma_{\text{MLE}}^2 &= \frac{1}{|\mathcal{T}_{\text{train},\epsilon}|} \sum_{\mu \in \mathcal{D}_{\text{train},\epsilon}} \sum_{n=1}^{|\mathbb{T}_{\text{train},\epsilon}|} (c_{\text{MLE}} \hat{\delta}_\epsilon^{\tau(n-1)}(\mu) - (\delta^{\tau(n)}(\mu) - \hat{\delta}_f^{\tau(n)}(\mu)))^2. \end{aligned} \quad (52)$$

4. Numerical Experiments

This section investigates the performance of the proposed T-MLEM methods. In particular, we consider all combinations of the 13 feature-engineering methods reported in Table 1 with the 7 deterministic regression function models listed in Table 2. For the regression methods in Category 2 (i.e., ARX and ANN-I), we construct two separate regression-function models: one using non-recursive training (NRT) and one using recursive training (RT) as described in Section 3.1.5. In total, we consider 117 candidate T-MLEM methods. We also compare the performance of the T-MLEM methods with that achieved by time-local Gaussian-process (GP) regression in parameter space [34]; Appendix C describes this method in detail.

We consider three examples. The first two examples employ approximate solutions generated by a ROM constructed via Galerkin projection (as discussed in Section 2.1.3), while the third example considers approximate solutions generated by a coarse-mesh lower-fidelity model (as discussed in Section 2.1.2).

4.1. Implementation and model evaluation details

We now provide details on the implementation of the machine-learning regression methods, training algorithms, hyperparameter grids, and evaluation metrics.

4.1.1. Training and model selection of machine learning algorithms

We implement k -nearest neighbors and GP regression algorithms with Scikit-learn [37], and all other machine-learning regression methods with Keras [10]. We employ the following workflow to train and test all machine-learning regression models:

1. Define the coarse time grid \mathbb{T} on which regression methods will operate.
2. Define the training set $\mathcal{T}_{\text{train}}$, validation set \mathcal{T}_{val} , and test set $\mathcal{T}_{\text{test}}$ according to (30) with $\mathbb{T}_{\text{train}} = \mathbb{T}_{\text{val}} = \mathbb{T}_{\text{test}} = \mathbb{T}$ and $\mathcal{D}_{\text{train}}$, \mathcal{D}_{val} , and $\mathcal{D}_{\text{test}}$ generated by drawing independent samples of the parameters $\boldsymbol{\mu} \sim \mathcal{U}(\mathcal{D})$, where $\mathcal{U}(\cdot)$ denotes the uniform distribution. We ensure that $|\mathcal{T}_{\text{train}}| = 4|\mathcal{T}_{\text{val}}|$ (i.e., we employ an 80/20 split between training and validation).
 - For Feature 5, Feature 6, and Feature 7, additionally extract the residual training set $\mathcal{T}_{\mathbf{r},\text{train}}$ from $\mathcal{D}_{\text{train}}$ and $\mathbb{T}_{\text{train}}$ according to (31).
3. Standardize features and responses according to their respective means and variances on the training set $\mathcal{T}_{\text{train}}$.
4. Define the hyperparameter grid for each considered regression model.
5. For each value of the hyperparameters, train the regression model by solving optimization problem (41), (42), or (43), depending on the category of the method. For the ARX, LARX, ANN, ANN-I, RNN, and LSTM models, we employ the Adam algorithm [26] with early stopping (assessed on a 20% holdout set) for this purpose. For regression methods employing the recursive training (RT) approach, as described in Section 3.1.5, BPTT is used to solve the optimization problem. Within the optimization problems, we employ ridge regularization such that $\kappa_f(\cdot) \equiv \alpha \|\cdot\|_2^2$ and $\kappa_g(\cdot) \equiv \alpha \|\cdot\|_2^2$, where $\alpha \in \mathbb{R}_+$ is a regularization hyperparameter. As the Adam algorithm is stochastic, each model is trained 20 times.
6. For each regression method, select the model—which corresponds to one value of the hyperparameters and one execution of the Adam algorithm—by evaluating validation criterion (44) or (45), depending on the category of the method.
7. Define the noise training set $\mathcal{T}_{\text{train},\epsilon}$ and test set $\mathcal{T}_{\text{test},\epsilon}$ according to (49) with $\mathbb{T}_{\text{train},\epsilon} = \mathbb{T}_{\text{test},\epsilon} = \mathbb{T}$, $\mathcal{D}_{\text{train},\epsilon}$ drawn randomly from $\mathcal{D}_{\text{test}}$, and $\mathcal{D}_{\text{test},\epsilon} = \mathcal{D}_{\text{test}} \setminus \mathcal{D}_{\text{train},\epsilon}$.
8. Train stochastic noise models corresponding to a stationary Gaussian, stationary Laplacian, or AR1 via (50), (51), and (52), respectively.
9. Evaluate the trained noise models using statistical validation criteria (e.g., empirical prediction intervals, Komolgorov–Smirnov test) on the test set $\mathcal{T}_{\text{test},\epsilon}$.

As discussed in Section 3.1.5, the validation procedure described in steps 5–6 could be replaced with a cross-validation process.

4.1.2. Hyperparameter grid and optimization

We now describe the specific hyperparameter grid employed by each considered regression method as defined in step 4.

- **k -nearest neighbors (kNN):** The hyperparameters for kNN correspond to the number of neighbors k , and the definition of the weights w . We employ the hyperparameter grid

$$(k, \text{weighting function}) \in \{1, \dots, 5\} \times \{\text{uniform, Euclidean distance}\}.$$

- **Artificial neural network (ANN):** The hyperparameters for ANN correspond to the network depth d and the number of neurons per layer p , which we set to be constant such that $p_i = p$, $i = 1, \dots, d$. We

also consider the regularization parameter α that appears in ridge regularization terms $\kappa_f(\cdot) \equiv \alpha \|\cdot\|_2^2$ and $\kappa_g(\cdot) \equiv \alpha \|\cdot\|_2^2$ as a hyperparameter. We employ the hyperparameter grid

$$(d, p, \alpha) \in \{1, 2\} \times \{10, 25, 50, 100\} \times \{10^{-i}\}_{i=1}^5.$$

Listing 1 provides the Python code for the Keras implementation of this method.

- **Autoregressive with exogenous inputs (ARX):** Because we consider only ARX(1,1) methods, the only hyperparameter for this technique is the regularization parameter α ; we employ the hyperparameter grid

$$\alpha \in \{10^{-i}\}_{i=1}^5.$$

We construct ARX models using both the NRT and RT approaches (see Section 3.1.5). We refer to the resulting models as ARX (NRT) and ARX (RT). Listing 2 provides the Python code for the Keras implementation of ARX (RT).

- **Integrated artificial neural network (ANN-I):** For ANN-I, we employ the same hyperparameter grid as for ANN. As with ARX, we construct two different ANN-I models: one with NRT and one with RT. We refer to the resulting models as ANN-I (NRT) and ANN-I (RT). Listing 3 provides the Python code for the Keras implementation of ANN-I (RT).
- **Latent autoregressive with exogenous inputs (LARX):** The hyperparameter for LARX is the number of latent variables N_h . We also consider the regularization term α and employ the hyperparameter grid

$$(N_h, \alpha) \in \{10, 25, 50, 100\} \times \{10^{-i}\}_{i=1}^5.$$

Listing 4 provides the Python code for the Keras implementation of LARX.

- **Recurrent Neural Network (RNN):** For RNN, we employ the same hyperparameter grid as for ANN. Listing 5 reports the Python code used to develop the RNNs used in this work; we employ Keras' `SimpleRNN` cell.
- **Long short-term memory Network (LSTM):** For LSTM, we employ the same hyperparameter grid as for ANN. Listing 6 gives the Python code used to develop the LSTM networks in this work; we employ Keras' `LSTM` cell.
- **GP Regression:** GP regression is characterized by one hyperparameter: the noise magnitude λ . We employ the hyperparameter grid

$$\lambda \in \{10^{-8+\frac{8(i-1)}{19}}\}_{i=1}^{20}.$$

Additionally, for feature methods employing the principal components of the residual or residual samples, the number of principal components n_r and number of residual samples n_s can be viewed as hyperparameters. Here, we employ $n_r = n_s$, where n_r is determined such that the retained singular values associated with the truncated residual principal components contain 99% of the total statistical energy (see, e.g., Ref. [9, Appendix A]).

4.1.3. Evaluation metrics

To evaluate the performance of the deterministic regression-function models, we employ the fraction of variance unexplained (FVU) computed on the test set $\mathcal{T}_{\text{test}}$, which is given by

$$\text{FVU} := 1 - r^2,$$

where the coefficient of determination is defined as

$$r^2 := 1 - \frac{\sum_{n \in \mathbb{T}_{\text{test}}, \mu \in \mathcal{D}_{\text{test}}} (\hat{\delta}_f^n(\mu) - \delta^n(\mu))^2}{\sum_{n \in \mathbb{T}_{\text{test}}, \mu \in \mathcal{D}_{\text{test}}} (\delta^n(\mu) - \bar{\delta})^2},$$

where the mean response is $\bar{\delta} := 1/|\mathcal{T}_{\text{test}}| \sum_{n \in \mathbb{T}_{\text{test}}, \mu \in \mathcal{D}_{\text{test}}} \delta^n(\mu)$.

4.2. Example 1: Advection–diffusion equation with projection-based reduced-order model

The first example considers the advection–diffusion equation and approximate solutions generated by a POD–Galerkin reduced-order model. The governing PDE is

$$\frac{\partial}{\partial t}u(x, t) + \mu_1 \frac{\partial}{\partial x}u(x, t) = \mu_2 \frac{\partial^2}{\partial x^2}u(x, t), \quad u(0, t) = u(2, t) = 0, \quad u(x, 0) = x(2 - x) \exp(2x), \quad (53)$$

on the domain $x \in \Omega = [0, 2]$ with $t \in [0, T]$ and $T = 0.3$ and $u : \Omega \times [0, T] \rightarrow \mathbb{R}$. We employ a parameter domain of $(\mu_1, \mu_2) \in \mathcal{D} = [-2, -0.1] \times [0.1, 1]$, where the parameter μ_1 is the wave speed and the parameter μ_2 is the diffusion coefficient.

To derive a parameterized dynamical system of the form (1) for the FOM, we apply a finite-difference spatial discretization to the governing PDE (53), which uses central differencing for the diffusion term and upwind differencing for the advection term. This discretization is obtained by partitioning the spatial domain into 101 cells of equal width, yielding a FOM with $N = 100$ degrees of freedom of the form

$$\frac{dx_k}{dt} + \mu_1 \frac{x_{k+1} - x_k}{\Delta x} = \mu_2 \frac{x_{k+1} - 2x_k + x_{k-1}}{\Delta x^2}, \quad k = 1, \dots, N,$$

where the state vector is $\mathbf{x}(t, \boldsymbol{\mu}) \equiv [x_1(t, \boldsymbol{\mu}) \cdots x_N(t, \boldsymbol{\mu})]^T$ and $x_k(t, \boldsymbol{\mu})$ is the finite-difference approximation to $u(x_k, t, \boldsymbol{\mu})$ with $x_k := 2k/(N+1)$ the k th point in the finite-difference discretization. The initial condition is characterized by $\mathbf{x}_0(\boldsymbol{\mu}) \equiv \mathbf{x}_0 = [x_1(2 - x_1) \exp(2x_1) \cdots x_N(2 - x_N) \exp(2x_N)]^T$.

To define the FOM ODE of the form (2), we employ a time step $\Delta t = 3 \times 10^{-4}$ with the implicit Crank–Nicolson scheme, which is characterized by multistep coefficients $\alpha_0 = 1$, $\alpha_1 = -1$, $\beta_0 = \beta_1 = 1/2$ in (3), which yields $N_t = 10^3$ time instances.

To construct approximate solutions, we employ projection-based reduced-order models as described in Section 2.1.3. For this purpose, we construct the trial-basis matrix $\boldsymbol{\Phi} \in \mathbb{R}_*^{N \times K}$ using proper orthogonal decomposition (POD) by executing Algorithm 1 in Appendix A with inputs $\mathcal{D}_{\text{ROM}} = \{0.1, 1.05, 2.0\} \times \{0.1, 0.55, 1.0\}$, $N_{\text{skip}} = 10$, reference state $\mathbf{x}_{\text{ref}}(\boldsymbol{\mu}) = \mathbf{x}_0(\boldsymbol{\mu})$, and $K = 5$. For the ROM, we employ Galerkin projection such that the ROM ODE corresponds to (12) with $\boldsymbol{\Psi} = \boldsymbol{\Phi}$. We employ the same time discretization for the ROM as was employed for the FOM, i.e., the Crank–Nicolson scheme with time step $\Delta t = 3 \times 10^{-4}$.

We model both the QoI error $\delta_s^n(\boldsymbol{\mu})$, where the QoI corresponds to the solution at the midpoint of the domain such that the associated functional is $g(\mathbf{x}; t, \boldsymbol{\mu}) \mapsto \mathbf{e}_{51}^T \mathbf{x}$ with \mathbf{e}_i the i th canonical unit vector, and the normed state error $\delta_{\mathbf{x}}^n(\boldsymbol{\mu})$.

4.2.1. Coarse time grid, training, validation, and test sets

We now describe how we execute Steps 1–2 and 7 described in Section 4.1.1. For Step 1, we set $\mathbb{T} = \{20n\}_{n=1}^{50}$; the coarse grid is selected such that the error responses on the training set are well represented. For Step 2, we employ set sizes of $|\mathcal{D}_{\text{train}}| = 40$, $|\mathcal{D}_{\text{val}}| = 10$, and $|\mathcal{D}_{\text{test}}| = 50$. To assess the impact of the training set size on the performance of the deterministic regression-function model, we consider four smaller training and validation sets with $(|\mathcal{D}_{\text{train}}|, |\mathcal{D}_{\text{val}}|) \in \{(8, 2), (16, 4), (24, 6), (32, 8)\}$, which are constructed by sampling the original sets $\mathcal{D}_{\text{train}}$ and \mathcal{D}_{val} . In Step 7, we set $|\mathcal{D}_{\text{train}, \epsilon}| = 20$.

4.2.2. Regression results

Figures 4–8 summarize the performance of the considered error models. First, Figure 4 reports the dependence of the performance of each deterministic regression-function model (with its best performing feature-engineering method) on the size of the training set $|\mathcal{D}_{\text{train}}|$. This figure illustrates several trends. First, we observe that traditional time-series-modeling methods, i.e., ARX and LARX, nearly always yield the worst performance. Here, ARX yields the worst performance, likely due to the fact that it is a low-capacity model and contains only a single latent variable. LARX outperforms ARX; this is likely due to its inclusion of additional latent variables. We observe that the performance of ANN-I is slightly better than ARX or LARX, but not as good as the (non-integrated) ANN. This indicates that, in this case, differencing the data provides no particular benefit. We also observe that recursive-neural-network models, i.e., RNN and LSTM, yield the best performance nearly uniformly, and generate FVU values at least one order of magnitude smaller than

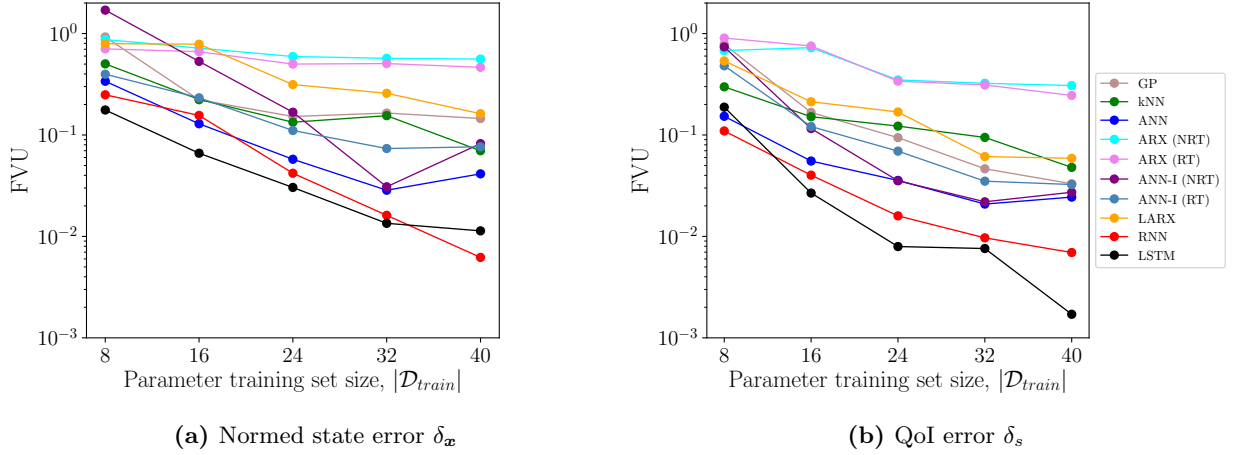


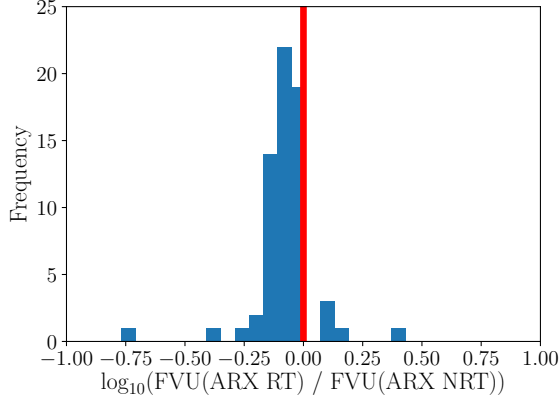
Figure 4: *Advection–diffusion equation.* Fraction of variance unexplained for all considered deterministic regression-function models, with each employing their best respective feature-engineering method.

both traditional time-series-modeling methods. This highlights that there is substantial benefit to modeling nonlinear latent dynamics as is done with RNN and LSTM models. Of these two, LSTM tends to yield best performance in most cases. Finally, LSTM and RNN outperform the GP regression-function model. This is likely due to the fact that the time-local GP method employs only the parameters μ as features, which are low quality compared to the residual-based quantities employed by the T-MLEM methods.

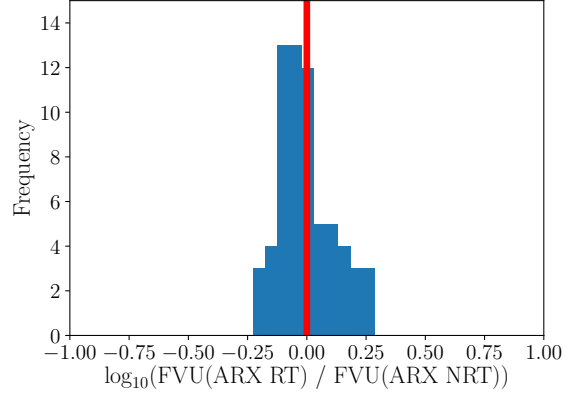
Figure 5 shows a histogram that, for regression methods in Category 2, compares the ratio of the fraction of variance unexplained using RT for training to fraction of variance unexplained using NRT for training. This figure shows that RT training generally outperforms NRT training; this is likely due to the fact that RT training properly accounts for the latent dynamics while training the model. For ARX, regression functions trained through RT outperform their NRT counterparts 90.8% of the time; for ANN-I the regression functions trained through RT outperform their NRT counterparts 72.3% of the time.

Next, Table 4 summarizes the percentage of cases that a given deterministic regression-function model produces results with the lowest FVU; each case is defined by one of the 13 feature-engineering methods and one of the 5 training-set sizes, yielding 65 total cases. We do not include the GP method in these results, as it employs only the parameters as features. Results are presented for the cases where (1) all feature methods are considered and (2) only feature methods that don’t include time are considered. The table shows that LSTM is the best overall performing regression-function model, leading to the lowest FVUs approximately 60% of the time. RNN is the next best performing regression-function model, followed by ANN. For the normed state error δ_x , recursive regression methods comprise the best performing regression-function models in 87.7% of cases when all feature-engineering methods are considered, and in 97.1% of cases when only feature-engineering engineering methods that omit time are considered; this shows that including time can improve the relative performance of non-recursive regression methods. For the QoI error δ_s , recurrent architectures comprise the best performing methods in over 97% of cases whether or not time is considered as a feature.

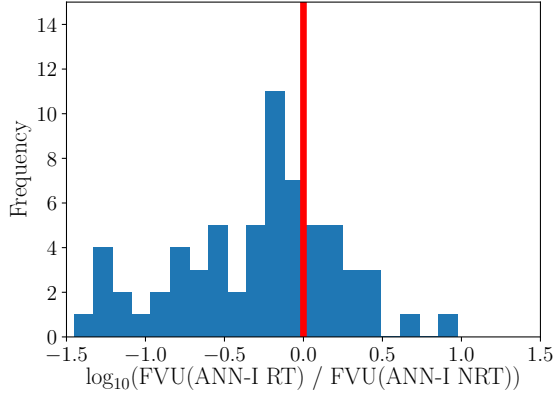
Figure 6 summarizes the performance of each combination of regression method and feature-engineering method for the case $|\mathcal{D}_{\text{train}}| = 40$. These results clearly show two critical trends. First, as hypothesized, using residual-based features can improve performance significantly; this is why they were considered high-quality features. This trend was also observed in Ref. [15]. Further, we note that—in this case—excellent results were obtained by computing only $7(\ll N)$ samples of the residual. Second, as hypothesized, the recurrent regression methods yield the best performance (even for low-quality features), with LSTM performing best



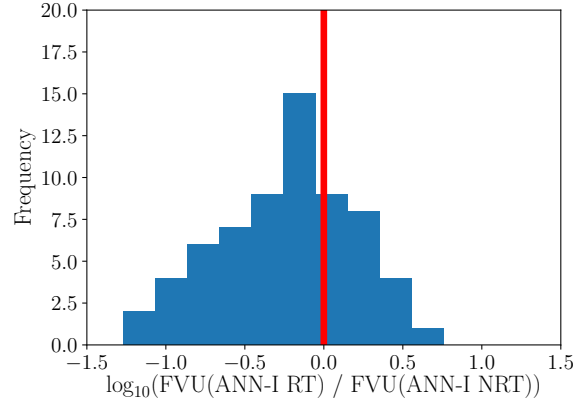
(a) Normed state error δ_x



(b) QoI error δ_s



(c) Normed state error δ_x



(d) QoI error δ_s

Figure 5: *Advection–diffusion equation.* Histogram of the ratio of the fraction of variance unexplained using RT for training to fraction of variance unexplained using NRT for training. Results are shown for ARX (top) and ANN-I (bottom). For ARX, RT outperforms NRT 90.8% of the time. For ANN-I, RT outperforms NRT 72.3% of the time.

error	include feat. eng. w/ time?	kNN	ANN	ARX (NRT)	ARX (RT)	ANN-I (NRT)	ANN-I (RT)	LARX	RNN	LSTM	Recursive total
δ_x	Yes	0.0	12.3	0.0	0.0	1.5	0.0	0.0	27.7	58.5	87.7
δ_x	No	0.0	2.9	0.0	0.0	2.9	0.0	0.0	31.4	60.0	97.1
δ_s	Yes	0.0	1.5	0.0	0.0	0.0	1.5	1.5	32.3	63.1	98.5
δ_s	No	0.0	2.9	0.0	0.0	0.0	2.9	2.9	40.0	51.4	97.1

Table 4: *Advection-diffusion equation.* Percentage of cases having the lowest predicted FVU for each regression method. Results are summarized over all values $|\mathcal{D}_{\text{train}}| \in \{8, 16, 24, 32, 40\}$ and all feature-engineering methods. Recursive total reports the sum of all regression methods in Category 2 and Category 3.

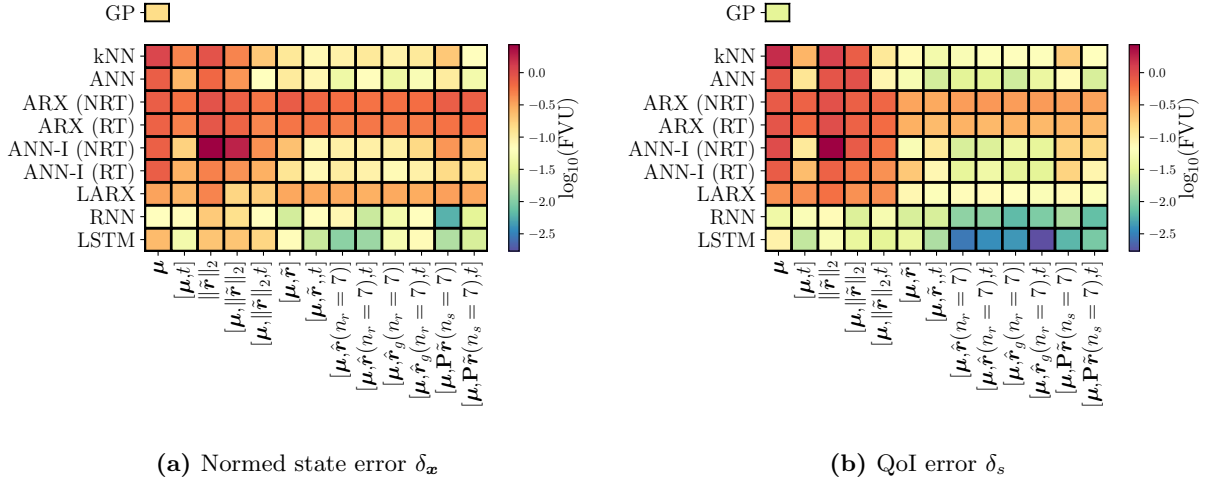


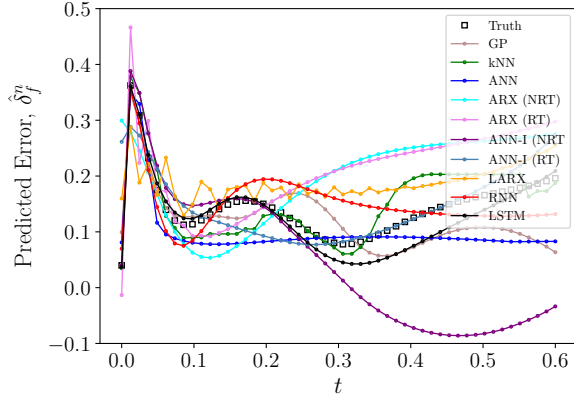
Figure 6: *Advection-diffusion equation.* Summary of the performance of each combination of regression method and feature-engineering method for the case $|\mathcal{D}_{\text{train}}| = 40$.

of all. In fact, LSTM and RNN outperform the time-local GP by approximately one order of magnitude. We also observe that including time slightly improves performance for these methods. Finally, we observe that for the deterministic regression-function models in Category 2, both training methods yield comparable results.

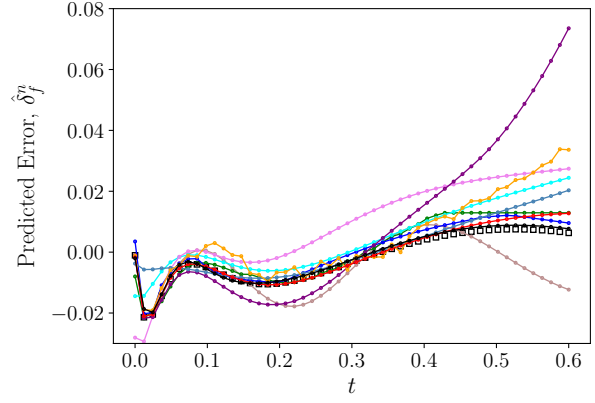
Figure 7 shows the predictions made by the different considered regression methods (for their best performing respective feature-engineering method) as a function of time for a randomly drawn element of $\mathcal{D}_{\text{test}}$ for cases $|\mathcal{D}_{\text{train}}| = 8$ and $|\mathcal{D}_{\text{train}}| = 40$. First, we note that the case $|\mathcal{D}_{\text{train}}| = 8$ yields significant errors for all considered models, with LSTM yielding the best performance. For the case $|\mathcal{D}_{\text{train}}| = 40$, all regression methods display substantially improved performance; LSTM, RNN, and ANN yield particularly accurate results.

Figure 8 shows the regression errors (i.e., the response error of the deterministic regression-function models) for the best performing regression method (i.e., LSTM) employing its best performing feature-engineering method. The figure compares the regression-error distribution with the distributions predicted by the Gaussian, Laplacian, and AR1 stochastic noise models. Table 5 reports validation frequencies of the approximated distributions, where $\omega(C)$ corresponds to the fraction of test data that lie within the C -prediction interval generated by the stochastic noise model. We also report the Kolmogorov–Smirnov (K-S) statistic. We observe that the Laplacian noise model yields the most accurate prediction-interval frequencies, with AR1 yielding similar performance to that of the Laplacian model.

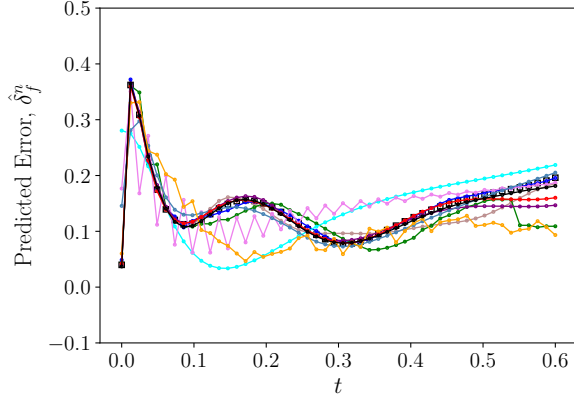
In summary, for the advection–diffusion example, the LSTM model yielded best performance, followed



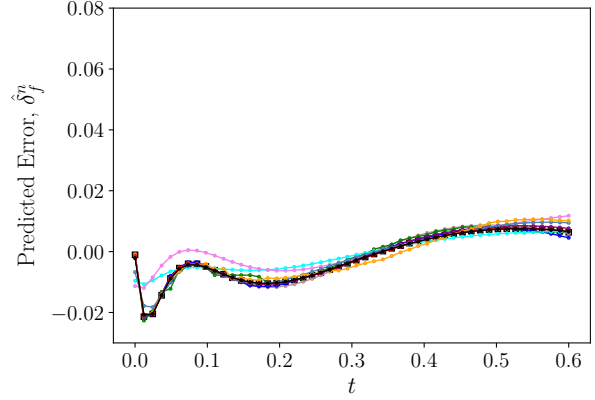
(a) Normed state error $\delta_{\mathbf{x}}$, $|\mathcal{D}_{\text{train}}| = 8$



(b) QoI error δ_s , $|\mathcal{D}_{\text{train}}| = 8$



(c) Normed state error $\delta_{\mathbf{x}}$, $|\mathcal{D}_{\text{train}}| = 40$



(d) QoI error δ_s , $|\mathcal{D}_{\text{train}}| = 40$

Figure 7: *Advection–diffusion equation.* Error response $\delta_{\mathbf{x}}$ (left) and δ_s (right) predicted by each regression method as a function of time. Results are shown for the best performing feature engineering method on the $|\mathcal{D}_{\text{train}}| = 8$ case (top) and the $|\mathcal{D}_{\text{train}}| = 40$ case (bottom).

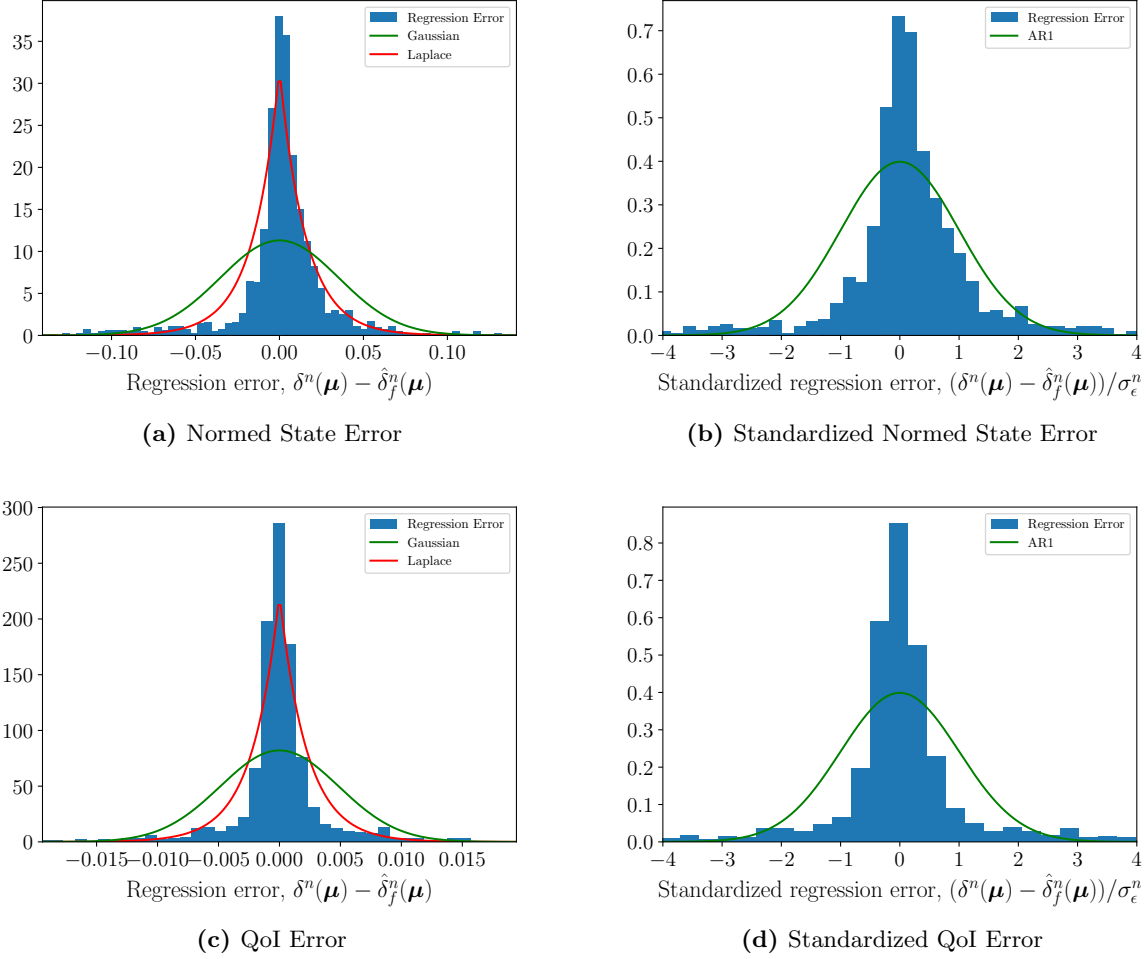


Figure 8: *Advection-diffusion equation.* Histogram of regression errors on the noise test set, $\mathcal{T}_{\text{test},\epsilon}$, for the normed state error (top) and QoI error (bottom). On the left, we show absolute errors $(\delta^n(\boldsymbol{\mu}) - \hat{\delta}_f^n(\boldsymbol{\mu}))$, $\boldsymbol{\mu} \in \mathcal{D}_{\text{test},\epsilon}$, $n \in \mathbb{T}$. On the right, we show standardized errors, $(\delta^n(\boldsymbol{\mu}) - \hat{\delta}_f^n(\boldsymbol{\mu}))/\sigma_\epsilon^n$, $\boldsymbol{\mu} \in \mathcal{D}_{\text{test},\epsilon}$, $n \in \mathbb{T}$. The true regression errors are compared to the distributions predicted by the Gaussian, Laplacian, and AR1 error models. Regression errors are shown for the LSTM deterministic regression function model with the best performing feature-engineering method on the $|\mathcal{D}_{\text{train}}| = 40$ case.

by RNN and ANN. We observed the residual-based features to yield best performance as well. Finally, the Laplacian model yielded the most accurate stochastic noise model.

Prediction interval	Gaussian		Laplacian		AR1	
	$\delta_{\mathbf{x}}$	δ_s	$\delta_{\mathbf{x}}$	δ_s	$\delta_{\mathbf{x}}$	δ_s
$\omega(0.68)$	0.842	0.805	0.724	0.673	0.714	0.725
$\omega(0.95)$	0.924	0.932	0.883	0.913	0.834	0.880
$\omega(0.99)$	0.943	0.967	0.868	0.967	0.868	0.913
K-S Statistic	0.216	0.216	0.114	0.088	0.146	0.131

Table 5: *Advection–diffusion equation.* Prediction intervals for the various stochastic noise models. Results correspond to those generated by the LSTM regression function model with its best performing feature-engineering method on the $|\mathcal{D}_{\text{train}}| = 40$ case, with samples collected over $\mathcal{T}_{\text{test},\epsilon}$.

4.3. Example 2: Shallow-water equations with projection-based reduced-order model

The second example considers the shallow water equations and approximate solutions generated by a POD–Galerkin reduced-order model. The governing system of PDEs is

$$\begin{aligned}\frac{\partial h}{\partial t} + \frac{\partial}{\partial \mathbf{x}}(hu) + \frac{\partial}{\partial \mathbf{y}}(hv) &= 0 \\ \frac{\partial hu}{\partial t} + \frac{\partial}{\partial \mathbf{x}}(hu^2 + \frac{1}{2}\mu_1 h^2) + \frac{\partial}{\partial \mathbf{y}}(huv) &= 0 \\ \frac{\partial hv}{\partial t} + \frac{\partial}{\partial \mathbf{x}}(huv) + \frac{\partial}{\partial \mathbf{y}}(hv^2 + \frac{1}{2}\mu_1 h^2) &= 0\end{aligned}$$

on the domain $(\mathbf{x}, \mathbf{y}) \in \Omega = [0, 5] \times [0, 5]$, $t \in [0, T]$ with $T = 10$, and where $h, u, v : \Omega \times [0, T] \rightarrow \mathbb{R}$, with h denoting the height of the water surface, u denoting the x -velocity, and v denoting the y -velocity. The parameter μ_1 is the “gravity” parameter.

The parameterized initial conditions are given by

$$h(\mathbf{x}, \mathbf{y}, 0) = 1 + \mu_2 e^{(\mathbf{x}-1)^2 + (\mathbf{y}-1)^2}, \quad u(\mathbf{x}, \mathbf{y}, 0) = v(\mathbf{x}, \mathbf{y}, 0) = 0, \quad (\mathbf{x}, \mathbf{y}) \in \Omega,$$

which corresponds to a Gaussian pulse centered at $(1, 1)$ with a magnitude of μ_2 . We consider a parameter domain $(\mu_1, \mu_2) \in \mathcal{D} = [2, 9] \times [0.05, 2]$.

To derive a parameterized dynamical system of the form (1) for the FOM, we apply a third-order discontinuous-Galerkin spatial discretization, which partitions the domain into a 16×16 grid of uniform square elements and employs tensor-product polynomials of order 2 to represent the solution over each element, yielding a FOM of dimension $N = 1.23 \times 10^4$. We employ slip-wall boundary conditions at the edge of the domain.

To define the FOM OΔE of the form (2), we employ a time step $\Delta t = 1.25 \times 10^{-2}$ with the implicit Crank–Nicolson scheme, which is characterized by multistep coefficients $\alpha_0 = 1$, $\alpha_1 = -1$, $\beta_0 = \beta_1 = 1/2$ in (3), which yields $N_t = 800$ time instances. Figure 9 shows elevation surfaces obtained from the solution to the FOM OΔE at one randomly chosen parameter instance.

As in the first example, we employ projection-based reduced-order models to construct approximate solutions. We again construct a POD trial-basis matrix $\Phi \in \mathbb{R}_*^{N \times K}$ by executing Algorithm 1 in Appendix A with inputs $\mathcal{D}_{\text{ROM}} = \{3, 6, 9\} \times \{0.05, 0.1, 0.2\}$, $N_{\text{skip}} = 1$, reference state $\mathbf{x}_{\text{ref}}(\boldsymbol{\mu}) = \mathbf{0}$, and $K = 78$. For the ROM, we employ Galerkin projection such that the ROM ODE corresponds to (12) with $\Psi = \Phi$. We employ the same time discretization for the ROM as was employed for the FOM.

We model both the QoI error $\delta_s^n(\boldsymbol{\mu})$, where the QoI corresponds to the water-surface height in the middle of the domain, and the normed state error $\delta_{\mathbf{x}}^n(\boldsymbol{\mu})$.

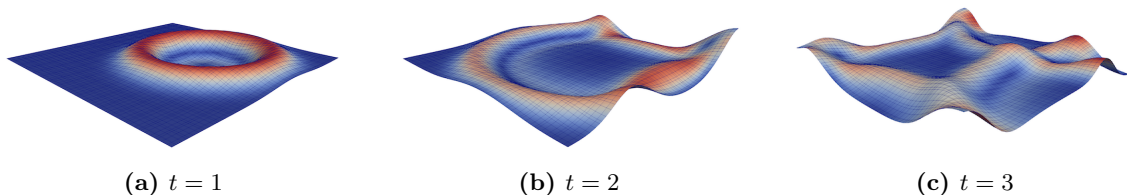


Figure 9: *Shallow-water equations.* Elevation surfaces of h for a randomly chosen parameter instance. Solutions are colored by velocity magnitude.

4.3.1. Coarse time grid, training, validation, and test sets

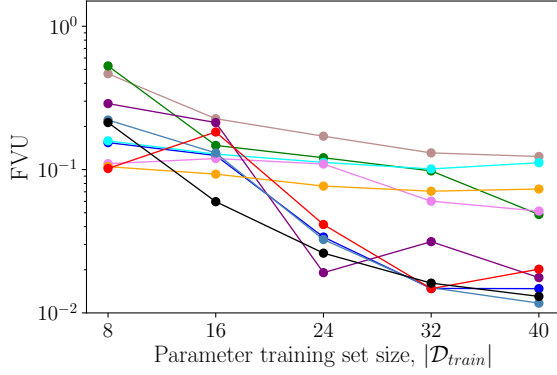
We now describe how we execute Steps 1–2 and 7 introduced Section 4.1.1. For Step 1, we set $\mathbb{T} = \{4n\}_{n=1}^{200}$; this coarse grid is again selected such that the error responses on the training set are well represented. For Step 2, we employ set sizes of $|\mathcal{D}_{\text{train}}| = 40$, $|\mathcal{D}_{\text{val}}| = 10$, and $|\mathcal{D}_{\text{test}}| = 20$. Again, to assess the impact of the training set size on the performance of the deterministic regression-function model, we consider four smaller training and validation sets with $(|\mathcal{D}_{\text{train}}|, |\mathcal{D}_{\text{val}}|) \in \{(8, 2), (16, 4), (24, 6), (32, 8)\}$, which are constructed by sampling the original sets $\mathcal{D}_{\text{train}}$ and \mathcal{D}_{val} . In Step 7, we set $|\mathcal{D}_{\text{train}, \epsilon}| = 10$.

Lastly, we note that we do not consider any feature-engineering methods that employ Feature 4, as the dimension of the residual $N = 1.23 \times 10^4$ is prohibitively large in this example.

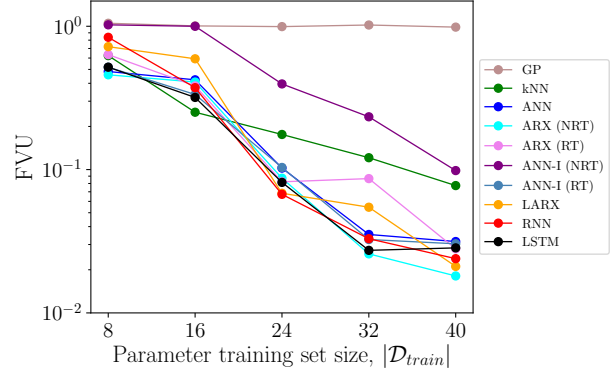
4.3.2. Regression results

Figures 10–13 summarize the performance of the deterministic regression-function models and stochastic noise models. First, Figure 10 reports the dependence of the performance of each deterministic regression-function model (with its best performing feature-engineering method) on the size of the training set $|\mathcal{D}_{\text{train}}|$. Figures 10a–10b considers all feature-engineering methods, while Figures 10c–10d limit consideration to feature-engineering methods that omit time from the set of features. When time is included as a feature, LSTM and RNN yield the best overall performance, followed closely by ANN; ANN slightly outperforms RNN in predicting the normed state error when time is included as a feature. ARX and LARX do not perform well for predicting the normed state error $\delta_{\mathbf{x}}$, but do perform very well in predicting the QoI error δ_s . We additionally observe that both methods for training ARX yield similar trends. ARX (RT) outperforms ARX (NRT) in predicting the normed state error, and ARX (NRT) outperforms ARX (RT) in predicting the QoI error. Next, we again observe that ANN-I performs worse than the standard ANN. We also observe that, in general, ANN-I (RT) performs slightly better than ANN-I (NRT) and yields similar results to ANN. Next, in comparing Figures 10a and 10b to Figures 10c and 10d, it is observed that the non-recursive regression methods are more reliant upon time to yield good performance than the recursive regression methods. This indicates that the non-recursive methods will likely not generalize well for problems characterized by phase shifts or for prediction beyond the training time interval. Lastly, the time-local GP benchmark is the worst performing method, and is particularly poor at predicting the QoI errors. This is thought to be due to the fact that the parameters are low quality features.

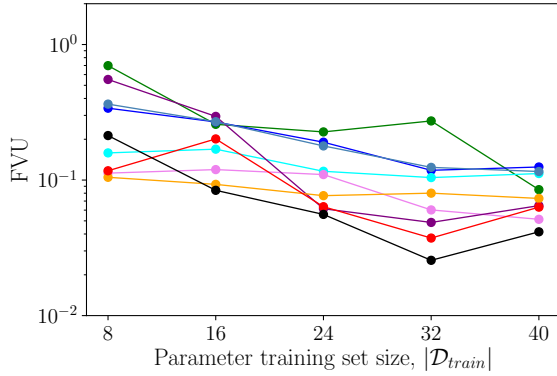
Table 6 summarizes the percentage of cases that a deterministic regression-function model produces results with the lowest FVU, where each case is defined by one of the 11 feature-engineering methods (recall that the residual, i.e., Feature 4 is not considered in this example) and one of the 5 training-set sizes, yielding 55 total cases. We again present results for the cases where (1) all feature methods are considered and (2) only feature methods that don’t include time are considered. Again, the results indicate that LSTM yields the best overall performance, followed by LARX and RNN. Recursive methods yield the best performance for predicting the normed state error in 81.8% of cases when all feature engineering methods are considered, and in 86.7% of cases when only feature engineering methods that do not include time are considered. For the QoI prediction, recursive methods yield the best performance in 85.5% and 86.7% of cases, respectively. As before, this shows that including time as a feature can (slightly) improve the relative performance of non-



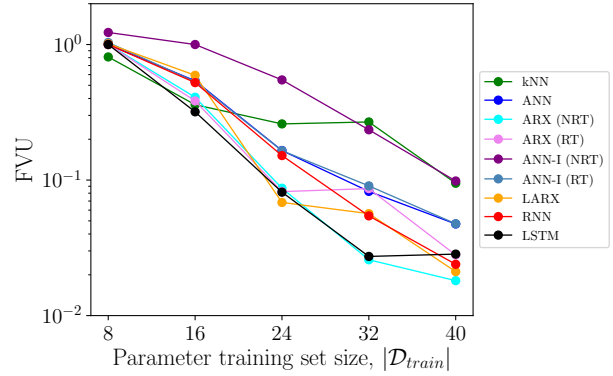
(a) Normed state error δ_x (All feature-engineering methods)



(b) QoI error δ_s (All feature-engineering methods)



(c) Normed state error δ_x (Feature-engineering methods without time)



(d) QoI error δ_s (Feature-engineering methods without time)

Figure 10: *Shallow-water equations.* Fraction of variance unexplained for all considered deterministic regression-function models, with each employing their best respective feature-engineering method.

recursive regression methods. Also as observed previously, including time as an input feature is observed to be more beneficial in predicting the normed state error than the QoI error.

error	include feat. eng. w/ time?	kNN	ANN	ARX (NRT)	ARX (RT)	ANN-I (NRT)	ANN-I (RT)	LARX	RNN	LSTM	Recursive total
$\delta_{\mathbf{x}}$	Yes	9.1	9.1	0.0	5.5	9.1	9.1	5.5	7.3	45.5	81.8
$\delta_{\mathbf{x}}$	No	13.3	0.0	0.0	10.0	6.7	0.0	10.0	3.3	56.7	86.7
δ_s	Yes	14.5	0.0	12.7	5.5	5.5	7.3	20.0	16.4	18.2	85.5
δ_s	No	13.3	0.0	16.7	3.3	3.3	3.3	16.7	13.3	30.0	86.7

Table 6: *Shallow-water equations.* Percentage of cases having the lowest predicted FVU for each regression method. Results are summarized over all values $|\mathcal{D}_{\text{train}}| \in \{10, 20, 30, 40, 50\}$ and all feature-engineering methods. Recursive total reports the sum of all regression methods in Category 2 and Category 3.

Figure 11 summarizes the performance of each combination of regression method and feature-engineering method for the cases $|\mathcal{D}_{\text{train}}| = 8$ (top) and $|\mathcal{D}_{\text{train}}| = 40$ (bottom). For the case $|\mathcal{D}_{\text{train}}| = 40$, the recursive regression methods generally display better overall performance than the non-recursive regression methods in predicting the normed state error $\delta_{\mathbf{x}}$. The low-dimensional feature engineering methods are additionally seen to lead to better overall performance than the high-dimensional feature engineering methods in this case, as using a small number of features typically leads to lower-capacity models that generalize with limited training data (see Consideration 3). For the QoI error, all regression methods perform poorly for the case $|\mathcal{D}_{\text{train}}| = 10$, with the lowest observed FVU value around FVU = 0.5. For the case $|\mathcal{D}_{\text{train}}| = 40$, all methods perform substantially better; here, it is clear that residual-based features are essential for obtaining good performance. LSTM, RNN, ANN, and ANN-I (RT) generally yield the best performance for the normed state error $\delta_{\mathbf{x}}$; however, ANN and ANN-I (RT) perform well only when time is included as a feature. For the QoI prediction, LSTM, RNN, LARX, and ARX (NRT) generally perform best.

Figure 12 shows the predictions made by the different considered regression methods (for their best performing respective feature-engineering method) as a function of time for a randomly drawn element of $\mathcal{D}_{\text{test}}$ for case $|\mathcal{D}_{\text{train}}| = 40$. The figure shows that all approaches except GP provide reasonably accurate predictions for both the normed state and QoI errors.

Figure 13 and Table 7 summarize the performance of the stochastic noise models, where results are shown for the LSTM regression method employing its best performing feature-engineering method for the case $|\mathcal{D}_{\text{train}}| = 40$. Similar to the previous case, the Laplacian noise model yields the best performance.

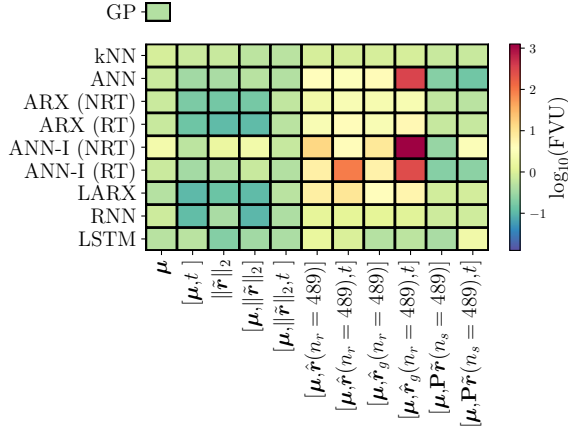
Prediction interval	Gaussian		Laplacian		AR1	
	$\delta_{\mathbf{x}}$	δ_s	$\delta_{\mathbf{x}}$	δ_s	$\delta_{\mathbf{x}}$	δ_s
$\omega(0.68)$	0.956	0.971	0.801	0.848	0.927	0.972
$\omega(0.95)$	0.991	0.995	0.966	0.960	0.984	0.990
$\omega(0.99)$	0.998	0.996	0.987	0.988	0.987	0.991
K-S Statistic	0.265	0.323	0.125	0.146	0.231	0.350

Table 7: *Shallow-water equations.* Prediction intervals for the various stochastic noise models. Results correspond to those generated by the best LSTM regression function model with its best performing feature-engineering method on the $|\mathcal{D}_{\text{train}}| = 40$ case, with samples collected over $\mathcal{T}_{\text{test}, \epsilon}$.

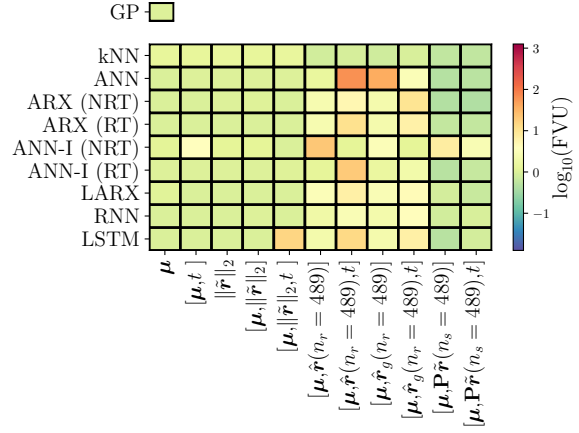
4.4. Example 3: Inviscid Burgers' equation with coarse-mesh low-fidelity model

The final example considers the one-dimensional inviscid Burgers' equation and approximate solutions generated by a low-fidelity model provided by a coarse spatial discretization. The governing PDE is

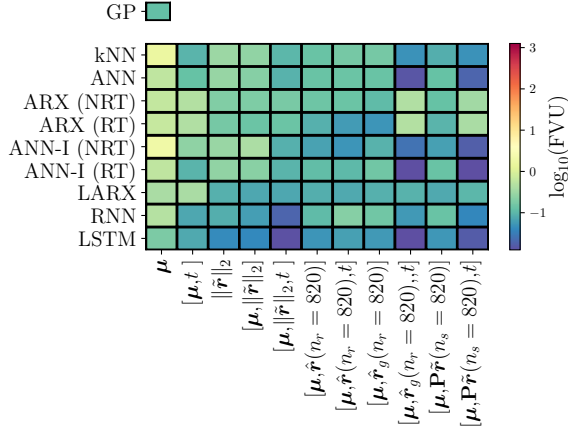
$$\frac{\partial u}{\partial t} + \frac{1}{2} \frac{\partial u^2}{\partial x} = \mu_1 e^{\mu_2 x}, \quad u(0, t) = \mu_3, \quad u(x, 0) = \mu_4 \text{ for } x \in (0, 100] \quad (54)$$



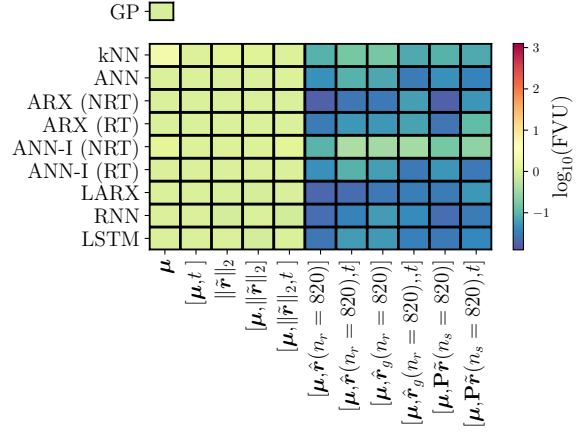
(a) Normed state error δ_x , $|\mathcal{D}_{\text{train}}| = 8$



(b) QoI error δ_s , $|\mathcal{D}_{\text{train}}| = 8$



(c) Normed state error δ_x , $|\mathcal{D}_{\text{train}}| = 40$



(d) QoI error δ_s , $|\mathcal{D}_{\text{train}}| = 40$

Figure 11: *Shallow-water equations.* Summary of the performance of each combination of regression method and feature-engineering method for the cases $|\mathcal{D}_{\text{train}}| = 8$ (top) and $|\mathcal{D}_{\text{train}}| = 40$ (bottom).

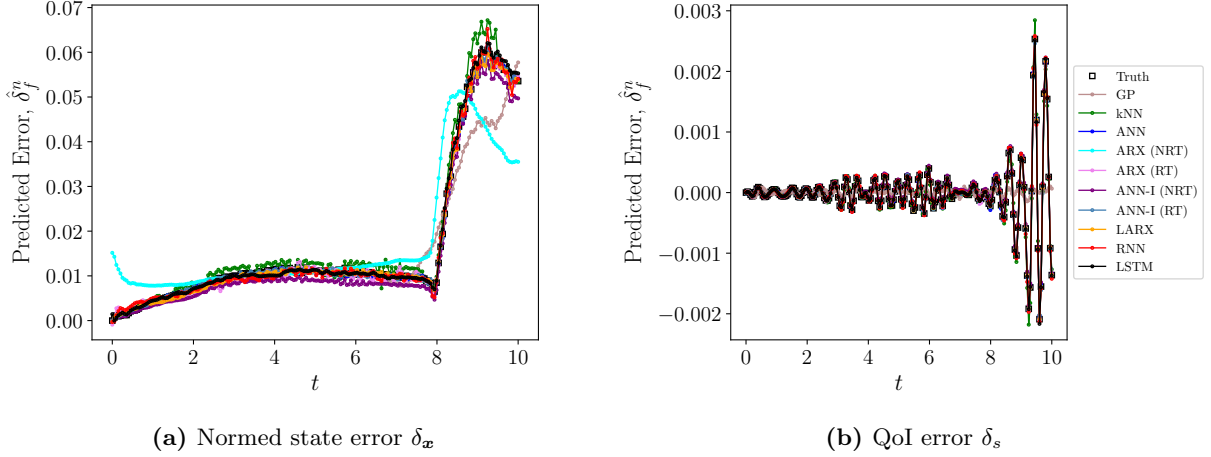


Figure 12: *Shallow-water equations.* Error response δ_x (left) and δ_s (right) predicted by each regression method as a function of time. Results are shown for the best performing feature engineering method on the $|\mathcal{D}_{\text{train}}| = 40$ case.

on the domain $x \in \Omega = [0, 100]$ with $t \in [0, T]$ and $T = 40$, and $u : \Omega \times [0, T] \rightarrow \mathbb{R}$. We employ a parameter domain of $(\mu_1, \mu_2, \mu_3, \mu_4) \in \mathcal{D} = [0.005, 0.05] \times [0.005, 0.05] \times [3, 5] \times [0.5, 2.5]$.

To derive a parameterized dynamical system of the form (1) for the FOM, we apply a finite-volume spatial discretization to the governing equations (54), which uses an upwind flux at the cell interfaces and a uniform control-volume width of $\Delta x = 0.1$, yielding a FOM with $N = 1000$ degrees of freedom.

To define the FOM ODE of the form (2), we employ a time step $\Delta t = 0.05$ with the implicit Euler scheme, which is characterized by multistep coefficients $\alpha_0 = 1$, $\alpha_1 = -1$, $\beta_0 = 1$ in (3), which yields $N_t = 800$ time instances.

To construct approximate solutions, we employ coarse-mesh low-fidelity models as described in Section 2.1.2. In particular, to define the LFM ODE of the form (7), we employ the same finite-volume scheme as that employed by the FOM, but use a uniform control-volume width of $\Delta x = 2$ such that $N_{\text{LF}} = 50$. The prolongation operator \mathbf{p} consists of a linear interpolation of the coarse-grid solution onto the fine grid.

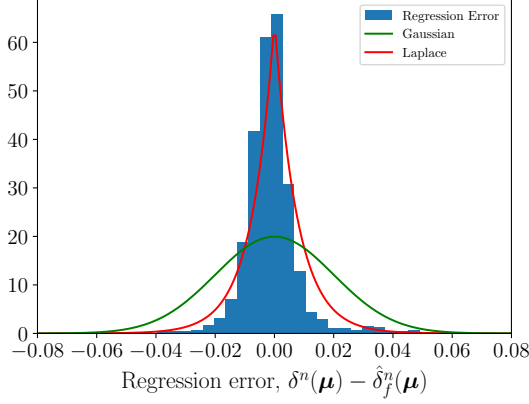
We model the QoI error $\delta_s^n(\mu)$, where the QoI corresponds to the solution at the midpoint of the domain such that the associated functional is $g(x; t, \mu) \mapsto e_{501}^T x$.

4.4.1. Coarse time grid, training, validation, and test sets

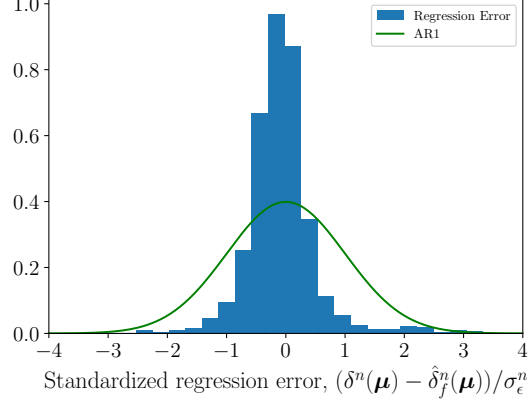
We now describe how we execute Steps 1–2 and 7 described in Section 4.1.1. For Step 1, we set $\mathbb{T} = \{8n\}_{n=1}^{100}$. For Step 2, we employ the same approach as in the previous section. Namely, we employ set sizes of $|\mathcal{D}_{\text{train}}| = 40$, $|\mathcal{D}_{\text{val}}| = 10$, and $|\mathcal{D}_{\text{test}}| = 50$. To assess the impact of the training set size on the performance of the deterministic regression-function model, we consider four smaller training and validation sets with $(|\mathcal{D}_{\text{train}}|, |\mathcal{D}_{\text{val}}|) \in \{(8, 2), (16, 4), (24, 6), (32, 8)\}$, which are constructed by sampling the original sets $\mathcal{D}_{\text{train}}$ and \mathcal{D}_{val} . In Step 7, we set $|\mathcal{D}_{\text{train}, \epsilon}| = 20$.

4.4.2. Regression results

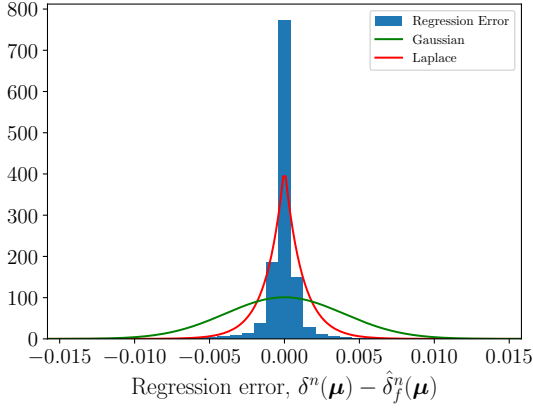
Figures 14 through 17 summarize the performance of the deterministic regression-function models and stochastic noise models. First, Figure 14 reports the dependence of the performance of each deterministic regression-function model (with its best performing feature-engineering method) on the size of the training set $|\mathcal{D}_{\text{train}}|$. Figure 14a considers all feature-engineering methods, while Figure 14b limits consideration to feature-engineering methods that omit time from the set of features. We observe that LSTM and RNN again yield the best performance, although their improvement over ANN is less significant than what was



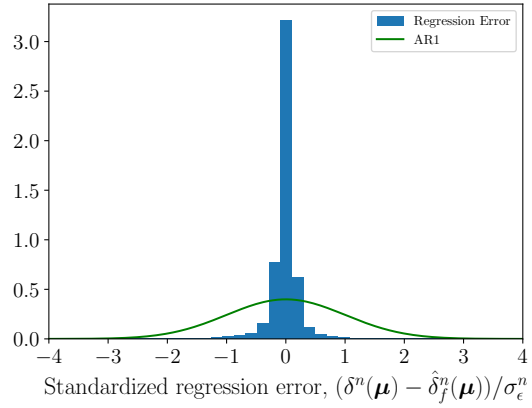
(a) Normed State Error



(b) Standardized Normed State Error



(c) QoI Error



(d) Standardized QoI Error

Figure 13: *Shallow-water equations.* Histogram of regression errors on the noise test set, $\mathcal{T}_{\text{test},\epsilon}$, for the normed state error (top) and QoI error (bottom). On the left, we show absolute errors $(\delta^n(\mu) - \hat{\delta}_f^n(\mu))$, $\mu \in \mathcal{D}_{\text{test},\epsilon}$, $n \in \mathbb{T}$. On the right, we show standardized errors, $(\delta^n(\mu) - \hat{\delta}_f^n(\mu))/\sigma_\epsilon^n$, $\mu \in \mathcal{D}_{\text{test},\epsilon}$, $n \in \mathbb{T}$. The true regression errors are compared to the distributions predicted by the Gaussian, Laplacian, and AR1 error models. Regression errors are shown for the LSTM deterministic regression function model with the best performing feature-engineering method on the $|\mathcal{D}_{\text{train}}| = 40$ case.

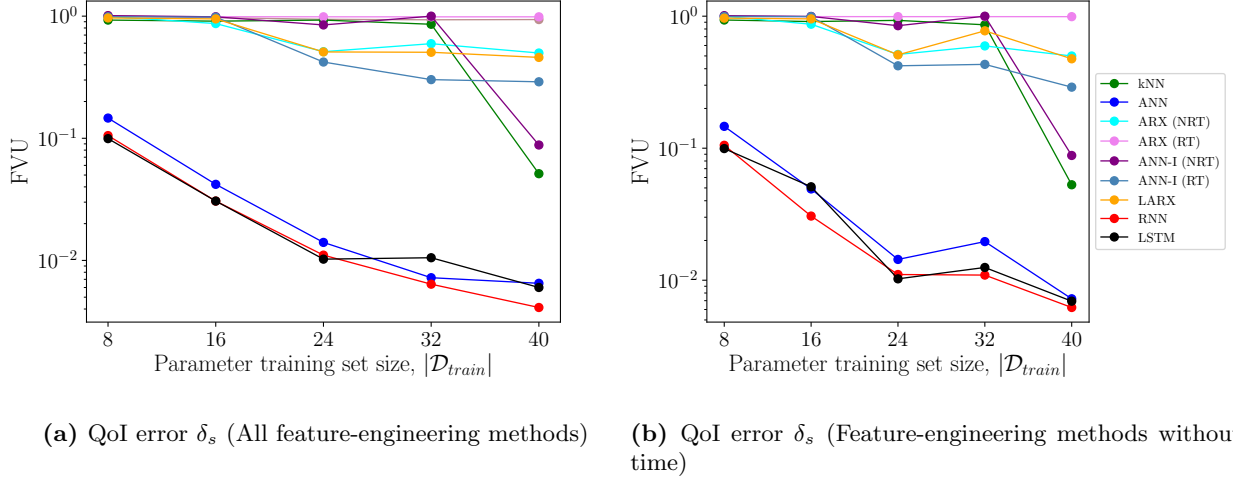


Figure 14: *Inviscid Burgers' equation*. Fraction of variance unexplained for all considered deterministic regression-function models, with each employing their best respective feature-engineering method.

observed in the previous two examples. We observe that all other methods—including the time-local GP benchmark—perform substantially worse than these three techniques.

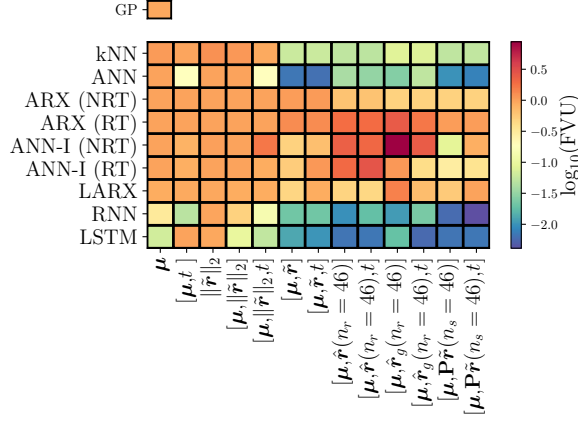
Next, Table 8 summarizes the percentage of cases that a deterministic regression-function model produces results with the lowest FVU, where each case is defined by one of the 13 feature-engineering methods and one of the 5 training-set sizes, yielding 65 total cases. Results are presented for the cases where (1) all feature methods are considered and (2) only feature methods that don't include time are considered. The table shows that LSTM is the best overall performing regression-function model, leading to the lowest FVUs in over half of cases. RNN yields the next best performance, followed by ANN. We again observe that recursive regression methods yield the best performance in the vast majority of cases; we also again observe that including time can improve the relative performance of non-recursive regression methods.

error	include feat. eng. w/ time?	kNN	ANN	ARX (NRT)	ARX (RT)	ANN-I (NRT)	ANN-I (RT)	LARX	RNN	LSTM	Recursive total
δ_s	Yes	0.0	12.3	0.0	0.0	0.0	0.0	1.5	35.4	50.8	87.7
δ_s	No	0.0	5.7	0.0	0.0	0.0	0.0	2.9	34.3	57.1	94.3

Table 8: *Inviscid Burgers' equation*. Percentage of cases having the lowest predicted FVU for each regression method. Results are summarized over all values $|\mathcal{D}_{\text{train}}| \in \{8, 16, 24, 32, 40\}$ and all feature-engineering methods. Recursive total reports the sum of all regression methods in Category 2 and Category 3.

Figure 15 summarizes the performance of each combination of regression method and feature-engineering method for the case $|\mathcal{D}_{\text{train}}| = 40$. We once again observe that feature-engineering methods employing elements of the residual lead to the best performance. We also observe that the LSTM and RNN methods yield the best performance, and substantially outperform the time-local GP method; indeed, they generate FVU values around 0.1 when they use only the parameters μ as features. These methods also generate FVU values lower than 0.01 when using only 46 residual samples in the set of features.

Figure 16 shows the predictions made by the different considered regression methods (for their best performing respective feature-engineering method) as a function of time for a randomly drawn element of $\mathcal{D}_{\text{test}}$ for cases $|\mathcal{D}_{\text{train}}| = 8$ and $|\mathcal{D}_{\text{train}}| = 40$. Here, we observe that LSTM, RNN, and ANN provide the most accurate predictions; indeed, their predictions are already very accurate for only $|\mathcal{D}_{\text{train}}| = 8$. The time-local



(a) QoI error δ_s

Figure 15: *Inviscid Burgers' equation*. Summary of the performance of each combination of regression method and feature-engineering method for the case $|\mathcal{D}_{\text{train}}| = 40$.

GP benchmark and ARX models perform the worst.

Lastly, Figure 17 and Table 9 summarize the performance of each stochastic noise model for the LSTM regression method employing its best performing feature-engineering method. Similar to the previous cases, the Laplacian stochastic noise model provides the best stochastic noise model.

Prediction interval	Gaussian δ_s	Laplacian δ_s	AR1 δ_s
$\omega(0.68)$	0.943	0.810	0.933
$\omega(0.95)$	0.970	0.946	0.959
$\omega(0.99)$	0.976	0.975	0.965
K-S Statistic	0.273	0.111	0.274

Table 9: *Inviscid Burgers' equation*. Prediction intervals for the various stochastic noise models. Results correspond to those generated by the best performing regression method (i.e., LSTM) with its best performing feature-engineering method on the $|\mathcal{D}_{\text{train}}| = 40$ case, with samples collected over $\mathcal{T}_{\text{test}}$.

5. Conclusions

This work proposed the Time-Series Machine-Learning Error Modeling (T-MLEM) method for constructing error models for approximate solutions to parameterized dynamical systems. The T-MLEM method extends the machine learning error modeling (MLEM) [15] method to dynamical systems. The key contribution of this work as compared to previous works on error modeling for dynamical systems is the use of residual-based features and recursive regression methods (e.g., recurrent neural networks, long short-term memory networks) that employ latent variables. The use of these latent variables enables these regression models to model dependence on temporally non-local quantities, which is essential for modeling errors in this context (as illustrated by classical approaches for error quantification).

Similar to the MLEM method, the T-MLEM method entails four steps: feature engineering, data generation, training a deterministic regression-function model that maps from features to the conditional expectation of the error, and training a stochastic noise model. For feature engineering, we considered a variety

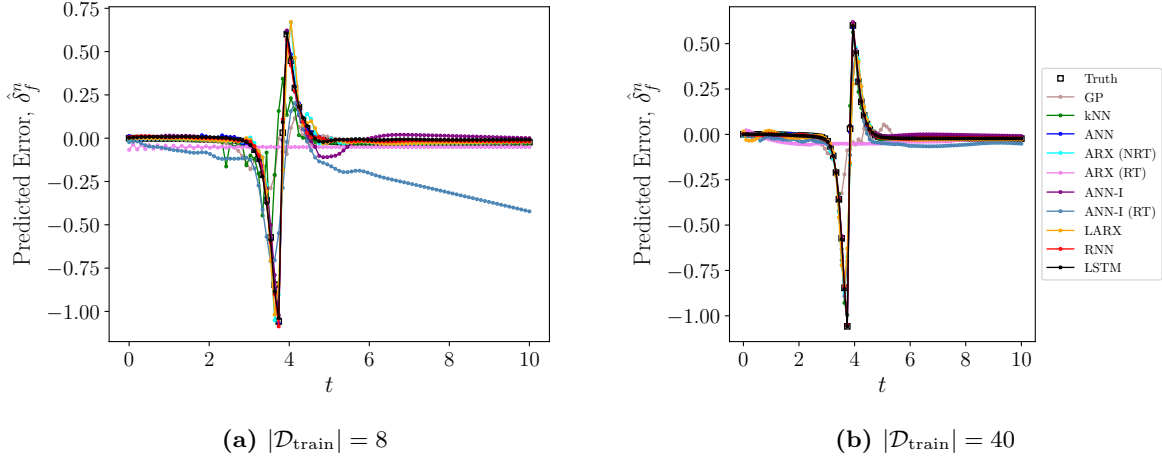


Figure 16: *Inviscid Burgers' equation.* Error response δ_s predicted by each regression method as a function of time. Results are shown for the best performing feature engineering method on the $|\mathcal{D}_{\text{train}}| = 8$ case (left) and the $|\mathcal{D}_{\text{train}}| = 40$ case (right).

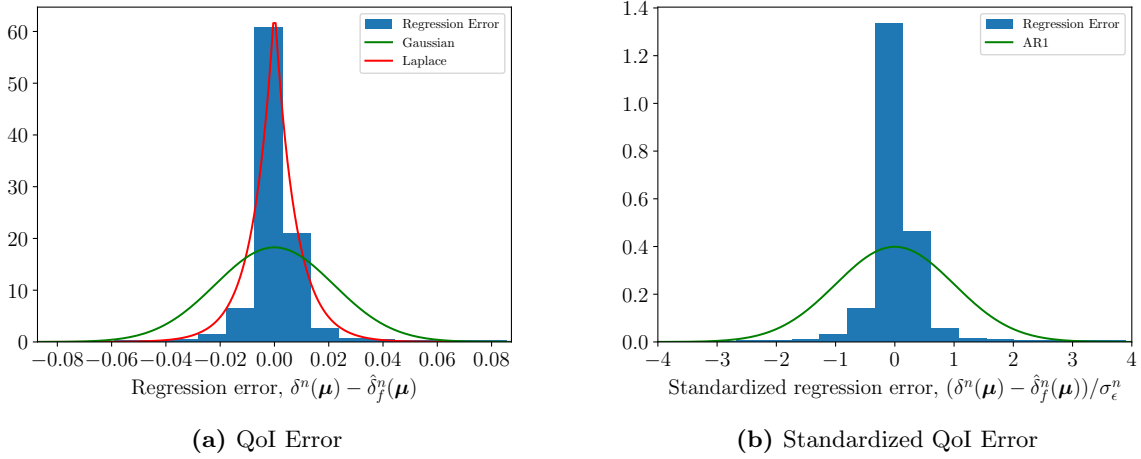


Figure 17: *Inviscid Burgers' equation.* Histogram of regression errors on the noise test set, $\mathcal{T}_{\text{test},\epsilon}$, for the QoI error. On the left, we show absolute errors $(\delta^n(\mu) - \hat{\delta}_f^n(\mu))$, $\mu \in \mathcal{D}_{\text{test},\epsilon}$, $n \in \mathbb{T}$. On the right, we show standardized errors, $(\delta^n(\mu) - \hat{\delta}_f^n(\mu))/\sigma_\epsilon^n$, $\mu \in \mathcal{D}_{\text{test},\epsilon}$, $n \in \mathbb{T}$. The true regression errors are compared to the distributions predicted by the Gaussian, Laplacian, and AR1 error models. Regression errors are shown for the LSTM deterministic regression function model with the best performing feature-engineering method on the $|\mathcal{D}_{\text{train}}| = 40$ case.

of techniques based on those proposed in Ref. [15], along with several new techniques that include the time variable as a feature. The majority of these feature-engineering methods employ residual-based quantities inspired by classic error-quantification approaches. Next, we considered a hierarchy of regression methods that employ both non-recurrent and recurrent regression functions as well as linear and nonlinear latent-variable dynamics. These techniques include classic time-series modeling techniques (e.g., ARX), as well as time-series modeling techniques emerging from the deep-learning community (e.g., LSTM). Lastly, we examined three different stochastic noise models: Gaussian, Laplacian, and autoregressive Gaussian.

Across three benchmark problems and two different types of approximate solutions, the numerical experiments illustrated the best overall performance was obtained using the T-MLEM framework with an LSTM regression-function model. We attribute this favorable performance to LSTM’s ability to capture dependencies on long-term non-local quantities through its use of a “cell state”, as well as its amenability to training. While the best-performing feature-engineering method varied across the considered problems, generally feature-engineering methods that employ residual-based features yielded the best performance. Lastly, we observed the Laplacian stochastic noise model to provide the best statistical model for the prediction noise. In particular, we emphasize that the T-MLEM method with an LSTM regression-function model and residual-based features significantly outperformed both (1) the classical model-discrepancy method [25], which constructs an error model by applying Gaussian-process regression in parameter space, and (2) error models constructed using non-recursive regression models as was proposed in Ref. [45].

Future work involves the application of the T-MLEM framework on truly large-scale problems, as well as in more difficult scenarios, e.g., predicting errors beyond the training time interval.

6. Acknowledgements

E. Parish acknowledges an appointment to the Sandia National Laboratories’ John von Neumann Postdoctoral Research Fellowship in Computational Science. The authors thank Brian Freno for providing the data that was used in the third numerical experiment. This work was partially sponsored by Sandia’s Advanced Simulation and Computing (ASC) Verification and Validation (V&V) Project/Task #103723/05.30.02. This paper describes objective technical results and analysis. Any subjective views or opinions that might be expressed in the paper do not necessarily represent the views of the U.S. Department of Energy or the United States Government. Sandia National Laboratories is a multimission laboratory managed and operated by National Technology and Engineering Solutions of Sandia, LLC., a wholly owned subsidiary of Honeywell International, Inc., for the U.S. Department of Energy’s National Nuclear Security Administration under contract DE-NA-0003525.

Appendix A Proper orthogonal decomposition

Algorithm 1 provides the algorithm for computing the POD basis used in this work. We note that the basis dimension K can be determined from the decay of the singular values; for simplicity, we treat it as an algorithm input.

Algorithm 1 Proper orthogonal decomposition (POD)

Input: Training parameter instances $\mathcal{D}_{\text{ROM}} \equiv \{\boldsymbol{\mu}_{\text{ROM}}^i\} \subseteq \mathcal{D}$; number of time steps between collected snapshots $N_{\text{skip}} \leq N_t$; reference state $\mathbf{x}_{\text{ref}}(\boldsymbol{\mu})$; desired basis dimension K .

Output: POD basis $\boldsymbol{\Phi} \equiv [\boldsymbol{\phi}_1 \cdots \boldsymbol{\phi}_K] \in \mathbb{R}_{\star}^{N \times K}$.

Steps:

1. Solve the FOM ODE (2) for $\boldsymbol{\mu} \in \mathcal{D}_{\text{ROM}}$ and collect the snapshot matrix

$$\mathbf{S}(\boldsymbol{\mu}, N_{\text{skip}}) := \left[\mathbf{x}^{N_{\text{skip}}}(\boldsymbol{\mu}) - \mathbf{x}_{\text{ref}}(\boldsymbol{\mu}) \cdots \mathbf{x}^{\text{floor}(N_t/N_{\text{skip}})N_{\text{skip}}}(\boldsymbol{\mu}) - \mathbf{x}_{\text{ref}}(\boldsymbol{\mu}) \right]. \quad (55)$$

2. Compute the (thin) singular value decomposition

$$\left[\mathbf{S}(\boldsymbol{\mu}_{\text{ROM}}^1, N_{\text{skip}}) \cdots \mathbf{S}(\boldsymbol{\mu}_{\text{ROM}}^{N_{\text{train,ROM}}}, N_{\text{skip}}) \right] = \mathbf{U} \boldsymbol{\Sigma} \mathbf{V}^T, \quad (56)$$

where $\mathbf{U} \equiv [\mathbf{u}_1 \cdots \mathbf{u}_{N_{\text{train,ROM}}N_t/N_{\text{skip}}}]$.

3. Truncate the left singular vectors such that $\boldsymbol{\phi}_i = \mathbf{u}_i$, $i = 1, \dots, K$.
-

Appendix B Q-sampling

Feature engineering methods explored in this work that employ either the gappy principal components (Feature 6) or sampled residual (Feature 7) require the specification of the sampling matrix \mathbf{P} . In this work, we compute this sampling matrix via q-sampling [11]. Algorithm 2 provides the associated algorithm.

Appendix C Gaussian-process regression

The numerical experiments consider time-local Gaussian-process regression models as a benchmark error-modeling method. This method is analogous to employing the “model-discrepancy” method of Kennedy and O’Hagan [25] at each time instance. This approach constructs a separate GP model to predict the error for each time instance of interest. As such, the approach can only be used to make predictions at time instances for which training data exist, i.e., prediction beyond the training time interval is not possible. We note that the use of time-local GP regression was considered in Ref. [34], wherein GP models were constructed in parameter space over time windows.

We begin by setting $\mathcal{D}_{\text{train}} \equiv \{\boldsymbol{\mu}_i\}_{i=1}^{N_s}$, where $N_s := |\mathcal{D}_{\text{train}}|$, and consider an arbitrary test point $\boldsymbol{\mu} \in \mathcal{D}$. We define the vector of training responses and the *model* of the test response at time instance $n \in \mathbb{T}$ as

$$\bar{\boldsymbol{\delta}}^n(\boldsymbol{\mu}) := \begin{bmatrix} \boldsymbol{\delta}_{\text{train}}^n \\ \hat{\boldsymbol{\delta}}^n(\boldsymbol{\mu}) \end{bmatrix},$$

where $\boldsymbol{\delta}_{\text{train}}^n := [\delta^n(\boldsymbol{\mu}_1) \cdots \delta^n(\boldsymbol{\mu}_{N_s})]^T$. We then assume the data are drawn from the prior distribution

$$\bar{\boldsymbol{\delta}}^n(\boldsymbol{\mu}) \sim \mathcal{N}(\mathbf{0}, \bar{\boldsymbol{\Sigma}}^n(\boldsymbol{\mu}) + \lambda \mathbf{I}),$$

Algorithm 2 Algorithm for generation of sampling matrix through q-sampling.

Input: Residual training set $\mathcal{T}_{\mathbf{r},\text{train}} \equiv \{\tilde{\mathbf{r}}^n(\boldsymbol{\mu}) \mid \boldsymbol{\mu} \in \mathcal{D}_{\text{train}} \equiv \{\boldsymbol{\mu}_i\}_{i=1}^{|\mathcal{D}_{\text{train}}|}, n \in \mathbb{T}_{\text{train}}\}$

Output: Sampling matrix $\mathbf{P} \in \{0, 1\}^{n_s \times N}$

Steps:

1. Compute the residual snapshot matrix:

$$\mathbf{S}_{\mathbf{r}} := \begin{bmatrix} \tilde{\mathbf{r}}^{\tau(1)}(\boldsymbol{\mu}_1) & \cdots & \tilde{\mathbf{r}}^{\tau(\bar{N}_t)}(\boldsymbol{\mu}_1) & \cdots & \tilde{\mathbf{r}}^{\tau(1)}(|\boldsymbol{\mu}_{\mathcal{D}_{\text{train}}}|) & \cdots & \tilde{\mathbf{r}}^{\tau(\bar{N}_t)}(\boldsymbol{\mu}_{|\mathcal{D}_{\text{train}}|}) \end{bmatrix}.$$

2. Compute the column mean of $\mathbf{S}_{\mathbf{r}}$

$$\bar{\mathbf{r}} := \frac{1}{|\mathcal{T}_{\mathbf{r},\text{train}}|} \sum_{\tilde{\mathbf{r}} \in \mathcal{T}_{\mathbf{r},\text{train}}} \tilde{\mathbf{r}}$$

3. Compute the (thin) singular value decomposition:

$$\mathbf{S}_{\mathbf{r}} - \bar{\mathbf{r}}\mathbf{e}^T = \mathbf{U}\boldsymbol{\Sigma}\mathbf{V}^T,$$

where $\mathbf{e} \in \{1\}^{|\mathcal{T}_{\mathbf{r},\text{train}}|}$.

4. Compute the QR factorization of \mathbf{U}^T with column pivoting

$$\mathbf{U}^T[\mathbf{P}^*]^T = \mathbf{Q}\mathbf{R},$$

where $\mathbf{P}^* \equiv [\mathbf{p}_1 \quad \cdots \quad \mathbf{p}_{|\mathcal{T}_{\mathbf{r},\text{train}}|}]^T$, $\mathbf{p}_i \in \{0, 1\}^N$.

5. From the permutation matrix \mathbf{P}^* , select the first $n_s \leq |\mathcal{T}_{\mathbf{r},\text{train}}|$ rows to form the sampling matrix

$$\mathbf{P} := [\mathbf{p}_1 \quad \cdots \quad \mathbf{p}_{n_s}]^T.$$

where $\lambda \in \mathbb{R}_+$ is an additive noise hyper-parameter and $\bar{\Sigma}^n(\boldsymbol{\mu})$ is a positive definite $(N_s + 1) \times (N_s + 1)$ covariance matrix of the form

$$\bar{\Sigma}^n(\boldsymbol{\mu}) = \begin{bmatrix} \Sigma_{\text{train}}^n & \Sigma_{\text{test}}^n(\boldsymbol{\mu})^T \\ \Sigma_{\text{test}}^n(\boldsymbol{\mu}) & 1 \end{bmatrix},$$

where we employ radial-basis-function kernels such that

$$\begin{aligned} [\Sigma_{\text{train}}^n]_{ij} &:= \exp \frac{\|\boldsymbol{\mu}_i - \boldsymbol{\mu}_j\|_2^2}{h^2}, \quad i, j = 1, \dots, N_s, \\ [\Sigma_{\text{test}}^n(\boldsymbol{\mu})]_{1i} &= \exp \frac{\|\boldsymbol{\mu} - \boldsymbol{\mu}_i\|_2^2}{h^2}, \quad i = 1, \dots, N_s, \end{aligned} \quad (57)$$

Given the training data, the posterior distribution of the model of the test response is

$$\hat{\delta}^n(\boldsymbol{\mu}) \sim \mathcal{N} \left(\Sigma_{\text{test}}^n(\boldsymbol{\mu}) (\Sigma_{\text{train}}^n + \lambda \mathbf{I})^{-1} \boldsymbol{\delta}_{\text{train}}^n, 1 + \lambda - \Sigma_{\text{test}}^n(\boldsymbol{\mu}) (\Sigma_{\text{train}}^n + \lambda \mathbf{I})^{-1} (\Sigma_{\text{test}}^n(\boldsymbol{\mu}))^T \right),$$

Comparing with Eq. (26), we see that this model corresponds to the following quantities in the present T-MLEM framework:

$$\begin{aligned} \hat{\delta}_f^n(\boldsymbol{\mu}) &= \Sigma_{\text{test}}^n(\boldsymbol{\mu}) (\Sigma_{\text{train}}^n + \lambda \mathbf{I})^{-1} \boldsymbol{\delta}_{\text{train}}^n \\ \hat{\delta}_\epsilon^n(\boldsymbol{\mu}) &\sim \mathcal{N} \left(0, 1 + \lambda - \Sigma_{\text{test}}^n(\boldsymbol{\mu}) (\Sigma_{\text{train}}^n + \lambda \mathbf{I})^{-1} (\Sigma_{\text{test}}^n(\boldsymbol{\mu}))^T \right). \end{aligned} \quad (58)$$

This model requires specifying parameters λ and h . We compute the length-scale parameter h by maximizing the log-marginal likelihood of the posterior distribution (see Ref. [39]), while we treat the noise parameter λ as a hyper-parameter that is selected using a validation procedure with a grid search.

Appendix D Keras algorithms

We implement the ANN, ARX, ANN-I, LARX, RNN, and LSTM models using Keras. This appendix provides the Python code that was used to construct these networks. For ARX and ANN-I, only networks corresponding to the RT training formulation are presented.

D.1 Artificial neural network (ANN)

```

1 def build_nn(X, y, hyperparams):
2     neurons, depth, reg = hyperparams[0], np.int(hyperparams[1]), hyperparams[2]
3     model = Sequential()
4     model.add(Dense(neurons, input_shape=(None, np.shape(X)[-1]), activation='relu', use_bias=True,
5                     kernel_regularizer=regularizers.l2(10.**reg)))
6     for i in range(1, depth):
7         model.add(Dense(neurons, activation='relu', use_bias=True,
8                         kernel_regularizer=regularizers.l2(10.**reg)))
9     model.add(Dense(np.shape(y)[-1], activation='linear', use_bias=True))
10    model.compile(loss='mean_squared_error', optimizer='Adam')
11    return model

```

Listing 1: Python code for the initialization of ANN.

D.2 Autoregressive w/ Exogenous Inputs (ARX)

```

def build_model_arx(X,y,hyperparams):
2   neurons,reg = int(hyperparams[0]),np.int(hyperparams[1])
   model = Sequential()
4   model.add(SimpleRNN(np.shape(y)[-1],input_shape=(None,np.shape(X)[-1]),return_sequences=
       True,activation='linear',kernel_regularizer=regularizers.l2(10**reg),
       recurrent_regularizer=regularizers.l2(10**reg)))
   model.compile(loss='mean_squared_error', optimizer='Adam')
6   return model

```

Listing 2: Python code for the initialization of ARX.

D.3 Integrated Artificial Neural Network (ANN-I)

```

def build_model_nni(X,y,hyperparams):
2   neurons,depth,reg = hyperparams[0],np.int(hyperparams[1]),hyperparams[2]
   model = Sequential()
4   model.add(Dense(neurons,input_shape=(None,np.shape(X)[-1]),activation='relu',use_bias=True,
       kernel_regularizer=regularizers.l2(10**reg)))
   for i in range(1,depth):
6       model.add(Dense(neurons,activation='relu',use_bias=True,kernel_regularizer=regularizers.
           l2(10**reg)))
   model.add(Dense(np.shape(y)[-1],activation='linear',use_bias=True))
8   model.add(SimpleRNN(np.shape(y)[-1],return_sequences=True,activation='linear',use_bias=
       False,recurrent_initializer='ones',kernel_initializer='ones',name='RNN'))
   model.get_layer('RNN').trainable = False
10  model.compile(loss='mean_squared_error', optimizer='Adam')
   return model

```

Listing 3: Python code for the initialization of ANN-I.

D.4 Latent Auto-Regressive w/ Exogenous Inputs (LARX)

```

1  def build_model_rnn_linear(X,y,hyperparams):
   neurons,reg = int(hyperparams[0]),hyperparams[1]
3   model = Sequential()
   model.add(SimpleRNN(neurons,input_shape=(None,np.shape(X)[-1]),return_sequences=True,
       activation='linear',kernel_regularizer=regularizers.l2(10**reg),recurrent_regularizer=
       regularizers.l2(10**reg)))
5   model.add(Dense(np.shape(y)[-1],activation='linear',use_bias=True))
   model.compile(loss='mean_squared_error', optimizer='Adam')
7   return model

```

Listing 4: Python code for the initialization of LARX.

D.5 Recurrent neural network (RNN)

```

1  def build_rnn(X,y,hyperparams):
   neurons,depth,reg = int(hyperparams[0]),np.int(hyperparams[1]),hyperparams[2]
3   model = Sequential()
   model.add(SimpleRNN(neurons,input_shape=(None,np.shape(X)[-1]),
5       return_sequences=True, kernel_regularizer=regularizers.l2(10**reg),
       recurrent_regularizer=regularizers.l2(10**reg)))
7   for i in range(1,depth):
   model.add(SimpleRNN(neurons,
9       return_sequences=True,
       kernel_regularizer=regularizers.l2(10**reg),
11      recurrent_regularizer=regularizers.l2(10**reg)))
   model.add(Dense(np.shape(y)[-1],activation='linear',use_bias=True))
13  model.compile(loss='mean_squared_error', optimizer='Adam')
   return model

```

Listing 5: Python code for the initialization of the RNN.

D.6 Long short-term memory network (LSTM)

```

def build_lstm(X,y,hyperparams):
2   neurons,depth,reg = int(hyperparams[0]),np.int(hyperparams[1]),hyperparams[2]
   model = Sequential()
4   model.add(LSTM(neurons,input_shape=(None,np.shape(X)[-1]),return_sequences=True,
       kernel_regularizer=regularizers.l2(10**reg),recurrent_regularizer=regularizers.l2(10**
       reg)))
   for i in range(1,depth):
6       model.add(LSTM(neurons,return_sequences=True,kernel_regularizer=regularizers.l2(10**reg)
           ,recurrent_regularizer=regularizers.l2(10**reg)))
   model.add(Dense(np.shape(y)[-1],activation='linear',use_bias=True))
8   model.compile(loss='mean_squared_error',optimizer='Adam')
   return model

```

Listing 6: Python code for the initialization of LSTM.

References

- [1] J. ACKMANN, J. MOAROTZKE, AND P. KORN, *Stochastic goal-oriented error estimation with memory*, Journal of Computational Physics, 348 (2017), pp. 195–219.
- [2] M. AINSWORTH AND J. T. ODEN, *A posteriori error estimation in finite element analysis*, Computational methods in applied mechanics and engineering, 142 (1997), pp. 1–88.
- [3] I. BABUŠKA AND W. RHEINBOLDT, *A-posteriori error estimates for the finite element method*, International Journal for Numerical Methods in Engineering, 12 (1978), pp. 1597–1615.
- [4] G. BERKOOZ, P. HOLMES, AND J. L. LUMLEY, *The proper orthogonal decomposition in the analysis of turbulent flows*, Annu. Rev. Fluid Mech., 25 (1993), pp. 539–575.
- [5] P. J. BLONIGAN, *Least Squares Shadowing for sensitivity analysis of large chaotic systems and fluid flows*, PhD thesis, Massachusetts Institute of Technology, 2016.
- [6] T. BUI-THANH, K. WILLCOX, AND O. GHATTAS, *Model reduction for large-scale systems with high-dimensional parametric input space*, SIAM Journal on Scientific Computing, 30 (2008), pp. 3270–3288.
- [7] BUI-THANH, T. AND WILLCOX, K. AND GHATTAS, O., *Parametric reduced-order models for probabilistic analysis of unsteady aerodynamic applications*, AIAA Journal, 46 (2008), pp. 2520–2529.
- [8] C. PRUD’HOMME AND D.V. ROVAS AND K. VEROY AND L. MACHIELS AND Y. MADAY AND A. PATERA AND G. TURINICI, *Reduced-Basis Output Bound Methods for Parametrized Partial Differential Equations*, Proceedings SMA Symposium, (2002).
- [9] K. CARLBERG, M. BARONE, AND H. ANTIL, *Galerkin v. least-squares Petrov–Galerkin projection in nonlinear model reduction*, Journal of Computational Physics, 330 (2017), pp. 693–734.
- [10] F. CHOLLET ET AL., *Keras*. <https://keras.io>, 2015.
- [11] Z. DRMAC AND S. GUGERCIN, *A new selection operator for the discrete empirical interpolation method—improved a priori error bound and extensions*, SIAM Journal on Scientific Computing, 38 (2016), pp. A631–A648.
- [12] M. DROHMANN AND K. CARLBERG, *The ROMES method for statistical modeling of reduced-order-model error*, SIAM/ASA Journal on Uncertainty Quantification, 3 (2015), pp. 116–145.

- [13] M. S. ELDRED, A. A. GIUNTA, S. S. COLLIS, N. A. ALEXANDROV, AND R. M. LEWIS, *Second-order corrections for surrogate-based optimization with model hierarchies*, in 10th AIAA/ISSMO Multidisciplinary Analysis and Optimization Conference, American Institute of Aeronautics and Astronautics, 2004.
- [14] R. EVERSON AND L. SIROVICH, *Karhunen–Loève procedure for gappy data*, Journal of the Optical Society of America A, 12 (1995), pp. 1657–1644.
- [15] B. FRENO AND K. CARLBERG, *Machine-learning error models for approximate solutions to parameterized systems of nonlinear equations*, Computer Methods in Applied Mechanics and Engineering, 348 (2019), pp. 250–296.
- [16] S. E. GANO, J. E. RENAUD, AND B. SANDERS, *Hybrid variable fidelity optimization by using a kriging-based scaling function*, AIAA Journal, 43 (2005).
- [17] I. GOODFELLOW, Y. BENGIO, AND A. COURVILLE, *Deep Learning*, MIT Press, 2016. <http://www.deeplearningbook.org>.
- [18] M. GREPL AND A. PATERA, *A posteriori error bounds for reduced-basis approximations of parametrized parabolic partial differential equations*, ESAIM, 39 (2005), pp. 157–181.
- [19] M. HINZE AND M. KUNKEL, *Residual based sampling in POD model order reduction of drift–diffusion equations in parametrized electrical networks*, ZAMM-Journal of Applied Mathematics and Mechanics / Zeitschrift für Angewandte Mathematik und Mechanik, 92 (2012), pp. 91–104.
- [20] S. HOCHREITER AND J. SCHMIDHUBER, *Long short-term memory*, Neural Comput., 9 (1997), pp. 1735–1780.
- [21] C. HOMESCU, L. R. PETZOLD, AND R. SERBAN, *Error estimation for reduced-order models of dynamical systems*, SIAM Review, 49 (2007).
- [22] D. HUANG, T. T. ALLEN, W. I. NOTZ, AND R. A. MILLER, *Sequential kriging optimization using multiple-fidelity evaluations*, Structural and Multidisciplinary Optimization, 32 (2006).
- [23] D. HUYNH, D. KNEZEVIC, Y. CHEN, J. S. HESTHAVEN, AND A. PATERA, *A natural-norm successive constraint method for inf-sup lower bounds*, Computer Methods in Applied Mechanics and Engineering, 199 (2010), pp. 1963–1975.
- [24] I. BABUŠKA AND W.C. RHEINBOLDT, *Error estimates for adaptive finite element computations*, SIAM Journal on Numerical Analysis, 15 (1978), pp. 736–754.
- [25] M. C. KENNEDY AND A. O’HAGAN, *Bayesian Calibration of Computer Models*, J.R. Statist. Soc. B, 63 (2001), pp. 425–464.
- [26] D. P. KINGMA AND J. BA, *Adam: A method for stochastic optimization*, CoRR, abs/1412.6980 (2015).
- [27] K. LEE AND K. CARLBERG, *Model reduction of dynamical systems on nonlinear manifolds using deep convolutional autoencoders*, arXiv e-print, (2018).
- [28] J. C.-C. LU, *An a posteriori Error Control Framework for Adaptive Precision Optimization using Discontinuous Galerkin Finite Element Method*, PhD thesis, Massachusetts Institute of Technology, 2005.
- [29] Y. MADAY AND A. T. PATERA, *Numerical analysis of a posteriori finite element bounds for linear functional outputs*, Mathematical Models and Methods in Applied Sciences, 10 (2000), pp. 785–799.
- [30] A. MARCH AND K. WILLCOX, *Provably convergent multifidelity optimization algorithm not requiring high-fidelity derivatives*, AIAA Journal, 50 (2012).

- [31] M. C. MOZER, *A focused backpropagation algorithm for temporal pattern recognition*, Complex Systems, 3 (1989).
- [32] C. OLAH, *Understanding LSTM networks*, August 2015.
- [33] S. PAGANI, A. MANZONI, AND K. CARLBERG, *Statistical closure modeling for reduced-order models of stationary systems by the ROMES method*, arXiv:1901.02792, (2019).
- [34] S. PAGANI, A. MANZONI, AND A. QUARTERONI, *Efficient state/parameter estimation in nonlinear unsteady pdes by a reduced basis ensemble kalman filter*, SIAM/ASA Journal on Uncertainty Quantification, 5 (2017), pp. 890–921.
- [35] M. PARASCHIVOIU AND A. T. PATERA, *A hierarchical duality approach to bounds for the outputs of partial differential equations*, Computer Methods in Applied Mechanics and Engineering, 158 (1998), pp. 389–407.
- [36] M. PARASCHIVOIU, J. PERAIRE, AND A. T. PATERA, *A posteriori finite element bounds for linear-functional outputs of elliptic partial differential equations*, Computer Methods in Applied Mechanics and Engineering, 150 (1997), pp. 289–312.
- [37] F. PEDREGOSA, G. VAROQUAUX, A. GRAMFORT, V. MICHEL, B. THIRION, O. GRISEL, M. BLONDEL, P. PRETTENHOFER, R. WEISS, V. DUBOURG, J. VANDERPLAS, A. PASSOS, D. COURNAPEAU, M. BRUCHER, M. PERROT, AND E. DUCHESNAY, *Scikit-learn: Machine learning in Python*, Journal of Machine Learning Research, 12 (2011), pp. 2825–2830.
- [38] C. PRUD’HOMME, D. ROVAS, K. VEROY, L. MACHIELS, Y. MADAY, A. PATERA, AND G. TURINICI, *Reliable Real-Time Solution of Parametrized Partial Differential Equations: Reduced-Basis Output Bound Methods*, Journal of Fluids Engineering, 124 (2001), pp. 70–80.
- [39] C. E. RASMUSSEN AND C. K. I. WILLIAMS, *Gaussian Processes for Machine Learning*, The MIT Press, 2006.
- [40] A. J. ROBINSON AND F. FALLSIDE, *The utility driven dynamic error propagation network*, Tech. Rep. CUED/F-INFENG/TR.1, Engineering Department, Cambridge University, Cambridge, UK, 1987.
- [41] D. ROVAS, L. MACHIELS, AND Y. MADAY, *Reduced-basis output bound methods for parabolic problems*, IMA Journal of Numerical Analysis, 26 (2006).
- [42] D. E. RUMELHART, G. E. HINTON, AND R. J. WILLIAMS, *Learning representations by back-propagating errors*, Nature, 323 (1986), pp. 533–536.
- [43] E. D. RUMELHART, G. E. HINTON, AND R. J. WILLIAMS, *Learning representations by back-propagating errors*, Nature, 323 (1986), pp. 533–536.
- [44] Y. S. SHIMIZU, *Output-based error estimation for chaotic flows using reduced-order modeling*, in AIAA SciTech Forum, (AIAA 2018-0826), 2018.
- [45] S. TREHAN, K. CARLBERG, AND L. J. DURLOFSKY, *Error estimation for surrogate models of dynamical systems using machine learning*, International Journal for Numerical Methods in Engineering, 112 (2017), pp. 1801–1827.
- [46] D. A. VENDITTI AND D. L. DARMOFAL, *Adjoint error estimation and grid adaptation for functional outputs: Application to quasi-one-dimensional flow*, Journal of Computational Physics, 164 (2000), pp. 204 – 227.
- [47] D. A. VENDITTI AND D. L. DARMOFAL, *Grid adaptation for functional outputs: Application to two-dimensional inviscid flows*, Journal of Computational Physics, 176 (2002), pp. 40 – 69.

- [48] Y. WU AND U. HETMANIUK, *Adaptive training of local reduced bases for unsteady incompressible Navier–Stokes flows*, International Journal for Numerical Methods in Engineering, 103 (2015), pp. 183–204.
- [49] M. YANO AND A. T. PATERA, *An LP empirical quadrature procedure for reduced basis treatment of parametrized nonlinear PDEs*, Computer Methods in Applied Mechanics and Engineering, (2018).
- [50] M. ZAHR, *Adaptive model reduction to accelerate optimization problems governed by partial differential equations*, PhD thesis, Stanford University, 2016.
- [51] M. ZAHR, K. CARLBERG, AND D. KOURI, *An efficient, globally convergent method for optimization under uncertainty using adaptive model reduction and sparse grids*, SIAM/ASA Journal on Uncertainty Quantification, 6 (2019), pp. 877–912.
- [52] M. J. ZAHR AND C. FARHAT, *Progressive construction of a parametric reduced-order model for PDE-constrained optimization*, International Journal for Numerical Methods in Engineering, 102 (2015), pp. 1111–1135.